



University of
Stavanger

Faculty of Science and Technology

MASTER'S THESIS

Study program/ Specialization: <i>Master Konstruktion and material science</i>	Spring semester, 20..... Open / Restricted access
Writer: <i>Johan Andreas Thorkaas</i>	<i>J. A. Thorkaas</i> (Writer's signature)
Faculty supervisor: <i>Vidar Hansen</i>	
External supervisor(s):	
Thesis title: <i>Mechanical and Microstructural investigation of 3D-Printed Alloy 625</i>	
Credits (ECTS):	
Key words: <i>3D-Printing, Alloy 625 Charpy V, Tensile, dendritic</i>	Pages: <i>109</i> + enclosure: Stavanger, <i>15 June 2016</i> Date/year

Front page for master thesis
Faculty of Science and Technology
Decision made by the Dean October 30th 2009

Abstract

Additive manufacturing is in the wind and shows great promise as a manufacturing technique. In this thesis the properties of the additive manufactured EOS alloy 625 is investigated.

Tensile, CharpyV, Vickers, and pitting corrosion test have been performed to investigate the material properties, and it has been inspected in the SEM and with light microscopy.

The material properties were found to be within the range of the EOS specifications. Many interesting additional properties and details were found, as explained in the discussion and conclusion.

Apology

I wish to apologize for handing in such an unfinished work. The materials were delivered late, 11. March, and the extent of the experimental work of the thesis were so large that 3 months and 4 days' work, nearly 700hours, simply doesn't do it justice. Not counting the work done researching and deciding what specimens to order. If you are a student looking for an example thesis as a template for your own, this is probably not your best choice.

I'd like to apologize for the language in this thesis that probably has its faults. Should anything be unclear, or should you ever be in doubt of some results, please contact me for clarification.

Acknowledgements

I want to thank all involved parties, many more than I can make room for on a page, for contributing to the possibility of this work.

I would like to pay my respect to the pioneers and researchers who's shoulders we stand on today. This work had not been possible if they hadn't pushed the boundaries, dared to challenge established beliefs, and worked countless hours to prove their theories. We are all in great debt to the people who put science before all else, and to their families for their sacrifices.

I would like to thank my supervisor, Vidar Hansen for much good reflection and wisdom. Ingunn Cesilie Oddsen for great help with the lab work.

A huge thanks goes out to FMC with Jan Tore Kvåvik, and Geir Tandberg for making this thesis possible.

Thanks to my family for support, and my girlfriend for patience.

List of content

Abstract.....	2
Apology	3
Acknowledgements	4
List of figures	10
List of tables	12
1 Introduction.....	15
1.1 Additive manufacturing.....	15
1.2 Super alloys	16
2 Theory	17
2.1 Alloy 625	17
2.2 DMLS additive manufacturing.....	21
2.2.1 Introduction.....	21
2.2.2 Advantages of additive manufacturing over traditional manufacturing	23
2.2.3 Challenges.....	25
2.2.4 Anisotropic material	25
2.3 Tensile test.....	26
2.3.1 Introduction.....	26
2.3.2 Material properties	27
2.3.3 Test parameters	28
2.4 CharpyV.....	29
2.5 Vickers hardness test	30
2.6 Corrosion testing and pitting corrosion	31
2.7 Light microscopy.....	32
2.7.1 Introduction.....	32
2.7.2 Thin film interference	32
2.8 SEM.....	33
2.8.1 Introduction SEM	33
2.8.2 Signal generation	34
2.8.3 SE.....	36
2.8.4 QBSD.....	37

2.8.5	EDS	38
2.8.6	EBSD	39
3	Experimentation	40
3.1	General experimentation.....	40
3.1.1	Equipment	40
3.1.2	Specimen handling.....	42
3.2	Tensile	43
3.2.1	Introduction.....	43
3.2.2	Preparation	45
3.2.3	Testing	47
3.2.4	Post-test inspection	48
3.3	Charpy V.....	49
3.3.1	Introduction.....	49
3.3.2	Preparation	51
3.3.3	Testing	56
3.3.4	Post-test inspection	57
3.4	Vickers hardness test	58
3.4.1	Introduction.....	58
3.4.2	Preparation	58
3.4.3	Testing	59
3.4.4	Post-test inspection	59
3.5	Corrosion	60
3.5.1	Introduction.....	60
3.5.2	Preparation	60
3.5.3	Testing	62
3.5.4	Post-test inspection	63
3.6	SEM and light-microscopy	64
3.6.1	Introduction.....	64
3.6.2	Preparation	64
3.6.3	Microscopy	67
3.6.4	Post microscopy work.....	67

4	Results.....	68
4.1	Initial measurements of specimens.....	68
4.1.1	Measurements	68
4.1.2	Rough support and overhang surface.....	69
4.1.3	Bending by thermal contraction.....	69
4.2	Tensile	70
4.2.1	Curve shape, general characteristics.....	70
4.2.2	Tensile strength, UTS	71
4.2.3	Yield strength, $R_{p0.2}$	71
4.2.4	E-modulus.....	73
4.2.5	Elongation.....	74
4.2.6	Fracture surface.....	75
4.3	CharpyV.....	78
4.3.1	Energy absorbed	78
4.3.2	Fracture surface.....	79
4.4	Hardness Vickers.....	80
4.4.1	Resluts.....	80
4.5	Corrosion	81
4.5.1	Introduction.....	81
4.5.2	Measurements	81
4.5.3	Microscopy	82
4.6	Light microscopy results	84
4.6.1	Layer angle	84
4.6.2	Grain structure remaining over melting lines	84
4.7	SEM – microscopy	85
4.7.1	Pores.....	85
4.7.2	Dendritic structure	86
4.7.3	Aluminium particles	88
4.7.4	Crystal orientation, grain size. EBSD.....	90
4.7.5	Elemental composition	94

5	Discussion	95
5.1	Initial measurements and inspection.....	95
5.1.1	Overhang and support surfaces.....	95
5.1.2	Discoloration.....	95
5.1.3	Dimensional accuracy.....	95
5.1.4	Surface roughness	95
5.1.5	Thermal bending	95
5.2	Tensile	96
5.2.1	Modulus of elasticity (E-modulus)	96
5.2.2	% elongation	97
5.2.3	UTS and yield	97
5.2.4	Fracture surface.....	97
5.2.5	Y- specimen behaving like the L specimen	97
5.2.6	Anisotropic properties.....	97
5.3	CharpyV.....	98
5.3.1	Difference between printed and machined notch	98
5.4	Hardness Vickers	99
5.5	Corrosion	99
5.5.1	Presence of pitting	99
5.5.2	Surface finishing impact on pitting.....	99
5.5.3	Measurement accuracy of the surface area	100
5.5.4	Mass deviation	100
5.6	Light microscopy	100
5.7	SEM – microscopy	100
5.7.1	Pores.....	100
5.7.2	Dendrites	100
5.7.3	Aluminium rich spots.....	101
5.7.4	Crystallographic orientation	101
5.7.5	Material composition	101
6	Conclusion	102
7	Further work.....	103

8	References.....	104
	Attachments.....	109
7	Raw tensile test data.....	109
8	Raw CharpyV data.....	109

List of figures

Figure 2.2.1-1 Dendritic structure in welded 625 [8].....	20
Figure 2.2.1-1 Illustration of a typical DMLS machine [9]	21
Figure 2.2.1-2 DMLS layers of print illustration [10].....	22
Figure 2.2.2-1 Airbus A320 nacelle hinge bracket made by additive manufacturing. [11]	23
Figure 2.2.2-2 Nuts with honeycomb structure inside. [9].....	24
Figure 2.3.1-1 Example of stress strain curve. [23]	26
Figure 2.3.3-1 Presentation of Charpy-V testing [14].....	29
Figure 2.3.3-1 Vickers test illustrated [13].....	30
Figure 2.3.3-1 Illustration of pitting corrosion.....	31
Figure 2.7.2-1 Thin-film interference varying thickness. [16].....	32
Figure 2.7.2-2 Thin film interference cancellation [27].....	32
Figure 2.8.2-1 Emission volume SEM [29].....	34
Figure 2.8.2-2 Creation of characteristic x-rays and photons (to the left), and secondary electrons (to the right)	35
Figure 2.8.3-1 Everhart-Thornley (SE) detector illustration. [23]	36
Figure 2.8.4-1 BSE angular intensity	37
Figure 2.8.4-2 Backscatter detector illustration [33].....	37
Figure 2.8.6-1 Kikuchi lines silicone [24].....	39
Figure 3.1.1-1 Micrometre used in the experimentation	40
Figure 3.1.1-2 Struers Planopol with a Pedemax-2.....	41
Figure 3.1.2-1 Specimens in box after initial measurements	42
Figure 3.2.1-1 Orientation of the different specimens in the printing chamber.....	43
Figure 3.2.1-2 Top profile of T specimen.	44
Figure 3.2.1-3 Tensile test profile	44
Figure 3.2.2-1 Specimen U1 before machining.....	45
Figure 3.2.2-2 U-specimen after “SS5M8P2.MIN”.	45
Figure 3.2.2-3 U-Specimens after finished machining.....	46
Figure 3.2.3-1 Specimen U1 mounted and ready for testing.....	47
Figure 3.2.4-1 Tensile test ready for SEM.	48
Figure 3.3.1-1 CharpyV geometry for standard test specimen.....	49
Figure 3.3.1-2 Orientation of the Charpy test in the printing chamber.	50

Figure 3.3.2-1 Face milling off support structure on CharpyV-specimen.	51
Figure 3.3.2-2 Vice used to grind the CharpyV specimens.....	52
Figure 3.3.2-3 Grinding setup for a Charpy specimen	53
Figure 3.3.2-4 Control of printed V-notch radius.....	53
Figure 3.3.2-5 V-notch broaching machine.....	54
Figure 3.3.2-6 CharpyV-specimen after broaching.....	55
Figure 3.3.2-7 Control of broached CharpyV radius.....	55
Figure 3.3.3-1 Specimen being placed in the testing machine with a self-centring tong..	56
Figure 3.4.1-1 Illustration of Vickers test specimen surface.....	58
Figure 3.4.3-1 HV1 idents on Specimen LII 3 F.....	59
Figure 3.5.2-1 Fracture surface being cut off a CharpyV-sample in the Discotom	61
Figure 3.5.3-1 Corrosion tests in the heating cabinet after 24hours.....	62
Figure 3.6.2-1 Electropolishing setup.	65
Figure 3.6.2-2 Illustration of the electropolishing bath.....	65
Figure 4.1.1-1 Measurement points on the tensile specimens upon arrival	68
Figure 4.1.1-2 Measurement points on the Charpy specimens upon arrival	68
Figure 4.1.2-1 Rough overhang and support structure on specimen L1	69
Figure 4.1.3-1 Specimen L4 displaying bending due to thermal contraction/stress	69
Figure 4.2.1-1 Stress-Strain graph of tensile test, specimen L4.....	70
Figure 4.2.3-1 Yield point on stress-strain graph for specimen L1.....	72
Figure 4.2.4-1 Uneven curve at start of tensile test, specimen U2.....	73
Figure 4.2.6-1 Fracture surface of specimen L2.....	75
Figure 4.2.6-2 Pores on fracture surface of specimen T2.....	76
Figure 4.2.6-3 Specimen U2, cracks can be seen in the surface.	76
Figure 4.2.6-4 Specimen T2, showing tearing in the fracture surface.	77
Figure 4.2.6-5 Specimen U2, showing tearing at higher resolution in fracture surface....	77
Figure 4.3.1-1 CharpyV specimen orientations in 3D-printer.....	78
Figure 4.4.1-1 HV1 test on L II 3 F plotted in a 3D-plot.	80
Figure 4.5.1-1 Illustration of corrosion specimen measurements	81
Figure 4.5.3-1 Part of one of the surfaces of corrosion specimen 3	82
Figure 4.5.3-2 Mechanical mark on specimen 1	82
Figure 4.5.3-3 Oil from fingers on specimen 3	83
Figure 4.5.3-4 Dust on specimen 1	83
Figure 4.6.1-1 Multiple layers seen with laser angle difference in specimen L II 3 S.....	84

Figure 4.6.2-1 Grain growth across melting lines	84
Figure 4.7.1-1 Pores near about 100 μ m from the edge of specimen A II 3 S.....	85
Figure 4.7.1-2 Pore in surface of A II 3 S up close. Cracks visible at the bottom.	86
Figure 4.7.2-1 Backscatter image of dendritic structure of L II 3 F. Different grain orientations visible.	86
Figure 4.7.2-2 EDS line-mapping showing high amounts of Mo(magenta) and Nb(purple) at dendritic edges.....	87
Figure 4.7.3-1 Black spots of around 67nm diameter, found in all specimens.	88
Figure 4.7.3-2 Increase in Al at dark spots.....	89
Figure 4.7.4-1 EBSD orientation colour key.....	90
Figure 4.7.4-2 Grain orientation, specimen seen from the top and down, xy-plane.	91
Figure 4.7.4-3 Grain orientation seen from the side, zx-plane.....	91
Figure 4.7.4-4 Grain orientation density seen from the top, xy-plane.	92
Figure 4.7.4-5 Grain orientation density seen from the side, zx-plane.	92
Figure 4.7.4-6 Grains showing tints indicating smaler changes in crystallographic orientation.....	93
Figure 4.7.5-1 EDS analysis of the matrix, with plot and ZAF-table	94

List of tables

Table 2.1-1 W% composition of EOS Alloy 625 [6]	17
Table 2.1-2 Carbides in Alloy 625	18
Table 2.1-3 Mechanical properties of Alloy 625, EOS vs Special Metals Corporation ...	19
Table 2.5-1 Vickers test load designations [16]	30
Table 3.6-1 Mechanical grinding and polishing steps.....	64
Table 3.6-2 Time of exposure and order of electropolishing.....	66
Table 3.6-3 Polishing process steps OP-A or OP-S.	66
Table 4.2-1 Tensile strength, UTS, of tensile tests, [MPa]	71
Table 4.2-2 Yield strength of tensile test, Rp0.2 [MPa].....	71
Table 4.2-3 Yield strength as % of tensile strength.....	72
Table 4.2-4 E-modulus of tensile tests, [GPa].....	73
Table 4.2-5 % elongation at UTS	74
Table 4.2-6 % elongation at fracture	74
Table 4.3-1 CharpyV test results, printed notch.....	78
Table 4.3-2 CharpyV test results, machined notch.....	78

Table 4.3-3 Comparison between printed and machined notch	79
Table 4.4-1 Vickers test results	80
Table 4.5-1 Physical measurements and data of the corrosion specimens	81
Table 4.7-1 EDS analysis of dendritic intersection, bright area, at 20kV	87
Table 4.7-2 EDS analysis of black spot, at 20kV	89

Abbreviations

- EOS 625 - EOS NickelAlloy IN625, Attachment 5. DMLS (3D-printed) Alloy 625.
- Alloy 625 - UNS N06625, Inconel®¹ 625.
- DMLS - Direct Metal Laser Sintering. Additive manufacturing, 3D-printing technique
- AM Additive manufacturing.

¹ Inconel is a trademark of the Special Metals Corporation group of companies.

1 Introduction

1.1 Additive manufacturing

Early humans began to use stone tools 2.6 million years ago to ease the job of hunting and food gathering [1]. Since then we have continued to evolve tools to protect our existence, ease our lives, and explore the world and the universe. Production of metal tools or products have traditionally been done through forging, casting, welding, or subtractive machining. The different techniques are often combined to utilize each production technique's advantages. Even through combining different techniques, traditional manufacturing techniques have limitations in production possibilities and cost. This demands that the part or product is designed with production in mind to lower the cost and time of production, or to simply make it possible to produce it. Design for production rather than for function causes parts to be heavier, bulkier, and larger than necessary. For industries like aerospace, and the space industry having parts that weights more than needed is very costly because of increased fuel usage.

In the 1980s a new type of production techniques was invented. 3D-printing og additive manufacturing or additive manufacturing was a new technique were the part was built up into its finished shape, instead of being carved out of a block of material. The first patents were for polymers [2], but many of the techniques were applicable for metals to, and the introduction of metal AM machines, or 3D-printers.

To this day, much of the basics is still the same and the general improvements comes from better understanding og the printer parameters and their influence on the properties of the final products.

1.2 Super alloys

As we strive to better our living conditions we meet new challenges all the time. In engineering these challenges forces innovation in design, technique, and materials. In the offshore, and particularly the subsea industry, every project pushes the boundaries. High speed flow of hot crude oil with all its impurities going through a valve will wear it out no matter what it is made of. When it is on the bottom of the ocean and a crucial part of a billion-dollar oil producing operation, the cost of using specialised alloys fades compare to the cost of maintenance, the loss and environmental cost if it breaks.

A superalloy is in Oxford Dictionaries [3] defined as “An alloy capable of withstanding high temperatures, high stresses, and often highly oxidizing atmospheres.” and by Wikipedia [4] “...an alloy that exhibits several key characteristics: excellent mechanical strength, resistance to thermal creep deformation, good surface stability and resistance to corrosion or oxidation.” Superalloys are usually based on iron, nickel, or cobalt [5]. They are used in everything from valves, pipes, heat exchangers, to jet propulsion, and many more fields. It is mostly used where maintenance is costly or impossible, and failure is not an option, or where no other alloy is able to maintain its properties as in extreme temperature applications.

Nickle is element 28. It is probably generally most known by the fact that people can be allergic to skin contact with it from nickel coated zippers and jewellery, but it is also the basis for some quite impressive superalloys. Nickel is the main component in superalloys such as Inconel^{TM2}, Hastelloy^{TM3}, Waspaloy^{TM4}, etc. Nickel based superalloys are used in high temperature load bearing applications, up to 90% of its melting point. This is the highest for any common alloying system [5].

Now these alloys are being 3D-printed, and research is needed to control that the material properties remain.

² Inconel is a trademark of the Special Metals Corporation group of companies.

³ Hastelloy is a trademark of Haynes International, Inc.

⁴ Waspaloy is a trademark of United Technologies Corp

2 Theory

2.1 Alloy 625

Alloy 625, UNS N06625, Inconel™ 625 is an austenitic solution strengthened Nickel-Chromium superalloy. Due to its molybdenum and niobium content strengthening it is not necessary to precipitate harden treatments is not necessary. Precipitates are not as common in alloy 625 as in alloy 718 and other precipitate hardening material, but they can still be present. The alloy has many good properties like high creep resistance, a wide operational temperature range, good corrosion resistance, and other described in the following sections. Information given in this chapter will mainly focus on the information given by EOS GmbH on their additive manufactured EOS Alloy 625 [6]. Since this is the material being tested.

Composition

Table 2.1-1 W% composition of EOS Alloy 625 [6]

Element	Min		Max
Ni	58.00	≤	Remainder
Cr	20.00	-	23.00
Mo	8.00	-	10.00
Nb	3.15	-	4.15
Fe		≤	5.00
Al		≤	0.40
C		≤	0.10
Ta		≤	0.05
Si		≤	0.5
Mn		≤	0.5
P		≤	0.015
S		≤	0.015

Phases

Nickle-chromium superalloys have many phases, the ones listed here are the once suspected found in the specimens of this thesis.

γ - matrix phase

Structure: fcc

This is the main, matrix, phase of the Alloy 625. Since Alloy 625 is a solution hardened material, the matrix contains a lot of solid solution elements (Cr, Mo, Fe, Ta)

γ'' – Ni₃Nb

Structure: BCT

Formers: Nb

Metastable phase that transforms to the orthorhombic δ -phase(not mentioned in this thesis) at elevated temperatures over time.

Carbides

Table 2.1-2 Carbides in Alloy 625

Formula	Structure	Formers
MC	Cubic	Ta, Ti, Mo, Nb
M ₂₃ C ₆	fcc	Cr, Mo
M ₆ C	fcc	Mo

Surface Oxides

Forms on the surface and can grow to a thick protective barrier at elevated temperature.

Cr₂O₃, hexagonal close packed

Al₂O₃, Trigonal, hR30

Physical properties

EOS additive manufactured data is compared to Special Metals Corporations annealed rod material in Table 2.1-3. Different companies deliver the alloy in different states with different mechanical properties. Special Metals Corporation was chosen since they were the ones that developed the alloy.

Alloy 625 has good resistance against pitting and other corrosions, also at elevated temperatures. It has high creep resistance, also at elevated temperatures, and has the highest homologous service temperature of any common alloying system, 90% or $T_m=0.9$ [5]. High tensile strength and ductility, as seen in Table 2.1-3, coupled with good weldability makes it an interesting alloy for many uses.

Table 2.1-3 Mechanical properties of Alloy 625, EOS vs Special Metals Corporation

Property	EOS Alloy 625 [6]	Special Metals Corporation, Inconel 625 [7]
Density [g/cm^3]	8.4	8.44
Tensile strength (UTS) [MPa]:		
Horizontal, XY-plane	940 - 1040	827 - 1034
Vertical, Z-direction	850 – 950	827 - 1034
Yield strength, $R_{p0.2}$, [MPa]:		
Horizontal, XY-plane	675 - 775	414 - 655
Vertical, Z-direction	565 - 665	414 - 655
E- modulus [GPa]:		
Horizontal, XY-plane	150 - 190	207.5
Vertical, Z-direction	120 - 160	207.5
Elongation at fracture [%]:		
Horizontal, XY-plane	30 - 40	60-30
Vertical, Z-direction	37 - 47	60-30
Hardness		
Brinell	287	145-220
Rockwell	30	NA
Vicker's	302 ^C	145-231 ^C
CharpyV [J] Room temp	NA	92.9
		(Weld, filler Metal 625a)

*C = calculated

Applications and other properties

Alloy 625 can be used for many applications from propeller blades, valve housings, chemical plant parts, electrical connectors, etc. Due to its good corrosion resistance and mechanical properties, it is suitable for use in subsea oil applications.

Alloy 625 workhardens quickly and can be troublesome to machine. To overcome these problems it is often machined with deep cuts, hard cutting inserts, and at slow speeds. This is to avoid deformation of the cutting tool or the workpiece.

Alloy 625 is sometimes welded on-top of other alloys as a corrosion protection. Its good weldability makes this possible and also make it possible to joint alloy 625 parts, or joining with other materials using the proper filler material.

Dendritic structures

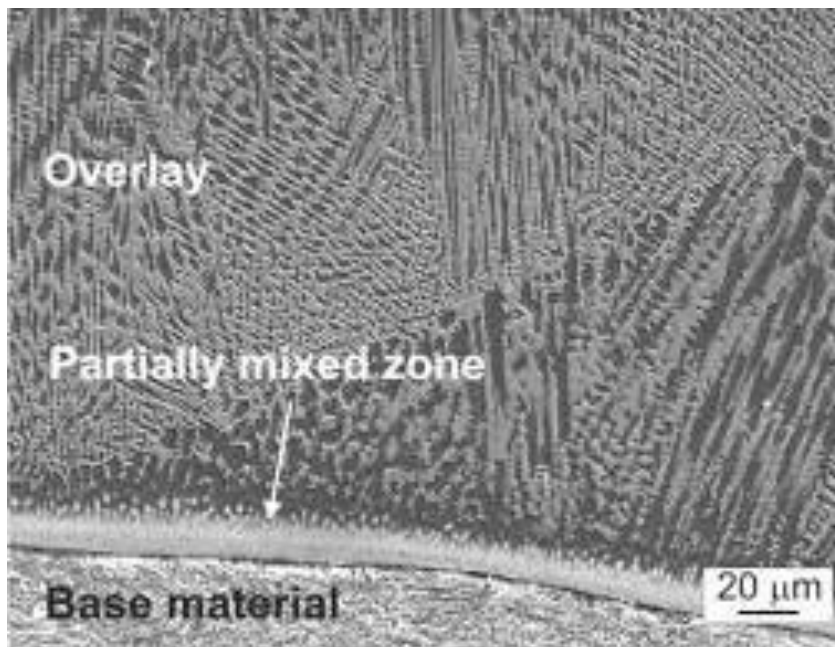


Figure 2.2.1-1 Dendritic structure in welded 625 [8]

A study on using alloy 625 as a protective layer for steel pipes shows that the alloy 625 layer gets a dendritic structure [8]. The study did find Mo and Nb rich precipitates in the boundary layer between the dendrites. Other studies of welds in other Nickel-Chromium alloys have found the same dendritic structure. Since EOS alloy 625 is a series of welds, see chapter 2.2, it is comparable, and the dendritic structure is expected.

2.2 DMLS additive manufacturing

This is a presentation of the DMLS technology and some of its benefits and limitations as found by the author in June 2016. The technology is rapidly developing and changes are expected.

2.2.1 Introduction

3D-printing of metals by DMLS is performed by using a laser to melt thin layers of metal powder to build up a 3D-part. The process is performed in an inert atmosphere and under strictly controlled conditions to achieve optimal results.

The whole process starts with a part being designed in a CAD software. After the design is done the digital part file is transferred into a slicing software. The slicing software slices the part into thin horizontal layers, about 20-100 μ m each. Machine code is made to tell the machine how to draw these layers with the laser. Support structure is generated if needed (more on this below). The machine code file is sent to the 3D-printer. The printer is prepared with the correct material, and if needed additives, and the production of the part begins.

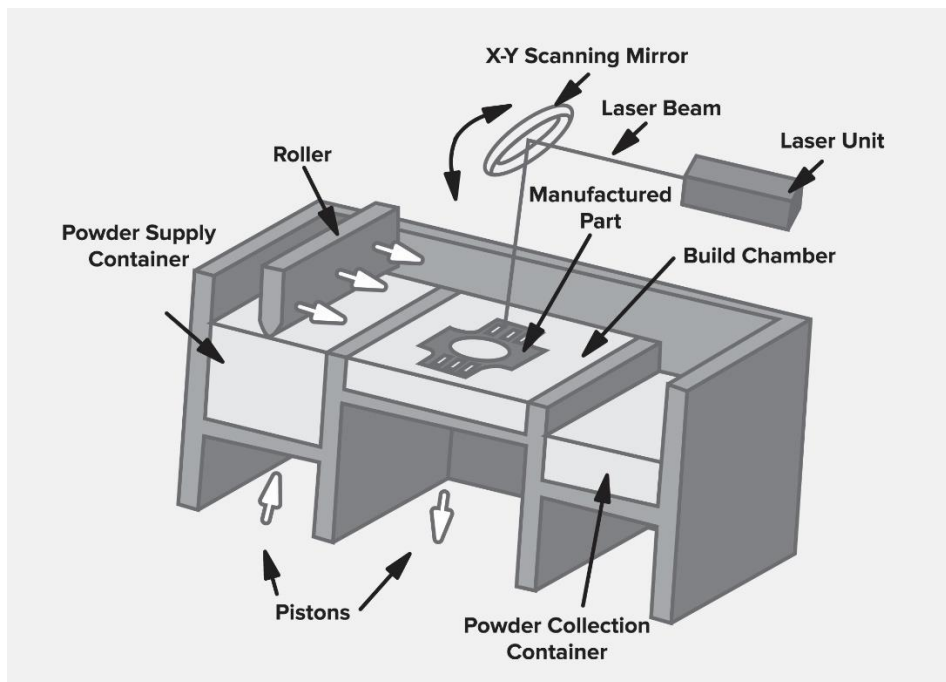


Figure 2.2.1-1 Illustration of a typical DMLS machine [9]

In the 3D-printer a fine layer of metal powder is distributed onto a metal plate, from now on known as the build plate. This is done with a roller or a wiper depending on machine type (see Figure 2.2.1-1 above). In the case of EOSINT M280 it is a stainless steel wiper blade. The laser scans over the part drawing the cross section of the part by melting the metal powder into the build plate. Then the build plate is lowered one layer height, and a new layer of metal powder applied over the first one. The laser melts the new cross section and the process then repeats itself until the part is done. See Figure 2.2.1-2 for layer build-up illustration.

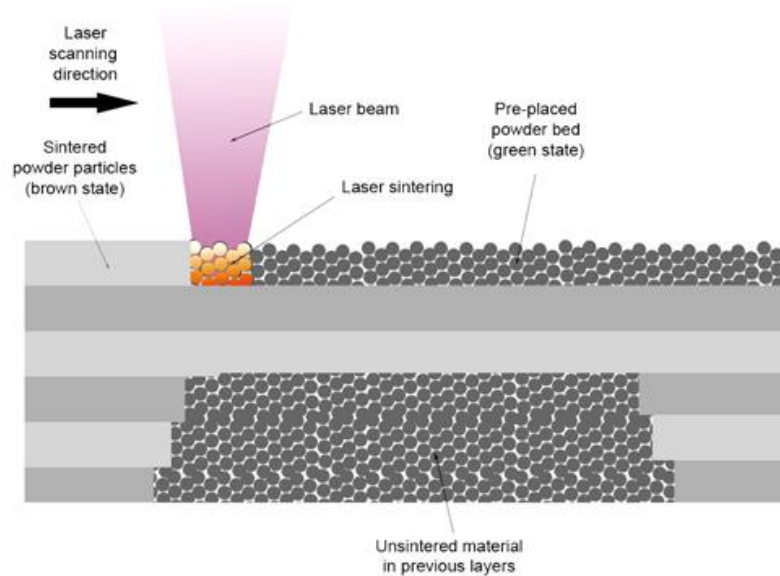


Figure 2.2.1-2 DMLS layers of print illustration [10]

Support material

For overhanging angles of 45° or less relative to the build plate support material generated. Support material is a light low density mesh that gives the overhanging part a solid surface around the powder to print on. This is needed since the melted powder needs something to stick to, if not it won't solidify in the correct position. Smaller gaps can be bridged without support material. The slicing software assists by suggesting the use of support structure if it finds sections that could need it.

Support material on the first layers

If the part itself is made directly onto the surface of the build plate, machining will be needed to remove the build plate from the 3D-printed part, and the build plate will be destroyed. To avoid this the 3D-printer first builds up a support structure beneath where the part will be made, and then it makes the part on top of this. The support structure can be broken off without damaging the part or the build plate. The build plate will need to be ground down to be flat again, but the heavy machining steps of milling off the build plate is omitted.

Similarities to welding

DMLS has clear similarities to welding. It is in fact welding, just a whole lot of it. This gives the produced part a lot of similar properties as a weld. Just as a weld, a part produced with DMLS might contain significant internal stress from thermal shrinkage. To release the internal stress, it is often necessary to anneal the parts after production.

When investigating the microstructure, it is also important to recognize that a lot of the work done on welding is applicable to the analysis of additive manufactured alloys too.

2.2.2 Advantages of additive manufacturing over traditional manufacturing

Additive manufacturing has many advantages over traditional manufacturing. Below are some of them listed.

Design for performance, not production

Traditional manufacturing starting with a solid block of material produces a lot of waste product and is limited in shape and features to what the manufacturing machines and tools can achieve. Complex geometries can quickly become quite costly and this drives the design to be production focused. With additive manufacturing, many (not all as some suggests) of the limitations in production cost and possibilities of traditional manufacturing. This allows for a design process where optimal design for function can be the focus, instead of production. Some production limitations still apply, but they are fewer than traditional manufacturing, and they are being worked on. A good example of utilisation of this technology is in aerospace where plate parts can be made with an organic shape that is lighter than a is possible with normal production techniques. Even though additive manufacturing is still more expensive than normal manufacturing. These lighter plane parts will pay for themselves with the reduced fuel consumption over time. See Figure 2.2.2-1 for an example of an optimised bracket.



Figure 2.2.2-1 Airbus A320 nacelle hinge bracket made by additive manufacturing. [11]

Material efficiency

Since only the material needed to make the part + support material is melted in the additive production process, the rest of the metal powder can be reused. This reduces material consumption and the need to ship it. This is good for the environment and economy since the energy needed to produce a part can be reduced, and you don't need to buy a large bulk of material that you will just turn into chips.

Hollow parts

With additive manufacturing the insides of a part can be tailored just as the outside. This opens the possibility for hollow or semi hollow parts that don't need to be solid to be strong enough. This can reduce material consumption and weight by a large deal as nearly everything can be made semi hollow and still keep enough mechanical strength to do the job.

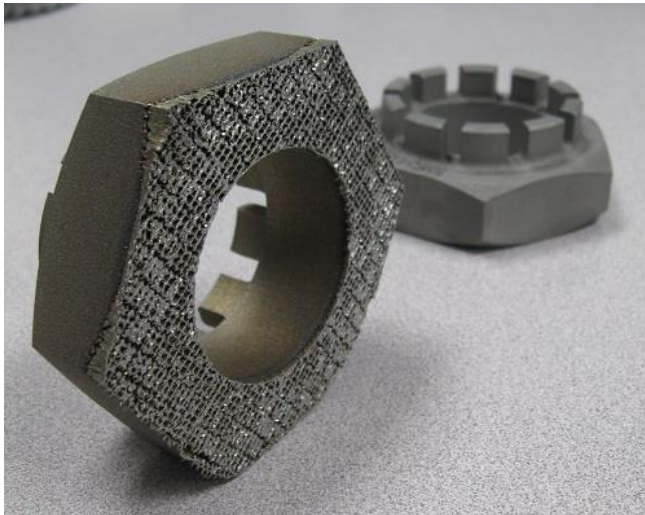


Figure 2.2.2-2 Nuts with honeycomb structure inside. [9]

An example where this has been used to solve an engineering weight problem is on a Howitzer artillery gun [12]. This artillery gun had strict weight limits since it had to be transportable beneath a helicopter. To add new parts to the Howitzer, weight had to be saved by optimising the existing design. The solution to the problem was to produce nuts with a honeycomb cross section, cutting the weight in half. See Figure 2.2.2-2. This gave enough weight savings to make room for new additions to the Howitzer.

Less need for stock parts and material

To have spare parts in stock is a costly operation, but the lead time on spare parts, and also the material needed to produce them can be quite costly too if production stops. To avoid this, some companies pay manufacturers to have material in stock in case they need to produce spare parts. Material might be needed in different dimensions for different parts, and over time material certificates can get lost, making this a costly practice to. If instead of having different dimensions of material in stock, the manufacturer could have metal powder, the storage needs and associated costs could be lowered significantly. The technology is not at this level today, but will be in a few years if the material properties of the printed material proves satisfactory for this type of production.

2.2.3 Challenges

Cost

Additive manufacturing is a valid growing industry today. Several products are made with additive manufacturing, but the cost of equipment, metal powder, and the slow production makes it more economical to use traditional manufacturing if that is possible.

Form stability. Heat shrinking.

When a weld solidifies and cools down, it shrinks to some extent. This is vibration of the atoms in a material is proportional to its heat. When the weld has just solidified it is very hot, and thus has lots of atomic vibration, making the atoms take up more space to avoid collision. When it cools down the atomic vibrations decrease, and the atoms don't need as much space anymore. If the workpiece is cold when welded, the weld will be like a spring on the surface when it cools, trying to bend the workpiece. This is an effect that is easy to observe on welds on thin sheet metal. In some metals and designs the heat shrinking can cause cracks and be a serious issue. To avoid cracking, the part(s) that are to be welded will be heated up before welding. Since the whole part then will shrink when cooled, the little extra shrinking in the weld won't be as much of a problem.

Additive manufacturing is a series of welds. Each weld works as a spring as seen above. Each layer will add a new set of springs trying to "pull" the edge surface into the cross section. This can cause an issue with the form stability and the dimensions of the finished part, that instead of being a straight piece can turn out more bent. Research on calculation compensating measures for this behaviour is ongoing on several locations around the world.

Depending on the material cracking because of the solidification from liquid metal to solid, also known as solidification cracking, can be an issue. This is an issue that it would be logical to assume could be dealt with in a similar way that it is done in the welding industry.

2.2.4 Anisotropic material

In an isotropic material the material properties are the same in all directions, for an anisotropic material they are not. Additive manufacturing produces an anisotropic material because of the laser welding techniques. The laser welding causes the grains of the material to have preferred growth orientation. To limit this effect, the "drawing" direction of the laser is changed for each layer. This can cause the material to be quite isotropic in the build cross section, but there will still be a difference between material in the build cross section plane(XY-plane), and along the build direction(Z-axis).

The sweep direction of the wiper or roller that applies metal powder for each layer could also might introduce some anisotropy in the build plane. This has not been a subject of investigation of this thesis.

2.3 Tensile test

2.3.1 Introduction

The purpose of tensile testing is to document the behaviour of a material under load. Yield strength, ultimate tensile strength (UTS), %elongation, %reduction of cross section, Young's modulus (E-modulus), and the type of fracture (brittle, ductile) are some of the more common properties found when performing a tensile test.

The test itself consists of putting a test specimen with a specific length of uniform cross section under axial load, often until it fractures. The length of a predefined section with uniform cross section is measured, and this section's length is constantly logged as the axial load increases. The axial load is also logged under the experimentation. To interpret the results, the load is plotted as a function of extension.

Stress strain curve

The cross section area can vary from specimen to specimen in a test, and the area might be several times larger for one test than another. The original length might also be much longer for

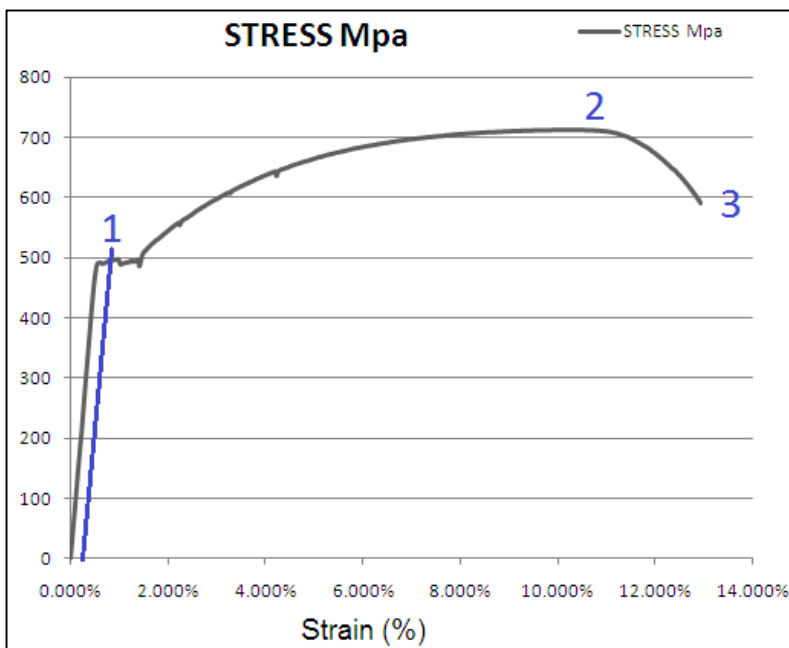


Figure 2.3.1-1 Example of stress strain curve. [23]

one test than for another. If load in [N] is plotted against extension [mm] the results of one specimen can't easily be compared with the result for another. To overcome this problem, the load is plotted as force per area, stress [MPa], and extension as extension per length unit original length [mm/mm]. A stress strain plot from a tensile test can look like the Figure 2.3.1-1 to the left. Note that strain is given in percent (100x mm/mm) in the figure. From the graph we can find different material properties

Note that stress is always calculated with the area of the original, pre test, cross section unless otherwise noted. This is because it is most practical for engineering purposes. In reality the stress is greater than displayed as the cross section is shrunk as the specimen is elongated.

2.3.2 Material properties

Young's modulus (E-modulus)

Young's modulus represents itself as the slope of line in the stress strain graph up to point 1 in Figure 2.3.1-1. This method is only valid for materials that have a fairly straight graph line in this region, known as the elastic region (see yield section below), of the graph.

For materials without a straight line in the elastic region, the following procedure is suggested [13]. The specimen is put under load up to and a little bit beyond the yield point, the load is noted and then relieved down to about 10%. When the load has reached 10%, it is reapplied slightly larger than before it was relieved. A line is drawn between the point of 10% load and load before relieved. The slope of this curve is the E-modulus.

Yield

The yield limit is the stress that, from and above, will permanently deform the material. Below the yield limit the material will return to its original form once the load has been relieved. Point 1 on Figure 2.3.1-1 is situated at the yield limit. For some materials there is a defined yield limit on the graph, like in the figure above, but some don't have an easily distinguishable mark. This has to do with the internal processes of the metal when it starts to plastically deform, to yield.

For materials without a clearly defined yield point, proof strength can be used instead. Proof strength is defined as the intersection between the stress strain graph and a line with the same slope as the E-modulus that is offset a known value from origin. The blue line below points 1 in Figure 2.3.1-1 is an example of this. The offset value is often given in % strain. 0.2% strain, corresponding to 0.002 mm/mm is frequently used. The proof strength with 0.2% strain would be noted as $R_{p0.2}$.

Ultimate Tensile Strength (UTS)

UTS is the largest load the specimen can handle before the load starts to decrease and the test specimen fractures. Point 2 in Figure 2.3.1-1 corresponds to the UTS. This is the largest load the material can handle and is important in an engineering perspective as yielding can be tolerated in some applications, but failure mostly can't.

Elongation

It is often of interest to know how much the elongation is at UTS and fracture (Point3 in Figure 2.3.1-1). This can be important for design purposes as some thing's purpose is to fail. The elongation is often given in % elongation, equal to % strain.

At UTS and point of failure/fracture the specimen is a spring under tension, and once the load is relived the specimen will contract just as an ordinary spring. The formula is used to calculate the unloaded, or plastic, elongation:

$$\%elongation_{relived} = \%elongation_{loaded} - \frac{Load^*}{E - modulus}$$

*Load is in stress [Pa]

The notation for plastic, relived, %elongation at UTS is A_g , and for fracture it is A .

For loaded % elongation A_{gt} is used for UTS, and A_t for fracture.

Cross sectional reduction

After fracture the smallest cross section is measured and the area calculated. Then the percentage reduction in are is calculated relative to the original, untested, cross sectional area. This is referred to as Z [13], or % Z .

Fracture surface

It can be of interest to know what mechanisms in the microstructure that fails, what causes the fracture. This can be investigated by inspecting the fracture surface. Fractograpy is not explained in this thesis, other sources should be sought out if insight or explanations are needed.

2.3.3 Test parameters

Speed of the test (Method)

The speed of the test is important for the result. If the test is done very slowly the internal structure of the material will have time to deform and distribute the load. On the other hand, if the test is performed quickly it won't be able to deform. This could lead to a fracture at much lower loads than if the test is performed slowly. For repeatability and scientific evaluation of the results from a tensile test, the way or method that the test is conducted is of great importance. There are two test methods, constant strain rate (A) or constant stress rate (B). For more reading, see chapter 10.3 and 10.4 in ISO 6892-1:2009 (or newer)

2.4 CharpyV

The purpose of a CharpyV impact test is to investigate the impact resistance of a material. This value can be anisotropic and has often a critical temperature where it will decrease significantly. This is useful information when performing material choices, especially for colder regions like the North Sea, Siberian, or polar regions. The fracture surface is also investigated to determine if the fracture is ductile or brittle.

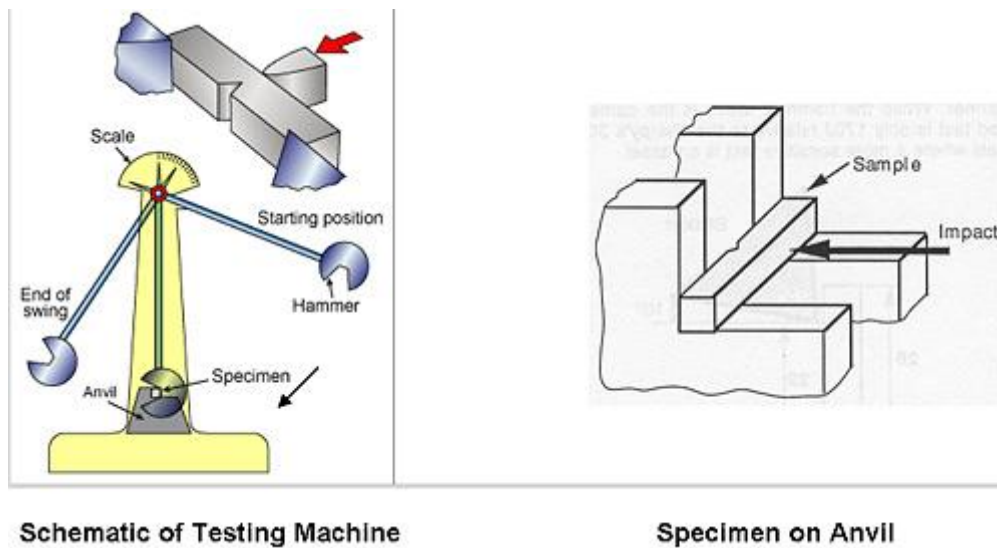


Figure 2.3.3-1 Presentation of Charpy-V testing [14]

The test is performed on a test piece with standardized geometry, 10x10x55mm. See section 3.3.1 for detailed geometry. A notch is made in the specimen with a V-shape, as seen in Figure 2.3.3-1 above. A pendulum hammer with a blade hits the specimen on the opposite side of the notch, and cleaves it in half, as seen in the figure above. Cleaving the specimen in half demands some energy, this is provided by the pendulum. This causes the pendulum to lose energy. A scale at the test machine indicates the energy absorbed by the specimen as a function of the angle of the pendulum after it has cleaved the specimen.

Other than the absorbed energy; type of fracture (ductile, brittle) and the fracture surface (fractography), deformation of the specimen (lateral expansion [15]), and transition temperature are properties that can be assessed. In this thesis the absorbed energy and its anisotropic nature, and the fracture surface is what will be evaluated. For further reading see ISO 148-1:2010 [15]

2.5 Vickers hardness test

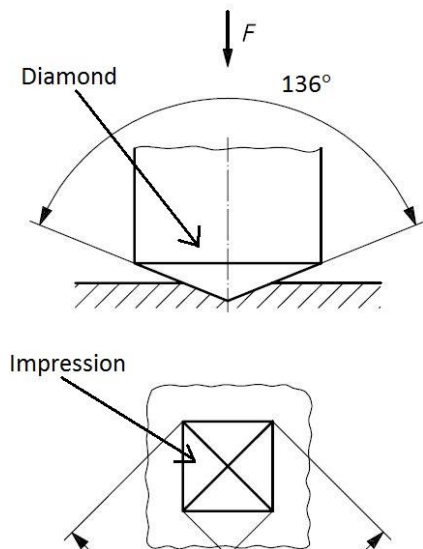


Figure 2.3.3-1 Vickers test illustrated [13]

Vickers hardness is a test to determine the hardness of a specimen. It is performed by pushing a pyramid shaped diamond down into the test specimen with a known force. See the upper part of Figure 2.3.3-1, This leaves an impression on the surface of the specimen. The two diagonals of the impression, d_1 and d_2 in the figure, is used to calculate the mean diagonal. The mean diagonal is used in the equation below to calculate the hardness value. The load is measured in kg and for 1kg load the test is designation is “HV1”.

The test time is also a parameter that can be of interest. The standard test time, according to ISO 6507-1:2005 [16], is 10-15s. If a test time outside of this range is used it shall be noted in the test report, see the example below.

$$\text{Vickers hardness} = \frac{w * \sin \frac{136^\circ}{2}}{d^2} = 0.102 * \frac{F * \sin \frac{136^\circ}{2}}{d^2}$$

w = test load in kg, F = test load in N, d = mean diagonal

Test result example for 350 Vickers hardness, 1kg load, and 20s test time:

350 HV1 /20

By varying the test load the impression size in a material will vary. This is useful to investigate different properties of the material. ISO 6507-1:2005 divides the load ranges into the three categories in Table 2.5-1 below. These categories are quite descriptive of their use.

Table 2.5-1 Vickers test load designations [16]

F [N]	HV [kg]	Designation
$F \geq 49.03$	$\geq \text{HV } 5$	Vickers hardness test
$49.03 > F \geq 1.961$	HV 5 to HV 0.2	Low-Force Vickers hardness test
$1.961 > F \geq 0.098$	HV 0.2 to HV 0.01	Vickers microhardness test

Since the surface is deformed when performing a test, it is important that the impressions is not done to closely together. This and other important test considerations are described, and parameters are given, in the test standard that you chose to follow.

2.6 Corrosion testing and pitting corrosion

Corrosion testing

Corrosion tests come in different categories for different purposes. Mainly there is two categories, to find the rate of corrosion, or to check if corrosion will occur. There are many different types of corrosion types, and many more corrosion environments. This calls for the results from the right test setup to be used for evaluation of a material for a specific job. Common parameters of a test are the state of the material (loaded? deformed? hardened? surface?), the temperature of the test, and the test atmosphere and composition (chlorine gas, salt water, etc.)

Pitting corrosion

Pitting is a localised corrosion attack that creates pits in the surface of the material. The process starts at a weak spot (dislocation, rupture in protective oxide layer, etc.), and creates an anodic pit with a cathode surrounding surface. See Figure 2.3.3-1 below. As corrosion continues the pit gets a high concentration of ions, leading to a very quick and aggressive corrosion attack. Because of the aggressive nature of pitting, it can cause material loss in critical areas and cause failures quickly. With a low total material loss and aggressive nature, it is hard to detect and catch via inspections. Pitting is therefore a type of corrosion that can't be allowed in critical applications.

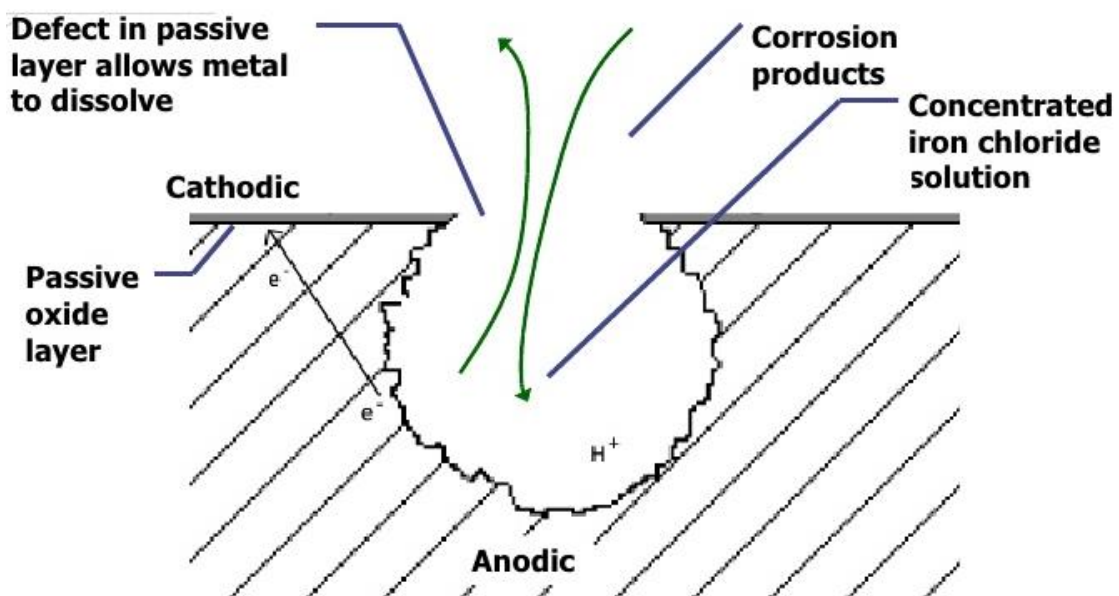


Figure 2.3.3-1 Illustration of pitting corrosion

Since the pitting starts at defects is important that the test surface is well documented. The best test is a worst case test where the specimen has no oxide layer and a rough surface where pitting can be started. A polished surface on the other hand can increase the pitting resistance.

2.7 Light microscopy

2.7.1 Introduction

Light microscopy uses photons with a wavelength in the visual spectrum, about 390 to 700 nm [17], or light as it is more commonly called. The specimen is lighted and the reflected light is sent through a series of optical lenses to achieve the wanted magnification. 200 nm is often seen as the limit to the resolution of a light microscope [18]. This has to do with the wavelength of visual light.

In a light microscope the colours of the specimen can be viewed. For a specimen with only one colour, different techniques can be utilised to distinguish different parts of the specimen. For metals etching, electropolishing, penetrating dye, and polarization filters are examples of methods used.

2.7.2 Thin film interference

In this thesis electropolishing has been performed. One of the results was a surface with different colours. One reason for the colours can be thin-film interference [19]. The effect appears when light hits a surface with a thin film on it. Some of the light is reflected off the surface of the film, but some goes through the film and is reflected by the surface of the main material. If the extra distance travelled by the light corresponds to $x.5$ times the wavelength of the light, the light will cancel itself out, see Figure 2.7.2-2. On the other hand, if it corresponds to x times the wavelength it will amplify the strength.

When white light, or multi wavelength light, is applied, one colour could stand out as its wavelength matches x times the extra distance travelled, while the other wavelength won't. See Figure 2.7.2-1 for an illustration. This is only an introduction, for further reading many online sources provide good in-depth explanations.

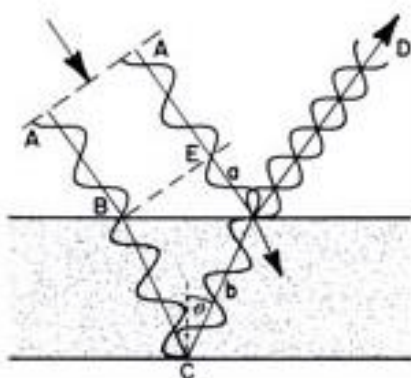


Figure 2.7.2-2 Thin film interference cancellation [27]

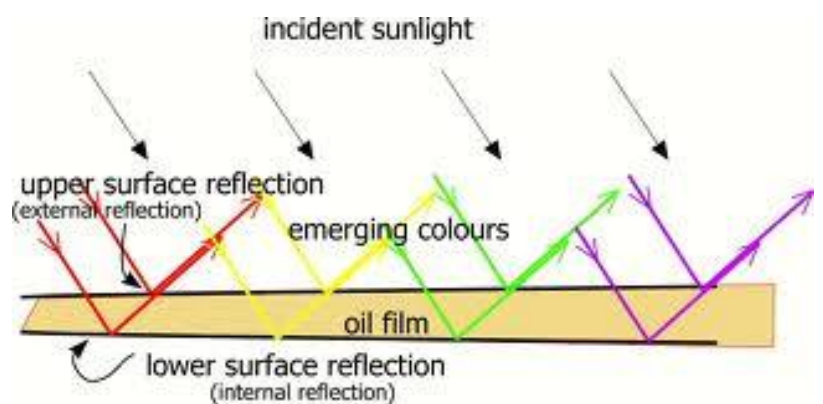


Figure 2.7.2-1 Thin-film interference varying thickness. [16]

2.8 SEM

This chapter is only a brief introduction to support this thesis. Good sources for further reading is available in books and online.

2.8.1 Introduction SEM

SEM stand for Scanning Electron Microscopy and is microscopy that uses electrons and detectors to inspect a specimen instead of light and the eye. Electrons, when in a high voltage acceleration field, can have a much lower wavelength than light (12.2pm at 10kV). This give a SEM a much higher resolution. The formula for the wavelength is displayed below [20]. This gives the SEM a possible resolution of less than 1nm, much finer than a light microscope. Another great characteristics of SEM is a much greater depth of field than light microscopy.

$$\lambda = \frac{h}{\sqrt{2meE}} * \frac{1}{\sqrt{1 + \frac{eE}{2mc^2}}}$$

λ = wavelength in m

h= planch = 6.626×10^{-34} J seconds

c= speed of light

E= acceleration voltage

m = electron mass = 9.1×10^{-31} kg

e= 1.6×10^{-19} electron charge

In a SEM electrons are sent through the microscope and down onto the specimen. Between the electron source there is an acceleration voltage, in this thesis 5-20kV. The electron beam is focused through magnetic field lenses, and aperture, to a cone shape which tip hits the surface of the specimen. The specimen has to be able to conduct the electrons that it is bombarded with. Inside the microscope there is a vacuum to avoid that the electrons collide with the atmosphere and not the specimen.

Through slight manipulation of a magnetic field working on the electron beam the beam is deflected to scan over the specimen just like your eyes scan over the lines of this thesis. Signals from one or more sensor or detector is used to generate a picture of the specimen. The signals are mostly used to create a grayscale image, meaning usually no colours, by simply using the signal intensity of the detector to decide the grayscale of each pixel. To increase the magnification, the beam simply scans over a smaller area of the specimen.

2.8.2 Signal generation

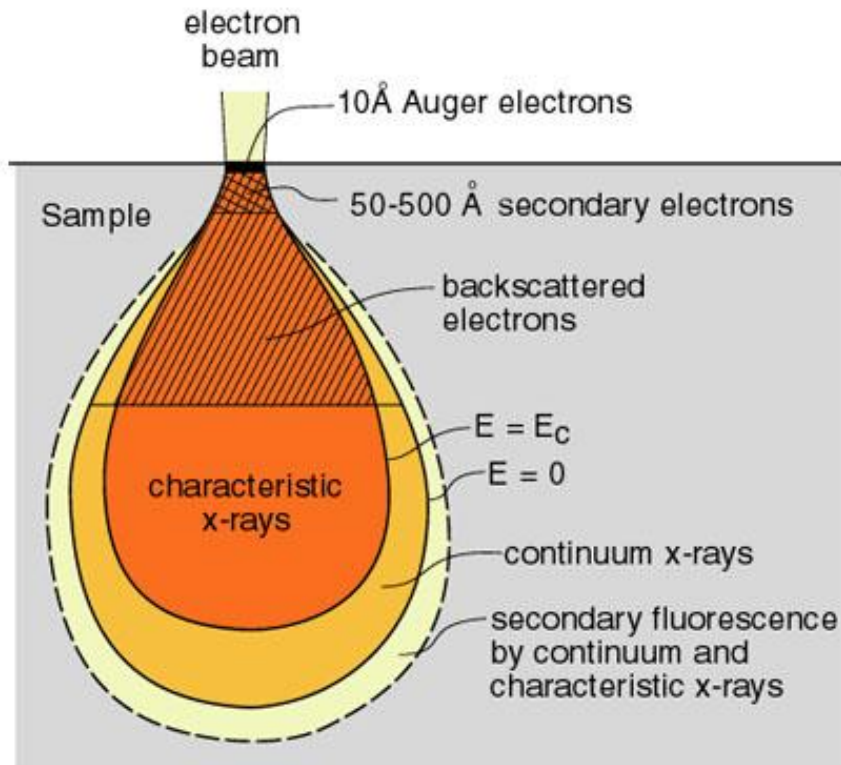


Figure 2.8.2-1 Emission volume SEM [29]

As the electron beam hits the surface it penetrates into the material, creating different kinds of signals as the electrons interact with the material, Figure 2.8.2-1. The electrons from the electron beam are called primary electrons. To an electron the surface of the material is not “solid”, but more like a dense bush to a baseball. It is important to notice from Figure 2.8.2-1 that the electrons are scattered when entering the material.

The depth and width of the emission volume is proportional to acceleration voltage and inverse proportional to the density of the material. It is important to be aware of this as this affects the real resolution of different analysis as EDS see 0. Formulas for estimating the emission depth “d1” and width “y” by Potts [21] p336-227 are listed below. Rajagopal, and for depth “d2” by Rajagopal [22] p162, p162, has another formula for the depth of the emission volume, “d2”, below.

$$d1 = E^{1.5} * \frac{0.1}{\rho} [\mu m] \quad y = E^{1.5} * \frac{0.077}{\rho} [\mu m] \quad d2 = E^{1.75} * \frac{4.28 * 10^{-10}}{\rho} [m]$$

$$E = \text{acceleration voltage in kV} \quad \rho = \text{material density [g/cm}^3\text{]}$$

The scattering of the electrons is either elastic or inelastic. In elastic scattering the speed and energy are nearly the same, but the trajectory of the electron changes. This is often backscatter electrons (BSE). For inelastic scattering some or nearly all of the energy of the electron is consumed by different interactions with the atoms in the material creating secondary electrons (SE), characteristic and continuous x-rays, photons, Auger electrons, and Cathodoluminescence (CL). In this thesis the focus will be on characteristic x-ray, SE, and BSE.

Characteristic x-rays are made when electrons that have been pushed to a higher electron shell by the primary electrons fall down again to its previous shell. Figure 2.8.2-2 The energy difference is emitted in a photon(x-ray) that has a characteristic wavelength for that specific jump electron shells in that specific element, making it distinguishable from those of other elements.

SE are electrons that have been shot out of its atom by a primary electron, Figure 2.8.2-2.

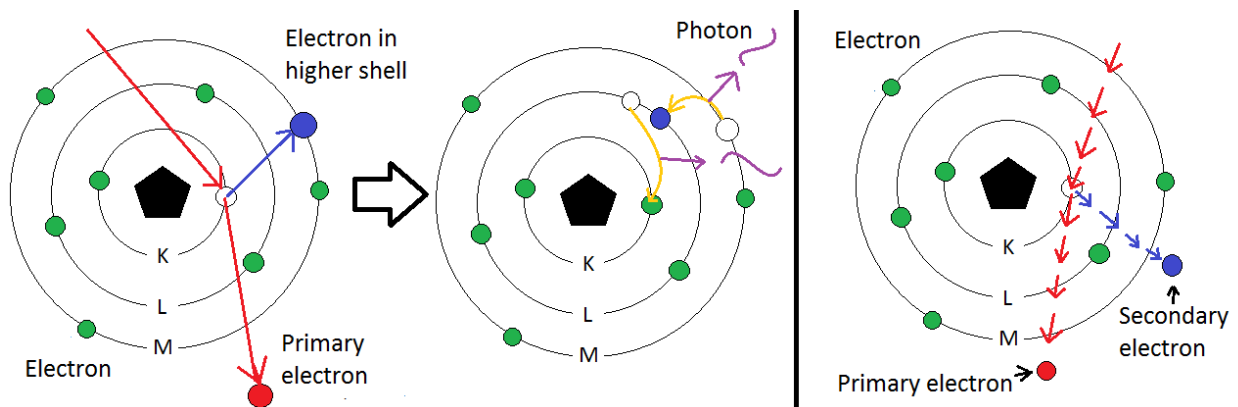


Figure 2.8.2-2 Creation of characteristic x-rays and photons (to the left), and secondary electrons (to the right)

2.8.3 SE

The SE detector is sometimes called the Everhart-Thornley detector, named after its inventors Thomas E. Everhart og Richard F. M. The detector consists of a scintillator material that the secondary electrons hits, this produces photons that are conducted through a light tube to the photomultiplier. In the photomultiplier the photon hits a dynode and electrons are emitted. These are accelerated against another dynode, emitting more electrons. This goes on for several steps until the electrons hit the anode at the end. The measures signal for the SE detector is the current to the anode. No or low current creates a black pixel and very high current gives a white pixel. To create photons, the SE electrons need to have enough acceleration voltage. To achieve this the scintillator has a bias voltage of 10-15 kV to accelerate the electrons. This bias voltage would interfere with the electron beam. To avoid this, a faraday cage is put around the scintillator to shield the electron beam. The faraday cage can also have a bias voltage to drag SE electrons into it.

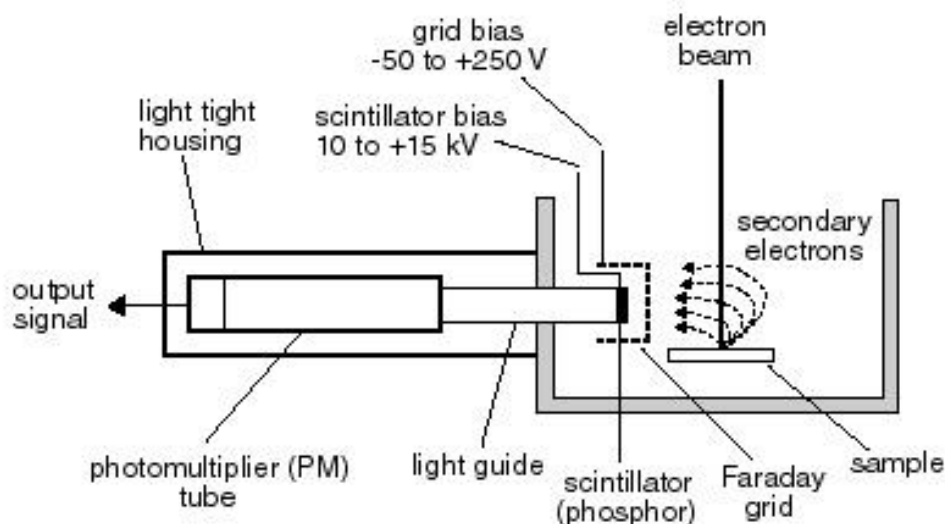


Figure 2.8.3-1 Everhart-Thornley (SE) detector illustration. [23]

Since the detector is located at one side of the electron beam, topography of the surface can cause some of the SE to not reach the detector. This creates “shadows” on the surface, making it a good detector to image the topography of the surface.

2.8.4 QBSD

The backscatter detector is located directly above the specimen, around the electron beam. In the case of the SEM used in this thesis, it is a QBSD, a 4 segment ring. See Figure 2.8.4-2. Each segment consists of a semiconductor Si(Li) (silicone doped with lithium). When electrons hit the detector, a small current travels between the two layers of the semiconductor. This current is amplified and used as the signal to draw the image on the screen.

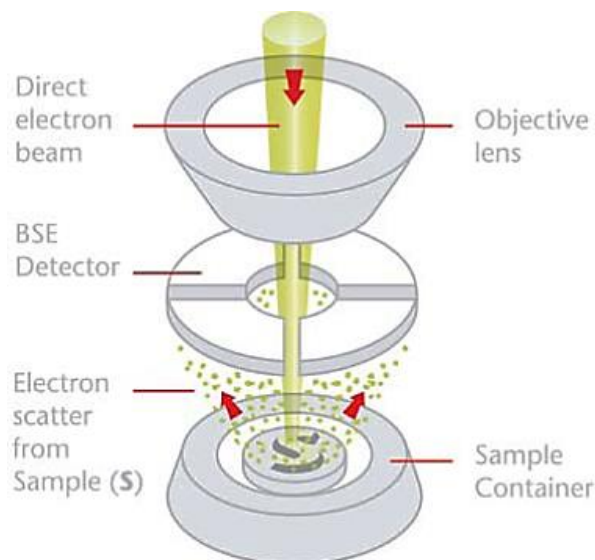


Figure 2.8.4-2 Backscatter detector illustration [33]

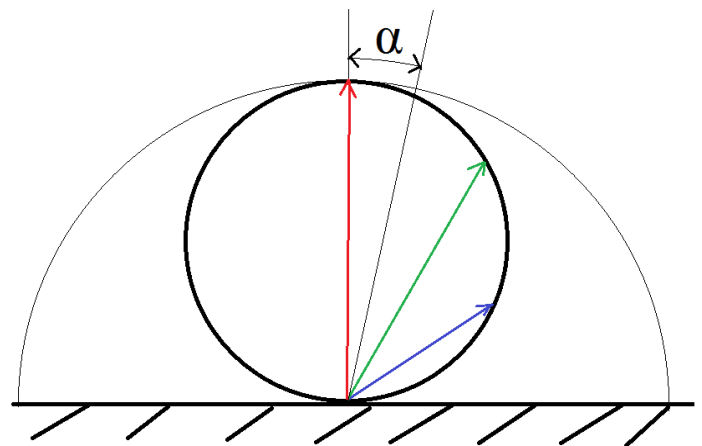


Figure 2.8.4-1 BSE angular intensity

The QBSD is located around the electron beam because the angular intensity distribution of the BSE, as seen in Figure 2.8.4-1. Directly above the specimen the intensity is greatest (red vector) but at an angle the intensity decreases (red and blue vectors).

The QBSD detector can be used to view differences in chemical composition in a material since the amount of BSE is related to the mean atomic number in the emission volume.

Since the detector is segmented into 4 individual pieces, each detectors signal can be added together to look at differences in mean atomic number, or one half of the detector can be subtracted from the signal of the other half (2 and 2 as there is 4 segments). The resulting signal is the difference between the two halves and can be used to image the topography of the specimen.

2.8.5 EDS

The x-rays from the emission volume can be analysed to get the elemental composition of the emission volume. This is done with an Energy Dispersive Spectrometer (EDS). The detector consists of a Si(Li) crystal that produces an energy burst proportional to the wavelength of the x-ray that hits it. The signal is amplified, and a graph is made with an x-axis of energy level, and a y-axis of intensity (number of times) of the different energy levels. This graph can be used to figure out the elemental composition of the emission volume.

The analysis can be performed in one spot to investigate a particle, etc., or with the electron beam scanning over a larger area to get the composition of the matrix of the material. It can also be used to map the differences in composition along a line, or to create a compositional map over the intensity of elements over an area. Maps and line analysis can give strong visual representations and visualise data making it easier to get a grasp of a complex compositional picture.

Finding the composition of the material is not as easy as just looking at the graph. First off it is important to have a high enough acceleration voltage to produce x-rays in the heaviest elements in the specimen. Then the different elements don't output equal amounts of x-rays and other factors make it necessary to do calculations to figure out the elemental composition. This is done with a ZAF analysis.

The Z stands for the atomic number and takes into account that heavier elements cause more of the electrons to backscatter, and the retardation of the electrons. A stands for absorption and compensates for the x-ray absorbed in the specimen before reaching the surface. F stands for fluorescence and compensates for x-rays from one element being able to be absorbed and produce more characteristic x-rays in another element. The ZAF analysis is an iterative process that converges towards a solution.

2.8.6 EBSD

Kikuchi-lines are a map telling the crystallographic orientation of a specimen. These can be found in specimen with ordered atomic structure like fcc and bcc metals. It is important that the surface of the specimen does not contain too many dislocations, if it does Kikuchi-lines will not be produced at the phosphorous screen as there is not enough ordered lattice structure to produce the diffraction. They are created continuously meaning that there is an image for every possible angle. See Figure 2.8.6-1 below for an example of Kikuchi lines.

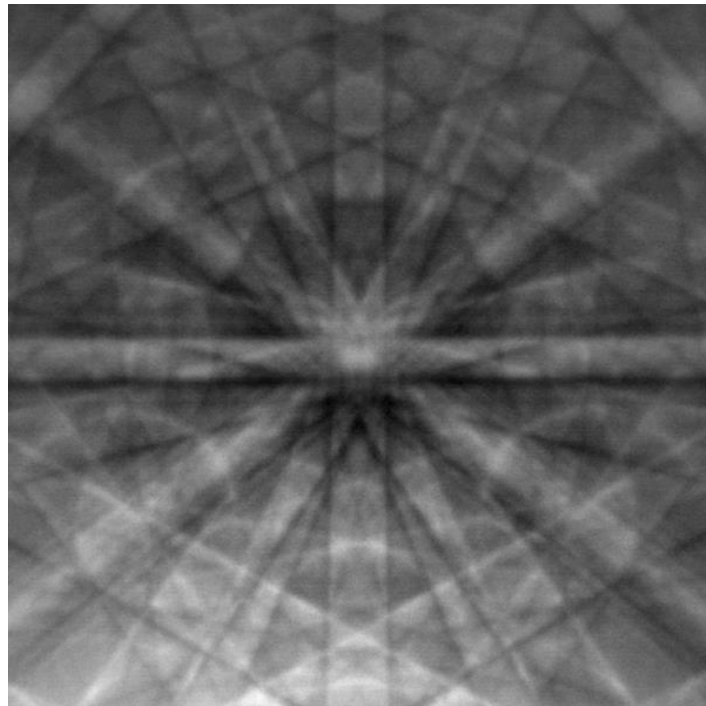


Figure 2.8.6-1 Kikuchi lines silicone [24]

In a SEM they can be found by tilting the specimen 70° towards a phosphor screen that is placed normal on the electron beam. A camera then films or photographs the phosphor screen to capture the Kikuchi lines. By scanning over the surface of the specimen and capture these Kikuchi lines, it is possible to map the crystal orientation of the specimen. This is useful to see if there is a preferred orientation, to be able to distinguish different grains, to measure grain size, etc.

3 Experimentation

This chapter explains the way the experimentation has been performed. The goal is to enable the reader to replicate the experiments performed, and evaluate the results presented in chapter 4.

3.1 General experimentation

This subchapter tries to provide information about the experimentation that don't fall correctly under any one of the experiments, is common to them all, or would be to sparsely presented to give any meaning.

3.1.1 Equipment

The equipment common for all the experiments is presented below.

Micrometre

The same micrometre was used for all the measurements in the experiments between 0 and 25mm. It is a Limit 9538-0101 micrometre with an accuracy of ± 0.004 mm, maximum parallelism deviation of $0.6\mu\text{m}$, and measuring range from 0 to 25 mm. The micrometre was bought specifically for these experiments and has not been used for other work, borrowed to other students, or dropped. When handled it was hold on the plastic protection to decrease the thermal inaccuracy caused by heat form the hands. No measurements were made on hot or corrosive specimens. The micrometre was always stored in its box.

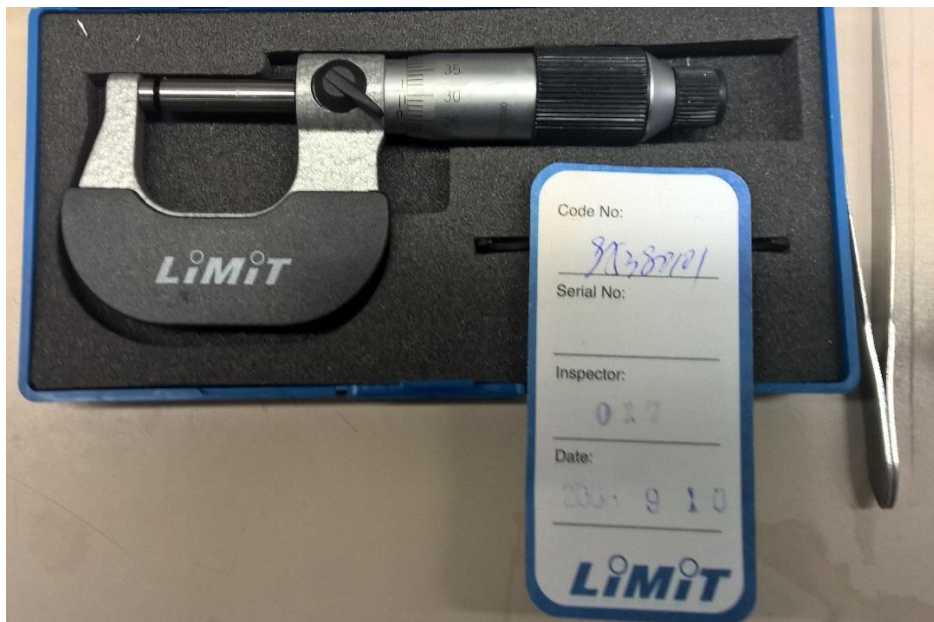


Figure 3.1.1-1 Micrometre used in the experimentation

Calliper

Only one set of callipers were used with an accuracy was $\pm 0.05\text{mm}$ when new.

Phone camera

Nearly all of the pictures in this report that was not taken by a microscope has been taken by a Nokia Lumia 1520 smartphone.

Leica MZ125

A Leica MZ125 was used to take some general surface pictures of the specimens and to document.

REICHERT-JUNG MeF3

The REICHERT-JUNG MeF3, was used for the more detailed light microscopy. The pictures themselves were taken with a JENOPTIC ProgRes STAR connected to a PC by FireWire and captured with ProgRes CapturePro 2.8.8 -JENOPTIC software.

SEM

Planopol

All polishing of the specimens were done with a Planopol with 300mm abrasive papers or felt discs. For some of the specimens a Pedemax-2 was used to rotate the specimens while they were polished. All polishing done were wet polishing.



Figure 3.1.1-2 Struers Planopol with a Pedemax-2.

3.1.2 Specimen handling

Having 43 test specimens in total being broken down into over 100 individual pieces throughout the experimentation demanded a strict system to avoid mixing up samples which could render the experimental data useless. The following system was put in place to achieve this. The specimens were stored in a wooden box with separate labelled compartments for each specimen, Figure 3.1.2-1, throughout the experimental testing and microscopy. Only the specimen(s) that were to be tested were taken out of the box. During an experiment one specimen would be taken out of the box at a time, tested/inspected, and then put back in the box before the next sample was taken out and tested. In the case were multiple specimens were taken out of the box, they were put in individual plastic bags and labelled appropriately. The only time this system broke down was with corrosion testing, see chapter 3.5.2 for more info.



Figure 3.1.2-1 Specimens in box after initial measurements

3.2 Tensile

3.2.1 Introduction

The tensile test was performed to investigate several areas of interest. The first and foremost the impact of printed vs machined surface on yield and ultimate stress on printed material. The second was to investigate the anisotropic properties of the material, and check if the yield and ultimate stress was within the specifications provided by EOS, Attachment 5. The test was performed according to NS-EN ISO 6892-1:2009 [13]. To test these properties 4 different specimens were needed.

The T, Y, and L specimens are oriented vertically, at 45°, and horizontally in the build chamber and will investigate the anisotropic properties. The U specimen are oriented vertically and will be machined to investigate the machined vs printed surface difference. See Figure 3.2.1-1 for specimen orientation. Specimen T was printed with the radius at the upper end going into a 45° chamfer since the printer did not support more than 45° overhang, Figure 3.2.1-2.

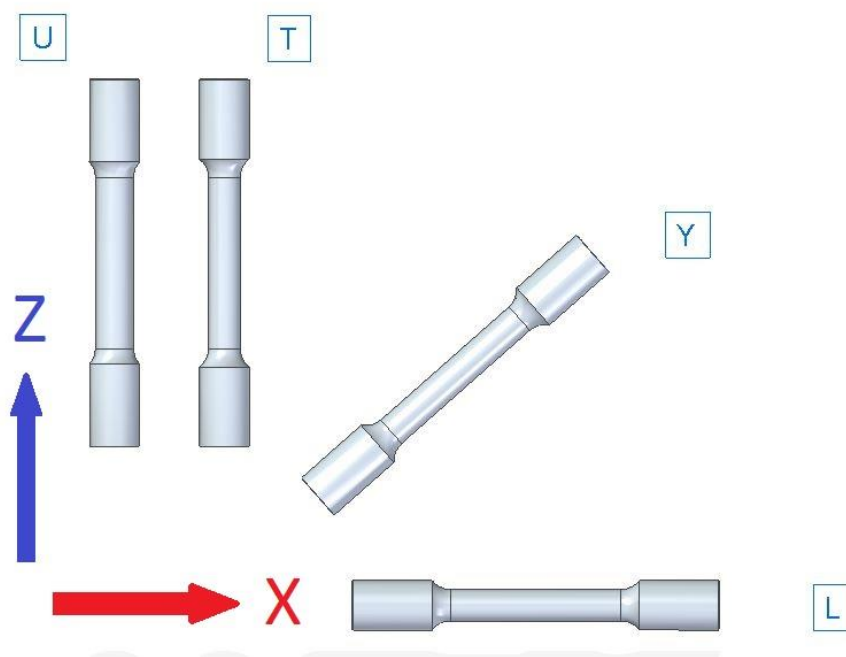


Figure 3.2.1-1 Orientation of the different specimens in the printing chamber. U and T specimens printed vertically, Y at 45°, and L horizontally in the printing chamber.

Each specimen had its type letter engraved into its end. This made it possible to distinguish the specimens, and the letters made it possible to know the orientation the specimen had in the printing chamber. Knowing the orientation could be useful since it enables an investigation in the effect of the brushing direction. This is not done in this study, but others might use the material and investigate it further in the future.

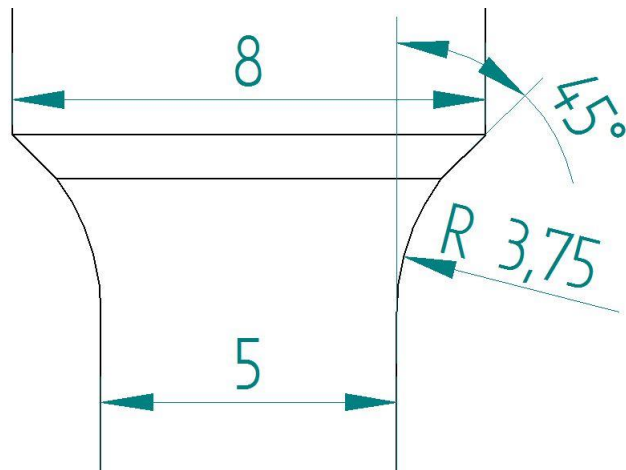


Figure 3.2.1-2 Top profile of T specimen. The 45° angle towards the end is necessary because of the overhang limit of 45° of the printing process.

Because of the high cost of printing larger test specimens, the smallest specimens given in Table D.1 in the standard [13] was chosen. Using threaded ends reduced the length of the tensile specimens down to 60mm and gave the following profile, Figure 3.2.1-3.

Test specimen geometry

- Diameter of reduced cross section - 5 mm
- Original gauge length - 25 mm
- Length of reduced cross-section - 28 mm
- Radius tangential to reduced cross-section - 3.75 mm
- Diameter of ends - 8 mm
- Threads on ends - M8x1.25

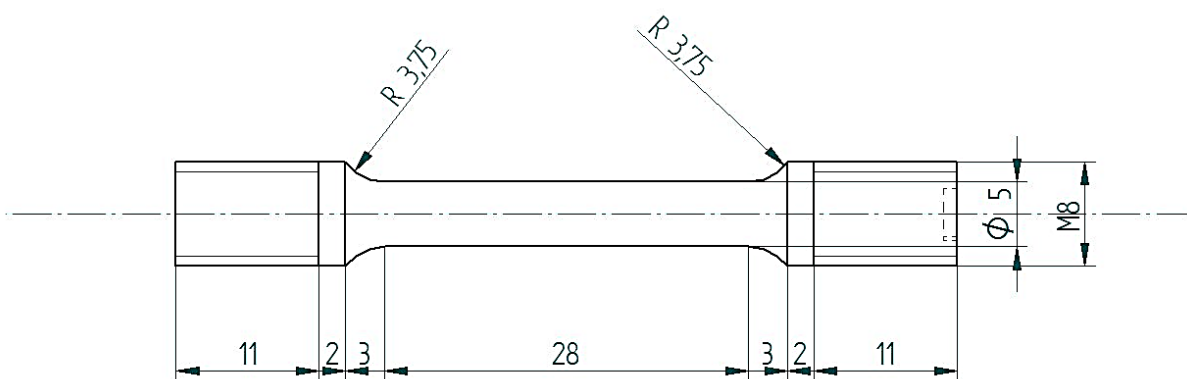


Figure 3.2.1-3 Tensile test profile

3.2.2 Preparation

The specimens were received and measured as described in chapter **Feil! Fant ikke referansekinden..** Comments and pictures of the specimens can be found in section 4.1.

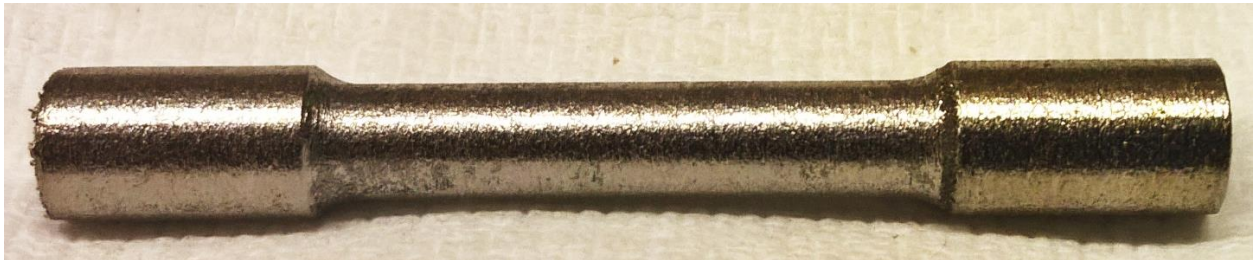


Figure 3.2.2-1 Specimen U1 before machining. Notice the golden discoloration on the top (right side), as discussed in chapter 5.1.2.

Machining of the specimens

The specimens were printed without the threads and the profile of the U-specimens needed to be machined. This was done on a CNC-lathe, an Okuma LB9 with a OSP500L controller, at UIS. Machining of the specimens were a three step process. This required some G-code files, all included in Appendix 1. First a centre hole was drilled in each end using “SS5M8P1.MIN”. This was done to allow for the tailstock to support the specimens. Then the U specimens were machined down to the profile given in Figure 3.2.1-3 by “SS5M8P2.MIN”.



Figure 3.2.2-2 U-specimen after “SS5M8P2.MIN”. The profile has been cut and one end threaded.

This operation did also cut the threads on the tailstock end, Figure 3.2.2-2 On the other specimens “SS5M8P3.MIN” were used to cut the threads at the end as the profile had already been printed. The specimens were then turned around and “SS5M8P3.MIN” were used to thread the other end.

During the threading of specimen L3 the cutting tool broke on both occasion and put heavy torque on the specimen, thus twisting it and ruining the specimen. The other specimens were inspected for similar damages, but none were found. After machining, the diameter of the U-

specimens was measured. The profile was slightly conical, and out of spec according to the standard [13]. Further work was done on a manual lathe with a fine file and abrasive paper. This made the profile cylindrical enough to pass inside the standard. New measurements were made and noted, attachment 6.



Figure 3.2.2-3 U-Specimens after finished machining.

3.2.3 Testing

Testing was performed on an Instron 5985 with an Instron AUTOX 750 extensometer at UIS. Special mounts were made with M8 threads to accommodate the specimens to give them enough grip to performed the test. One mount was fastened in the bottom clamp in the machine. A specimen was mounted and used to square and centre up the mount to achieve an as purely uniaxial test as possible. Then the other mount was fastened on the top of the specimen. The machines extensometer was brought in position and adjusted for each specimen to make sure that the extensometer measured on the reduced section. After adjusting the extensometer, the top clamp was brought down into position around the top mount, but not tightened. The machines sensors were balanced/nulled out, and then the top clamp was tightened. Figure 3.1.1-1 shows a specimen mounted and ready for testing.



Figure 3.2.3-1 Specimen U1 mounted and ready for testing. Extensometer in place and specimen fastened in mounts.

A test method was set up in the computer control software BlueHill3 together with the lab engineer. An expected E modulus of 140GPa was entered into the method file as this was the stated in EOS's specs (attachment 5). Constant strain rate was used and a strain of 0.02mm/s for the first 2 seconds, and then 0.2mm/s was used. The strain rate was measured with the extensometer. Each the specimens were tested in turn, U, T, Y, and L-specimens. One specimen was taken out of the box at a time, mounted, and tested. After testing each part of the tested specimen were put in its own bag, marked, and put back in its place in the wooden box. This to prevent mix-up and to protect the fracture surface from grinding against the other half of the specimen.

The test data was logged by the Bluehill3 software and stored in a test file.

3.2.4 Post-test inspection

After the test was completed the measurements from all the test specimens were exported in a pdf file. The information in this file was not enough to draw proper conclusions, and the raw test data was exported to .csv files, and worked in MATLAB to better investigate the tensile properties. The specimens were examined by eye and the Leica microscope (chapter 3.1.1).

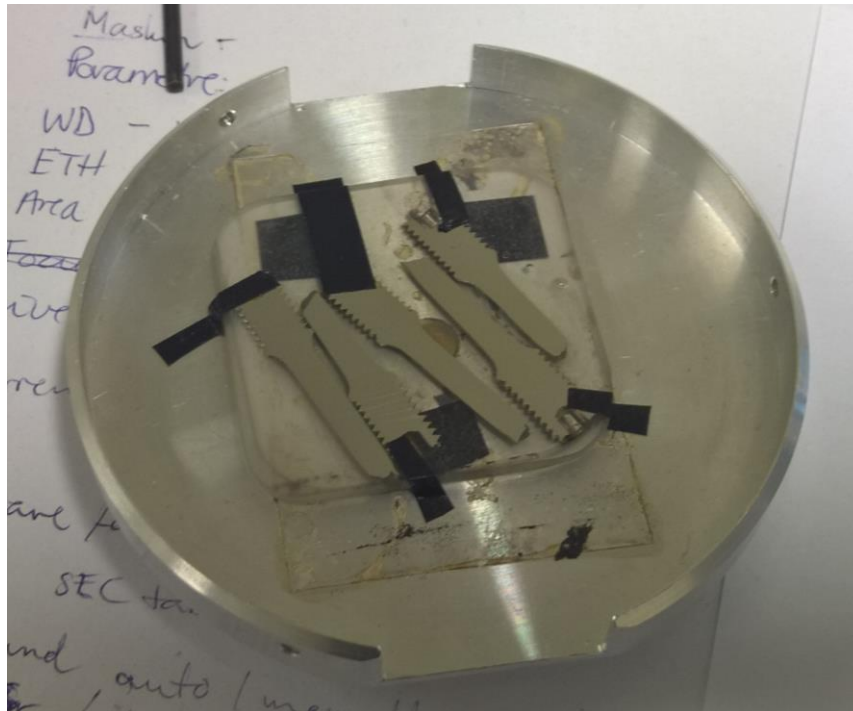


Figure 3.2.4-1 Tensile test ready for SEM. The specimens had been grinded in half after being encased in epoxy.

The fracture surface was inspected with the Leica light microscope and the SEM. To inspect the specimens axially in the SEM, specimen U2, T2, T3, Y2, and L3 were cast into epoxy and grinded down with 80grit abrasive paper until they had been cleaved in half. When the specimens had been cleaved they were grinded stepwise by 200 – 500 – 1200 – 2000grit abrasive paper, and 9 and 1 μ m diamonds at a polishing felt disc. The specimens were cleaned between each grit to avoid grit contamination. The polishing and grinding was done on the Planopol while holding the epoxy block manually. This was considered the easiest way available to cleave them in half without further deformation of the specimens.

Carbon double sided tape was used to mount the specimens in a holder for the SEM, and to establish electrical connection between the specimen and the base of the machine as seen in Figure 3.2.4-1. Both the Backscatter and Secondary Electron detector was used to inspect the specimens. Imaging near the edges proved hard because of the epoxy encasing.

3.3 Charpy V

3.3.1 Introduction

Charpy testing was done on the material since there were no data in the material data sheet from EOS (attachment 5), and no other studies on the toughness of AM Alloy 625 were found. It is of interest to know these properties for mechanical design, and consideration of the suitability of the material for certain operations. Effects of printed surface vs machined was also investigated. A Charpy V-notch test was performed according to NS-EN ISO 148-1:2009 [15] as it is a commonly used standard and notch type, and the university has equipment to perform it. A standard test specimen of 10x10mm was chosen since it gives better test data, and the width of the specimens did not have such high impact on the price as the length. The rest was performed at room temperature in agreement with FMC.

The α and I specimens were printed with a cross section of 10.1x10.1mm to allow for the specimens to be a little bent after production because of stress build-ups, and production tolerances. The β and II specimens were printed with a cross section of 11x11 mm to allow for proper machining and avoiding any surface effects from the printed surface to be present.

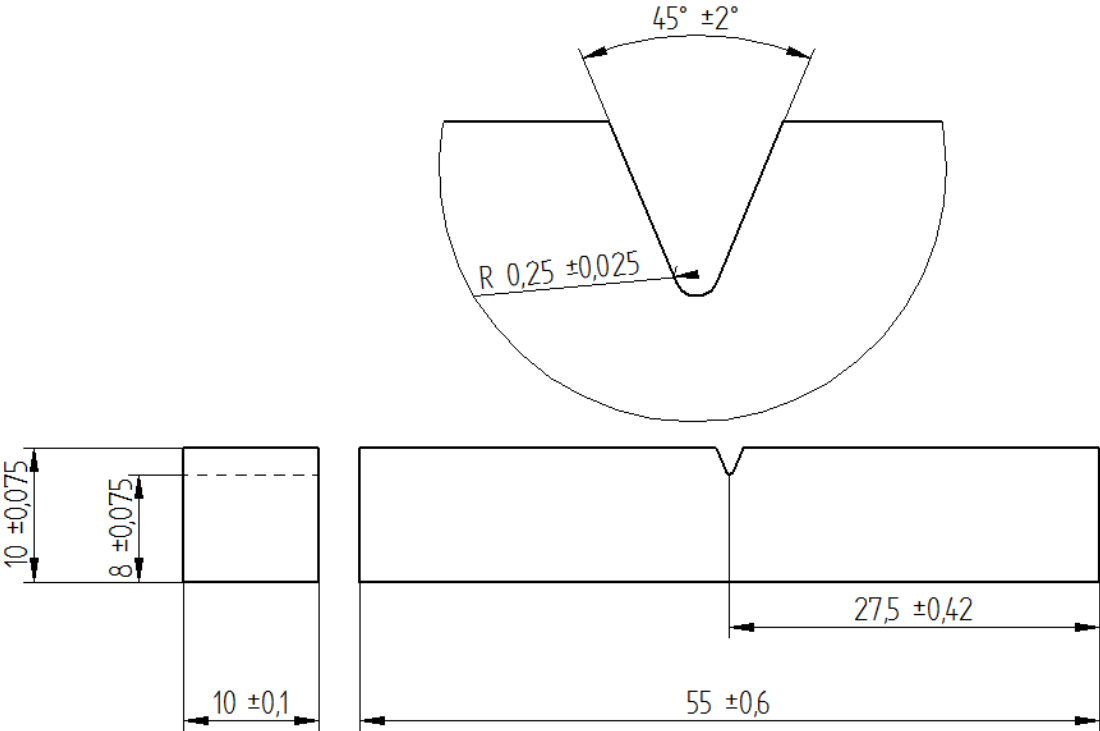


Figure 3.3.1-1 CharpyV geometry for standard test specimen. Measurements in mm. Generated from Figure 2 and Table 2 in NS-EN ISO 148-1:2009 [15].

5 specimen orientations were chosen for machined notch, and 4 for a printed notch. printed. The orientations can be seen in Figure 3.3.1-2 below. S specimens are printed vertically, A at 45°, and L horizontally. The specimens with a single line I or _ has a printed surface, while the specimens with double lines II og = was printed without the notch and machined down to size. L_ was not made as there was concerns that it would crack because of the internal stress in the specimen while being printed. This could have caused the printing powder to be unevenly distributed and ruined the whole print plater with all the other parts too.

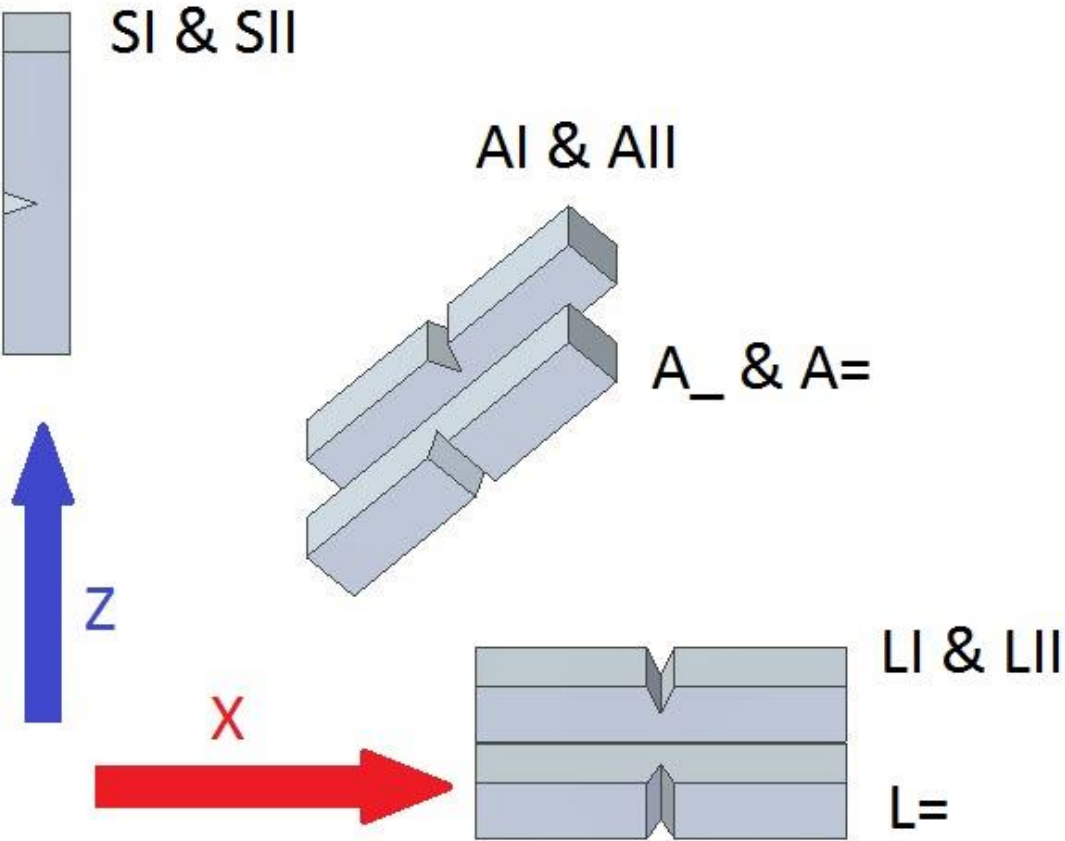


Figure 3.3.1-2 Orientation of the Charpy test in the printing chamber.

The reason for the _ and = specimens are to investigate if there is differences in which way you cleave a specimen relative to its layers. The material data sheet, attachment 5, and the manufacturing technique states that the material is anisotropic. This could cause differences in the way the material is cleaved. The reason no S_ and S= specimen is made is since the cleaving path through the printed layers is the same as for SI and SII.

3.3.2 Preparation

Machining

The standard calls for tight tolerances, Figure 3.3.1-1. Because of this care had to be taken when machining the specimens. Adding in that heating the specimen during machining, and work hardening would alter the results, grinding was chosen as the machining technique.



Figure 3.3.2-1 Face milling off support structure on CharpyV-specimen.

A mill with a surface-mill was used to remove support material from the specimens. This was done with adequate cooling to avoid any heat build-up as Alloy 625 is quite tough to machine and the mill had somewhat worn inserts in it before the machining started. Even though the support structure is very porous it had no problem to turn the inserts into shreds. This was an important first hands-on lesson in how hard this material can be, and that you have to respect the ridiculously low cutting speed that is advised.

To remove some of the support material on the end of the specimens a Struers Discotom-16 was used. The removed pieces were bagged in case a study in them would be of interest. The smaller pieces of support material were removed by a belt sander. The specimens were regularly dipped in water to avoid heat build-up. When the support material had been removed/ reduced considerably in thickness the specimens was grinded down to size in a surface grinder with a magnetic table.

To hold the specimens that are not magnetic, in the surface grinder, a special vice was made. The vice consisted of a base in S355 and grips in an unknown aluminium alloy. Both the top and bottom surface of the vice was surface grinded. Before grinding the specimens, the body of the vice was mounted on the magnetic table and grinded flat. This way the surface of the vice was parallel to the surface grinded, in other words the specimen could be grinded parallel to great precision. Grooves in the vice allowed for measuring the thickness with the micrometre while the specimen was still mounted in the vice.

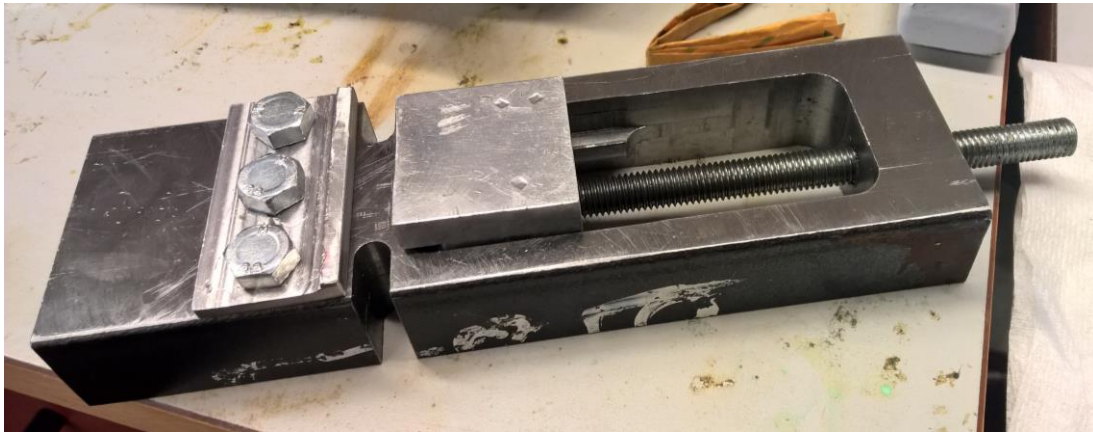


Figure 3.3.2-2 Vice used to grind the CharpyV specimens.

When a specimen was mounted in the vice it was first the surface of the vice was cleaned. Then the specimen was placed in the vice, and it was hand tightened. A piece of aluminium was put on top of the specimen and a hammer was used to make assure that the specimen rested on the surface of the vice. The vice as then carefully tightened with a wrench.

The specimens were grinded down in 0,02mm steps to avoid heat build-up. For the A and L specimens the top printed surface was first placed down in the vice, then the surface was grounded down until all the support material had been removed. For the I and _ specimens grinding was stopped when the surface on the other side of the V-notch was free of support structure. These specimens had very little material to remove and was nearly to small when delivered. Then the specimen was then deburred, and the ground surface put down in the vice and grinded until measurements was inside the tolerance and close to 10mm. The micrometre was used to take the measurements. The specimen was then deburred, turned 90° and the sides grinded down to size. See Figure 3.3.2-3 for the grinding setup. Coolant was used throughout the process and the specimen was regularly touched to control that I did not get warm.



Figure 3.3.2-3 Grinding setup for a Charpy specimen

When all the specimens had been grinded they were measured, see attachment 6. To control the radius of the printed V-notch, all the _ and I specimens were inspected in the Reichert-Joung (section 3.1.1) microscope. The support material in the notch on the SI specimens was roughly removed with a hack saw while keeping good distance from the specimen. The radius of the specimens was not written down, but some pictures were taken, Figure 3.3.2-4. All the radiuses were within the tolerance of the standard, and the SI specimens did not show any damages from the hack saw.

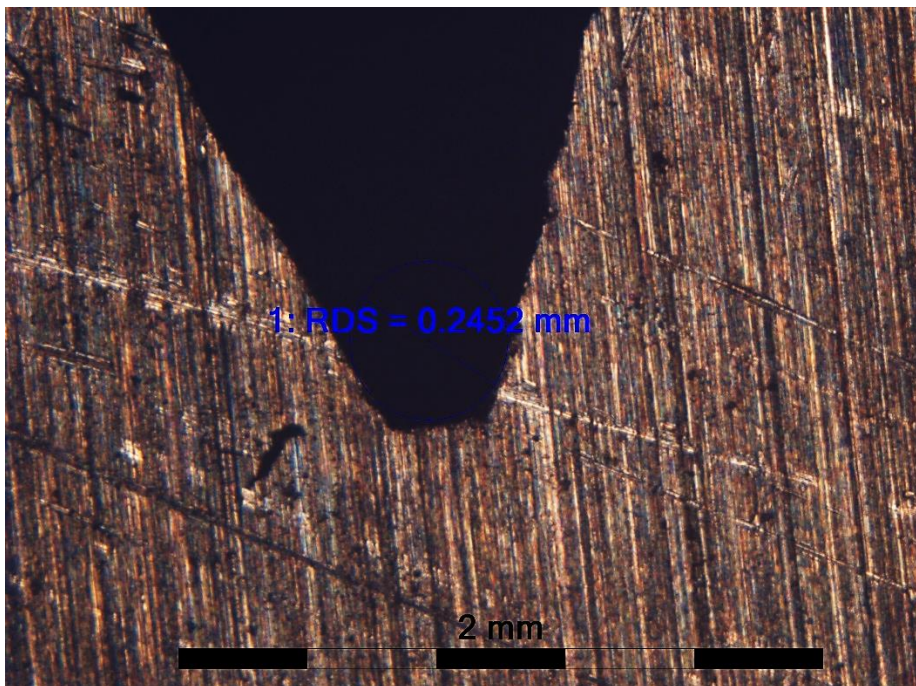


Figure 3.3.2-4 Control of printed V-notch radius. Specimen LI 2 with a radius of approximately 0,245mm, well within the tolerance.

A broaching machine was used to create the V-notch on the II and = specimens. The specimens were first marked to indicate what side should be broached. Before putting a specimen in the broaching machine the broach was cleaned with a soft steel brush, and the vice where the specimen would be placed was cleaned with a small painting brush. Then the specimen was put in the vice, and the vice as tightened. A guard was put in front of the broach and the machine was started. After the broach had made the V-notch, the specimen was removed from the vice before the broach was lifted back up. Then the guard was removed, and the broach and the vice was cleaned before the next specimen was machined.

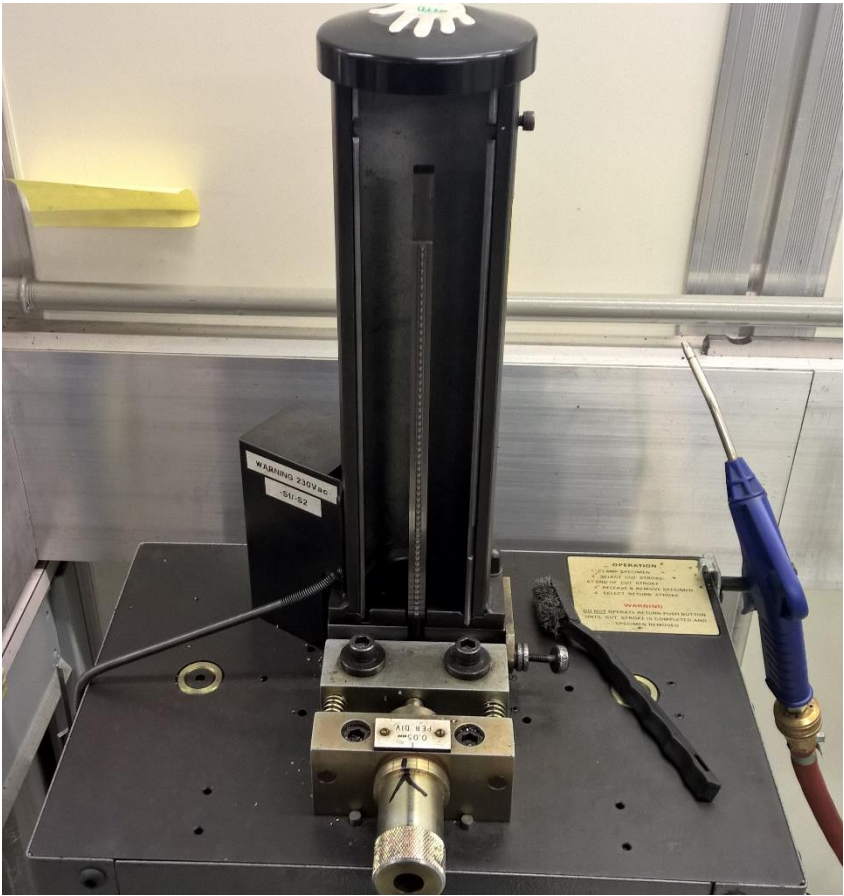


Figure 3.3.2-5 V-notch broaching machine.

There were some problems with the broaching machine that made it stop in the middle of the cut. The broach was then stuck in the specimen, and the machine would not continue the cut. Since lifting the broach back up again using the machine could damage the broach and the specimen, the screw mechanism, that drags the broach through the workpiece, was manually turned backwards until the specimen could be removed from the vice. The broach was then lifted up again, cleaned together with the vice, the specimen put back in the vice, and the cut was made again. The problem was not new, but lead to it taking 6 hours to make the V-notch in 27 specimens.

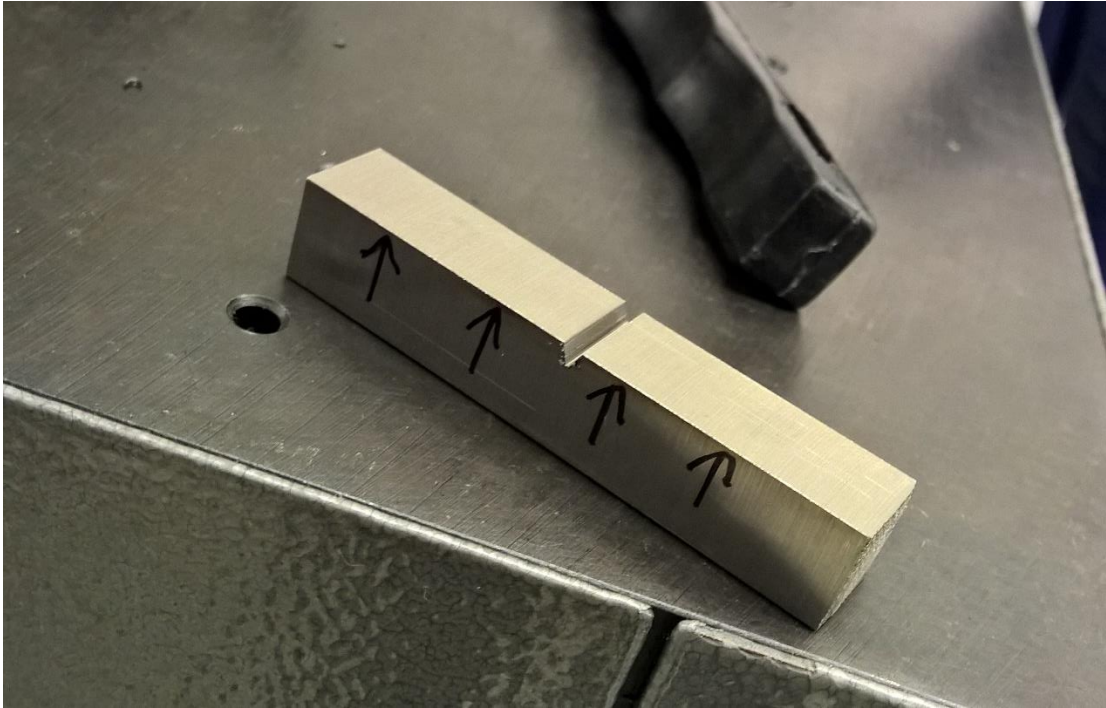


Figure 3.3.2-6 CharpyV-specimen after broaching. Specimen SII 1.

After the V-notch had been made the radius of the first, one in the middle, and the last machined specimen was studied in the Reichert-Joung microscope. All showed a radius inside, but on the lower end, of the tolerance as seen in Figure 3.3.2-7

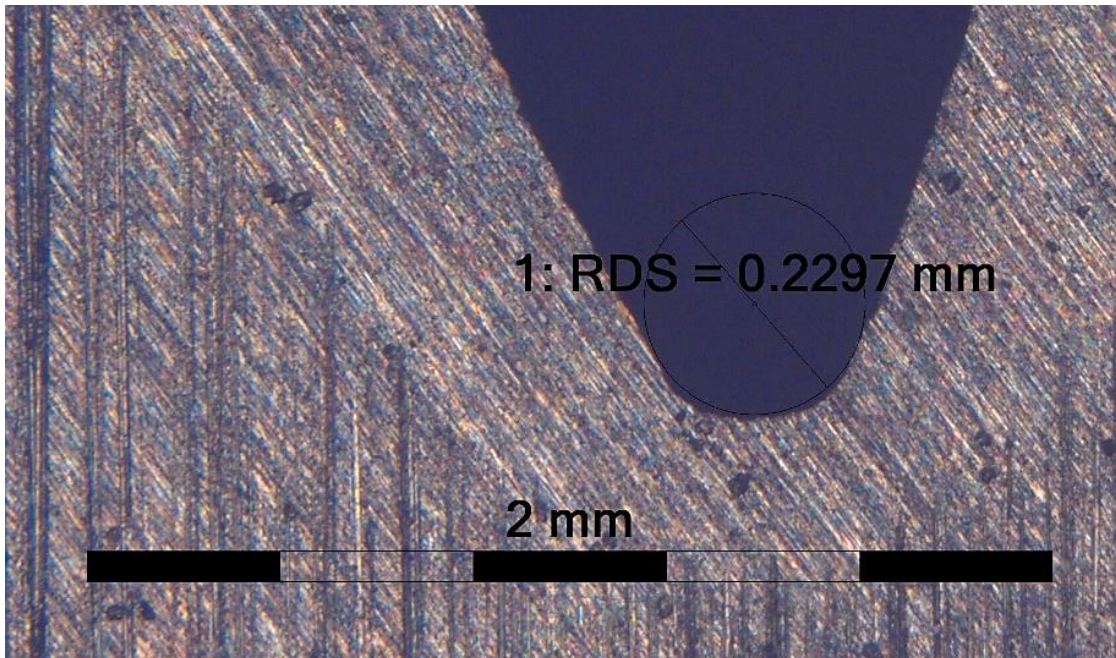


Figure 3.3.2-7 Control of broached CharpyV radius. Specimen AII with a radius of about 0.23mm within the tolerance of the standard, but close to the lower limit, 0.225mm.

3.3.3 Testing

Testing was performed on a Zwick / Roell RKP450 (capable of 450J), at UiS, with an analogue(clock) and digital readout. Both the analogue and digital values were noted. Placement of the specimen is crucial to the absorbed energy. A self-centring tong was used to ensure correct placement of the specimen, similar but not equal to those in Annex A in the standard [15]. To avoid ruining a EOS 625 specimen, training with test specimens in construction steel was done. When 5 consecutive test with construction steel showed an equal (± 2 Joule at 155J mean) value, testing of the EOS 625 specimens began. Since the test was to be performed at room temperature, there was plenty of time to reposition the specimen until it was in the right spot.



Figure 3.3.3-1 Specimen being placed in the testing machine with a self-centring tong. The wedge in the tong centres the specimen in the correct position relative to the wedge on the pendulum.

When a specimen was tested, first the analogue scale was reset, then the specimen was placed inside the machine with the use of the self-centring tongs, and then the machine was activated. The specimen was cleaved and both the analogue and digital readout was noted. The specimen parts were collected and bagged in new plastic bags with a subscript S for the piece with the specimen writing on it, and F for the one without engravings. No real important reason to do this was found at the time, but a reason might come around later that would make it interesting to be able to distinguish the two from each other. After bagging the specimens and putting them in the wooden box, the next specimen was tested.

All the specimens were cleanly broken into two parts, with the exception of AII 1 that was broken into two separate pieces but still got stuck together because of the lip of the fracture surface. AII 1 was still considered a clean fracture not a hinge since it was physically two parts.

3.3.4 Post-test inspection

The results from the test were plotted into a spreadsheet program and the mean value and the standard deviation was calculated. For the test results were one specimen had a significantly higher value than the other two, a new mean was calculated without this result. This was because the result probably was higher because of a small error in placement of the specimen in the test machine. The results can be viewed in section 4.3.



The fracture surface was inspected visually, by the Leica microscope, and in the SEM to determine the type of fracture (ductile or brittle), and other details.

3.4 Vickers hardness test

3.4.1 Introduction

The Vickers hardness test was performed after NS-EN ISO 6507-1:2005 [16]. The goal was to investigate if there was a difference in hardness from the printed surface and further into the specimen. Testing was done on a Struers DuraScan hardness testing machine. Specimen LII 3 S, LII 3 F, and SII 3 S was chosen.

LII 3 S and F investigates the printed “edge” surface from top(S) and the side(F). SII 3 S investigates the printed “top” surface from the side, and SII 3 F investigated the surface with support material. See Figure 3.4.1-1 for illustration.

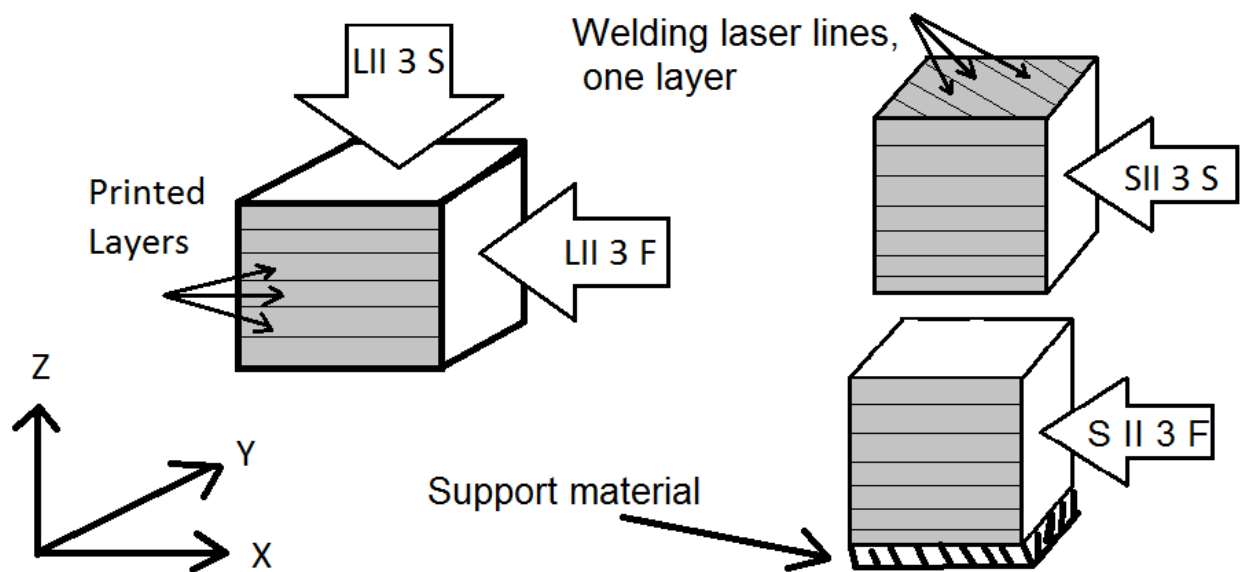


Figure 3.4.1-1 Illustration of Vickers test specimen surface

The standard [16] sets the following demands for the test:

- The mean diagonal should not be below 0.020 mm
- The distance between indentation centre and the edge of the specimen must be greater than 2.5 times the mean diagonal
- The distance between the centres of two indentations shall be at least 3 times the largest mean diagonal of the two indentations.
- The difference between the two diagonals shall not be greater than 5%
- The indentation shall be between 25 to 75 % of the width and height of the screen.

3.4.2 Preparation

The specimens were mechanically grinded and polished stepwise up to a finish of 1 μ m as a step in the preparation for SEM-microscopy, see chapter 3.6.2. This surface was used for testing.

3.4.3 Testing

Specimen LII 3 F was the first to be tested. This would test differences in hardness near the printed surface of the side of a part, and measured from the side. A load of 1kg, HV1, was used on the middle of the specimen to measure the diagonal and thus finding the distance from the edge and between the indentations. Then a test series of 15 indentations along the edge x 7 rows inwards was performed. See Figure 3.4.3-1 below. A similar HV1 test series was done on specimen LII 3 S, but with 5 indents per row instead of 15.

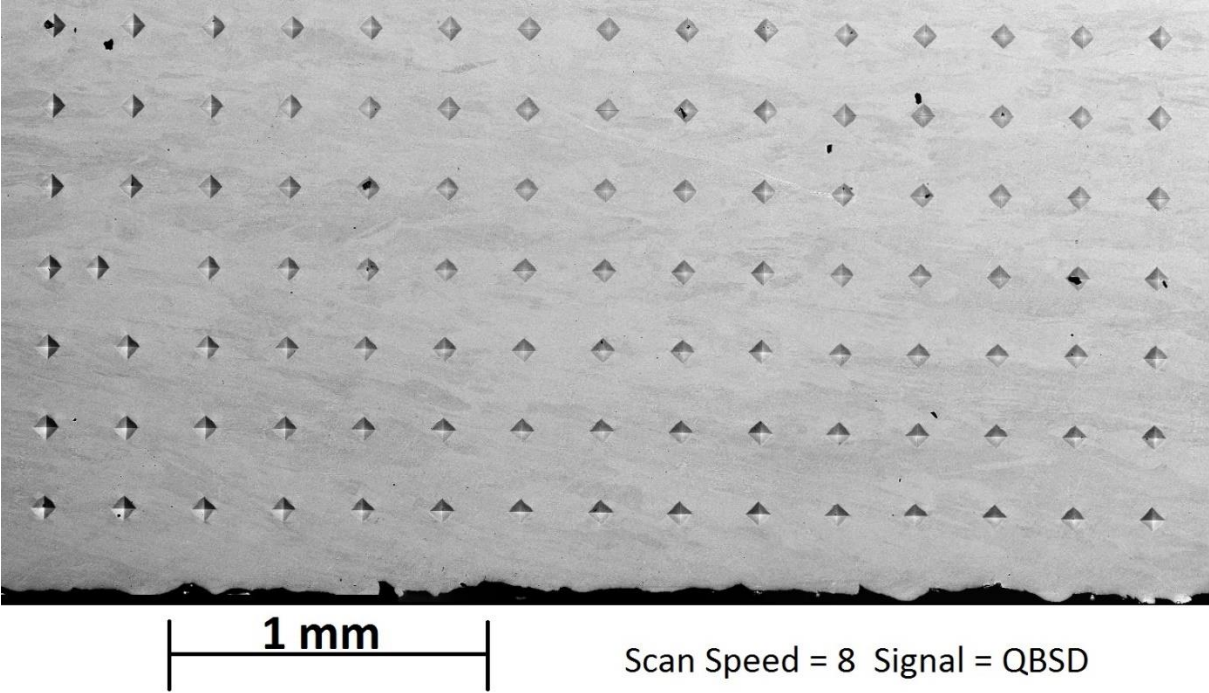


Figure 3.4.3-1 HV1 idents on Specimen LII 3 F.

HV1 tests gave inconclusive results, see chapter 4.4. To increase resolution the test load was lowered. The smallest load that still gave an impression filling over 25% of the screen was 0.1 kg, or HV0.1. All specimens were tested with the new test load.

To check for hardness variations caused by the polishing process, a series of 5 HV5 tests were performed on all specimens.

3.4.4 Post-test inspection

After the testing was done the data was processed in Matlab. The indents were inspected in the SEM while the work described in section 3.6 was performed.

3.5 Corrosion

3.5.1 Introduction

The purpose of the corrosion test is to confirm corrosion resistance of ALLOY 625 after being 3D-printed. The test was according to Norsok M-630 6:2013. [25] which, with a couple of additional specifications, refers to ASTM G48 Method A [26] The specifications call for the given preparation, testing, post testing, and acceptance criteria:

Preparation

- Surface finishing with 120grit or finer abrasive paper [26]
- Pickling with 20% HNO³ + 5% HF for 5 minutes at 60 °C [25]
- Weighting with a scale better than 0.001g resolution [26]
- Measuring of surface area [26]

Testing

- 600ml of 6w% FeCl₃ solution per test specimen [26]
- Temperature of 50°C [25]
- 24 hours' test [25]

Post testing

- Pickling with 20% HNO³ + 5% HF for 5 minutes at 60 °C [25]
- Weighting with a scale better than 0.001g resolution [26]
- Inspection of surface with 20X magnification [25]

Acceptance criteria

- No pitting at 20X magnification [25]
- Less than 4.0g/m² weight loss [25]

All of the specifications were followed with the exception of the pickling that was not performed.

3.5.2 Preparation

The test specimens were made from the tested Charpy-specimens LII_2_F, AII_2_F, and SII_2_F. Originally only the L and S specimens was planned, but enough solution as mixed, as explained on the next page, for 3 test and thus the A specimen was added too. These 3 samples were chosen since they would allow a larger surface area to be tested, and the influence of the printing direction could also be observed. The fracture surface was cut with the Discotom, Figure 3.5.2-1, and saved for further analysis. Then the rest of the specimen were grinded down on abrasive paper on the manual grinding machines, see chapter 3.1.1, with 80, 220, and 500 grit

abrasive paper. Pickling was not performed since all surfaces were grinded with 500 grit paper. Care was taken to grind down the marks on the surfaces from the CharpyV testing. This was done to avoid any deformation to influence the corrosion resistance of the specimens.

During the grinding the specimen got mixed up, and to keep a system they were renamed specimen 1, 2 and 3. They were weighted on a Sartorius Entris124I-1S that has a deviation of 0.1mg and measured with a resolution of 0.1mg. See chapter 4.5 for the measurements. The dimensions were measured with a micrometre, and the surface area calculated.

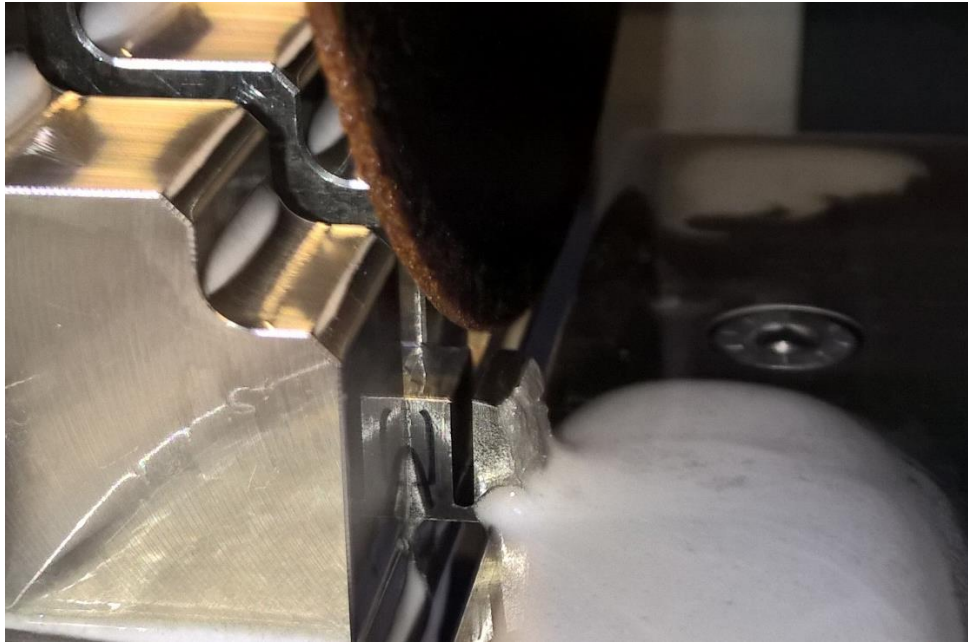


Figure 3.5.2-1 Fracture surface being cut off a CharpyV-sample in the Discotom

The corrosion solution was prepared by mixing 1200ml of distilled water, chapter 3.1.1, with 133.07g of anhydrous Iron(III)chloride. Using the recipe given in G48 by adding 900ml of water and 100g of $\text{FeCl}_3 \cdot 6\text{H}_2\text{O}$ was omitted because of lack of Iron(III)chloride available on the lab. All the equipment used was fresh out of the dishwasher (the washing method used on the corrosion lab). By intuition the colour of the solution was deemed too dark and it as discovered that the recipe in G48 called for the use of hydrous Iron(III)chloride. Additional 796ml of distilled water was added according to the calculations done in Attachments 2 to get the correct concentration. In total this added up to 1996ml of solution that was used to fill 3 1000ml beakers with 600ml solution each. The specimens were attached at the middle with light blue cotton sewing thread, and the other end of the tread tied to a bamboo skewer that rested on top of the beaker. The length of the tread was made to let the specimen be suspended in the centre of the beaker, and the middle of the solution.

3.5.3 Testing

The test was performed in a heating cabinet of model [INSERT HEATING Chamber MODEL]. The reason for this was that the alternative would be to use a corrosion machine that had a temperature fluctuation of ± 10 °C. The deviation caused by a heating cabinet was considered to be minor compared to that of the corrosion machine, and there was no time to build a custom solution.

The beakers with the corrosion solution, were placed in the heating cabinet with plastic wrap on top to preheat the solution. A thermometer was placed in one of the beakers to monitor the temperature. The heating cabinet was set to 50 °C and left for 4 hours to allow the temperature to stabilize. At 16:20 April 19th the specimens were added to the solution and the test started. A hole was made in the middle of the plastic wrap to accommodate the test specimens. The thermometer in the beaker for specimen Nr.2 read 49 °C at the start of the test.



Figure 3.5.3-1 Corrosion tests in the heating cabinet after 24hours. Test 1, 2, and 3 from left to right with the thermometer in the middle.

After 24 hours, on April 20th 16:20, the beakers were taken out of the heating cabinet. Figure 3.1.1-1 shows the specimens before they were taken out. The solution level is lower in the beaker even though they have been covered in plastic wrap. The solution level was about 550ml at the end of the test. The specimens were dipped in distilled water at the spot, and further rinsed at the microscopy lab. All the specimens had been dipped in distilled water within 3 minutes of the opening of the heating cabinet. At the opening of the cabinet, the thermometer read 48 °C. The test specimens were further rinsed with distilled water and cotton swabs, and put in an ultrasonic cleaner with ethanol for 15 minutes.

3.5.4 Post-test inspection

When the specimens had dried after the rinsing and ultrasonic cleaning, they were weighted again at the same scale as before. Weight loss per square meter were calculated.

The specimens were then inspected at the REICHERT-JUNG light microscope to look for pitting. 20x magnification was used to find details to further inspect, and 100x and 200x were used to photograph details. A detailed picture of one whole surface of specimen Nr.3 was made of a series of nearly a hundred pictures at 20x magnification. The picture in full size is included in Attachment 3, and a scaled down version is present in chapter 4.5. Details were pictured as they were found and a selection can be found in chapter 4.5.

After the inspection and documentation, the specimens were put in individual plastic bags and stored with the other specimens in the wooden box.

3.6 SEM and light-microscopy

3.6.1 Introduction

SEM and light-microscopy was performed to investigate the microstructure of the material. The goal was to uncover defects, grain structuring, elemental distribution, and other interesting details of the material. Specimen LII 3, AII 3, and SII 3; both S and F for all of them; was chosen for microscopy. This was done to include all three printing cases, and to inspect them from the “top” (S specimens), and the side (F specimens). The SII 3 specimens were both (S and F), grinded and polished to look for differences in the bottom and top surface. Both S and F specimens were needed since only one surface could be prepared on each specimen without ruining the other one because of the clamping solution during polishing.

3.6.2 Preparation

Mechanical grinding and Polishing

The specimens were polished on the Planopol polishing machine 3 at a time. Table 3.6-1 below shows the steps used. Both the machine and the specimens were thoroughly cleaned between each polishing step to avoid transfer of particles that could scratch up the surface. After the polishing was finished, the specimens were rinsed in water and then ethanol, and put in individual plastic bags.

Table 3.6-1 Mechanical grinding and polishing steps

	Grinding				Polishing	
Grit/Size	200	500	1200	2000	9 μ m	1 μ m
Surface	Paper	Paper	Paper	Paper	MD-Nap	felt disc
Material	SiC	SiC	SiC	SiC	Diamond	Diamond
Lubricant	Water	Water	Water	Water	Red	Red
RPM	300	300	300	300	300	300
F setting	1	1	1	1	1	1
Time [min]	Plane	2	2	2	10	10

Electro polishing

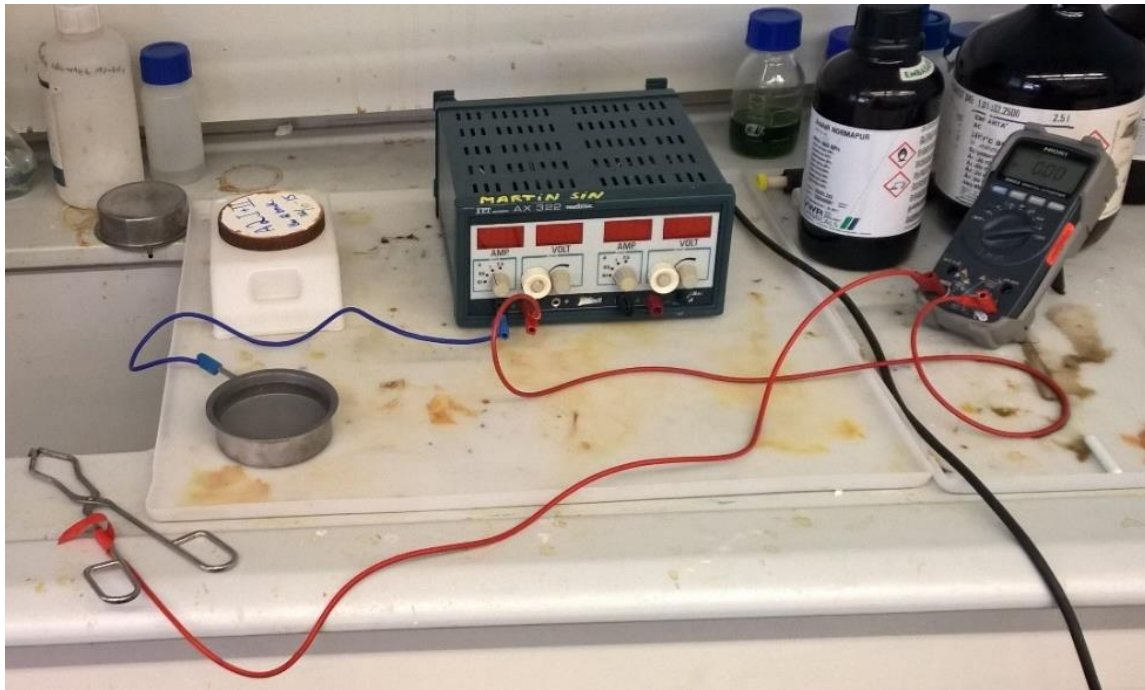


Figure 3.6.2-1 Electro polishing setup. Pan with A2 etchant connected to ground of the PSU. tong connected to positive voltage on the PSU, going through a multimeter to measure current when electro polishing.

Electro polishing was done to remove the deformed layer after mechanical polishing, to enable EBSD, and to look at HAZs in light microscopy. Electro polishing was performed with A2 electrolyte, at 30V, for a variable amount of time. This was based on the work of Kvåle and Randeberg [27]. A variable power supply was set to 30V and 1A current limit. The voltage was controlled with a multimeter. A pan was connected to the power supply ground, and filled with the electrolyte. The electrolyte used was unused leftovers from another student's experiments. A multimeter was connected in series between the positive terminal of the power supply, and a tong. This was done to have a second control of the current going through the electro polishing process.

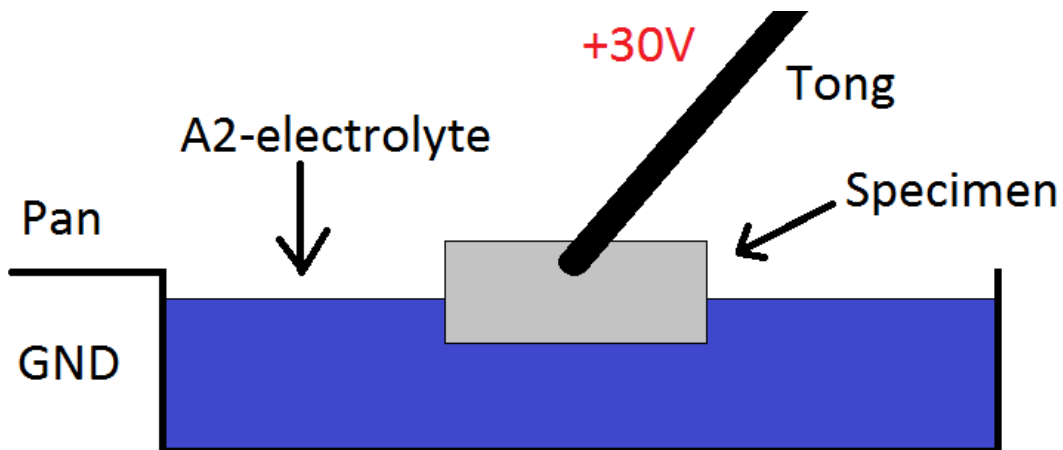


Figure 3.6.2-2 Illustration of the electro polishing bath.

Electropolishing was performed in the following way. All the specimens laid with the polished surface down in a piece of paper. A specimen was picked up with the clamp and the polished surface was put 2mm down into the electrolyte. Care was taken to avoid contact between the tong and the electrolyte. The specimen was hold in the electrolyte for the time and in the order listed in Table 3.6-2. After exposure the specimen was rinsed in running tap-water and ethanol. This was repeated for all the specimens.

The current was 1.1A for all the specimens, and would probably been higher

if the power supply had not been set to a 1A limit. The resulting surface of even specimen AII 3 S, was not suitable for EBSD analysis, but worked well for light microscopy.

Table 3.6-2 Time of exposure and order of electropolishing

Specimen	Time [s]
L II 3 F	30
L II 3 S	5
S II 3 F	5
S II 3 S	2
A II 3 F	2
A II 3 S	<1 (quickly dipped)

Mechanical polishing with Struers OP-S & OP-A

Studies performed by George Vander Voort [28] suggested that a grinding and polishing process finished by OP-A would give a suitable surface for EBSD. Tests with both OP-A and OP-S was performed, since OP-A initially wasn't available at the university. The differences between them, and the grinding and polishing steps are listed in Table 3.6-3 below.

Specimen S II 3 S was prepared with OP-S, and L II 3 S and L II 3 F was prepared with OP-A. Both worked, but OP-S produce a noticeable better surface for EBSD.

Table 3.6-3 Polishing process steps OP-A or OP-S.

	Grinding				Polishing			OP-S / OP-A
Grit/Size	180	220	320	2000	9µm	3µm	1µm	0.04 / 0.02 µm
Surface	Paper	Paper	Paper	Paper	MD-Nap	felt disc	felt disc	MD-Chem/MD-Nap
Material	SiC	SiC	SiC	SiC	Diamond	Diamond	Diamond	SiO ₂ / Al ₂ O ₃
Lubricant	Water	Water	Water	Water	Red	Red	Red	Alkaline / Acid
RPM	300	300	300	300	300	300	300	300 / 150
F setting	1	1	1	1	1	1	1	1
Time [min]	Plane	2	2	2	10	10	10	2 / 4

3.6.3 Microscopy

Light microscopy

Light microscopy was performed on electro polished specimens with the Reichert-Joung microscope. A glass ruler had been used to calibrate the scale in the CapturePro software to ensure that the scale on the pictures was correct.

The specimens were inspected and photographed to document the printed layers and other microscopic features that might be present.

SEM

SEM-microscopy was performed with secondary electron detector (SE2), backscatter detector (QBSD), EDS, and EBSD. The mechanically polished specimens were inspected with SE2 and QBSD. Defects were documented and QBSD was used to document dendritic subgrain structure, particles, and grain shape. EDS was used together with SE2 and QBSD to document chemical composition of interesting parts of the material and the matrix chemical composition. EBSD was used on the OP-A and OP-S polished specimens to investigate and document grain and subgrain orientation, and grain size.

20keV acceleration potential was used for nearly all SEM-microscopy. It was not possible to distinguish differences in metallurgical composition with the QBSD with a lower acceleration potential.

3.6.4 Post microscopy work

Some picture had to be merged to be meaningful. This was done with the free tool, Image Composite Editor. Paint was used to add information to the image after merge.

Certain picture, especially the light microscopy ones, needed contrast and brightness adjustments. These were done with the built in tool in Microsoft Word 2016.

4 Results

4.1 Initial measurements of specimens

This section gives some results on the geometry of specimens in the as delivered condition. The information is mainly meant as support for design and printing choices, and to back up some of the other results with information for discussion.

4.1.1 Measurements

EOS states that the accuracy of manufactured parts should be approximately $\pm 40\text{-}60\ \mu\text{m}$, or $\pm 0.04\text{-}0.06\ \text{mm}$. Both the tensile and Charpy specimens were thoroughly measured with the micrometre. Figure 4.1.1-1 and Figure 4.1.1-2 shows the measurement points. The measurements themselves can be seen in Attachment 6.

Over 150 measurements were made to control the printed geometry. Measurements were not made to where there was still support material present or where there had been overhang making the surface to rough, see 4.1.2, for an accurate measurement.

Off the measurements only one was smaller than the specified geometry. Most measurements were within $+0.06\ \text{mm}$, but there were a few of up to $+0.1\ \text{mm}$.

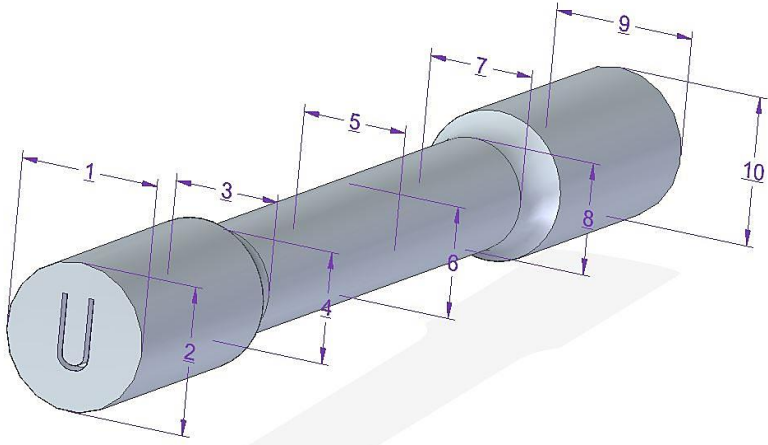


Figure 4.1.1-1 Measurement points on the tensile specimens upon arrival

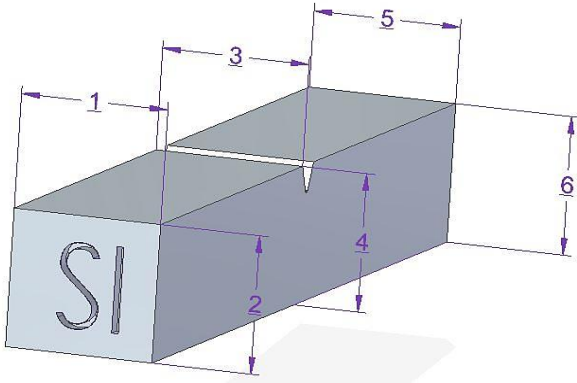


Figure 4.1.1-2 Measurement points on the Charpy specimens upon arrival

4.1.2 Rough support and overhang surface

The top(horizontally) and side(vertically) surfaces were clean and smooth. The Overhang and supported surfaces were much rougher. This can be seen in Figure 4.1.2-1 and Figure 4.1.3-1.



Figure 4.1.2-1 Rough overhang and support structure on specimen L1

4.1.3 Bending by thermal contraction

All the horizontal specimens experienced bending due to thermal contraction of the welds as described in 2.2.3 and seen in Figure 4.1.3-1 below. The amount of bending was not measured but considerable enough that there was no doubt of its present with visual inspection.

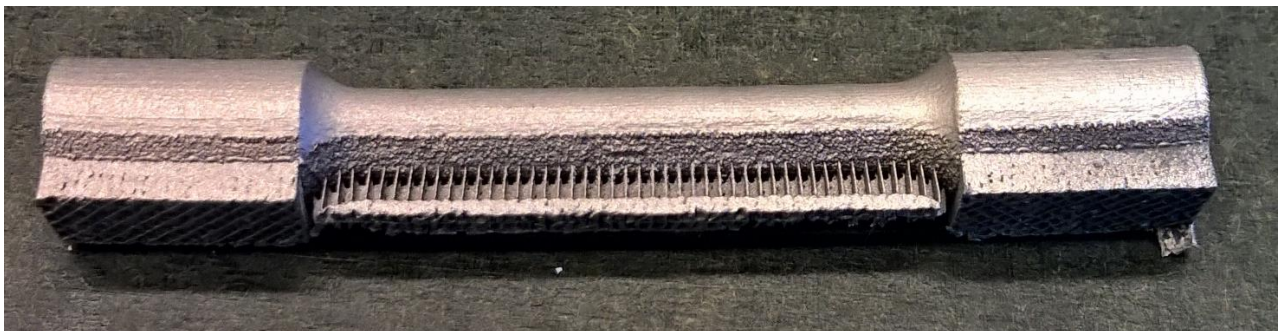


Figure 4.1.3-1 Specimen L4 displaying bending due to thermal contraction/stress

4.2 Tensile

All tests were performed with a strain rate of 0.02 mm/s in the first 2 seconds of the test and then 0.2mm/s. The separation was measured between the extensometer.

4.2.1 Curve shape, general characteristics

The general shape of the stress strain curve is shown in Figure 4.2.1-1 below. The long elongation before fracture, 32-40% depending on printing direction (see section 4.2.5), makes the curve look very steep in the elastic region. The yield limit, $R_{p0.2}$ varies between 640-720 MPa, see section 4.2.3. Tensile strength or UTS did also vary and was within the range 880-975 MPa, section 4.2.2 holds all the UTS results.

The E-modulus varies with nearly 100% within some specimens, this is thought to be measurement errors. The E-modulus is still presented in section 4.2.4 for information, but should not be considered as representable results for this material. This is discussed in section 5.2.1. There is no need to distrust the %elongation results as discussed in section 0.

Yield strength is quite consistently 71% of UTS over all the specimens. %elongation at UTS is in the range 74-80% of the %elongation at fracture.

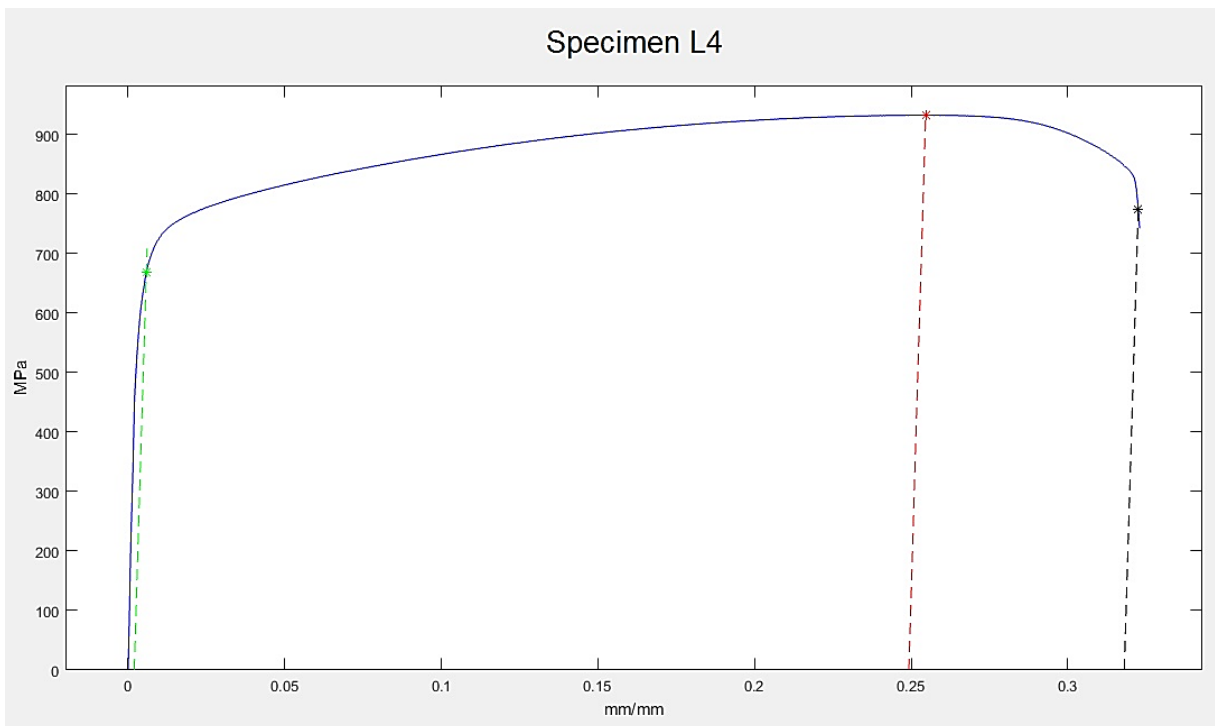


Figure 4.2.1-1 Stress-Strain graph of tensile test, specimen L4. Yield point shown with green mark, red mark indicates UTS, black mark indicates point of fracture. Lines indicate plastic deformation at the different points.

4.2.2 Tensile strength, UTS

Table 4.2-1 Tensile strength, UTS, of tensile tests, [MPa]

Specimen No.	Specimen type			
	U	T	Y	L
1	898	876	945	982
2	892	888	978	997
3	897	878	995	-
4	-	-	-	971
Mean	896	881	973	983
STD	3,2	6,4	25,4	13,1

The tensile strengths displayed in Table 4.2-1 is within the ranges specified by EOS [6], see Table 2.1-3. For U, T, and L the strength is slightly below the middle for the range.

There is a slight difference between the U and T specimens. This might have to do with pores in the printed surface as discussed in 5.7.1. The Y specimen (printed at 45°), has a nearly as high tensile strength as specimen L (horizontally printed).

Y and L specimens have a large standard deviation, this might be a result of the rough overhang and support surface (section 4.1.2), causing the real cross sectional area to vary.

4.2.3 Yield strength, $R_{p0.2}$

Table 4.2-2 Yield strength of tensile test, $R_{p0.2}$ [MPa]

Specimen No.	Specimen type			
	U	T	Y	L
1	636	628	686	701
2	649	664	708	728
3	640	637	764	-
4	-	-	-	689
Mean	642	643	719	706
STD	6,7	18,7	40,2	20,0

The yield strength seen in Table 4.2-2 is proportional to the tensile strength as seen in the comparative Table 4.2-3. Specimen Y shows an even larger variation in test results than for the tensile strength.

Table 4.2-3 Yield strength as % of tensile strength

Specimen No	Specimen type			
	U	T	Y	L
1	71 %	72 %	73 %	71 %
2	73 %	75 %	72 %	73 %
3	71 %	73 %	77 %	-
4	-	-	-	71 %
Mean	72 %	73 %	74 %	72 %
STD	1 %	2 %	2 %	1 %

The yield point was visible on the graph of nearly all the specimens, as seen in Figure 4.2.3-1 below.

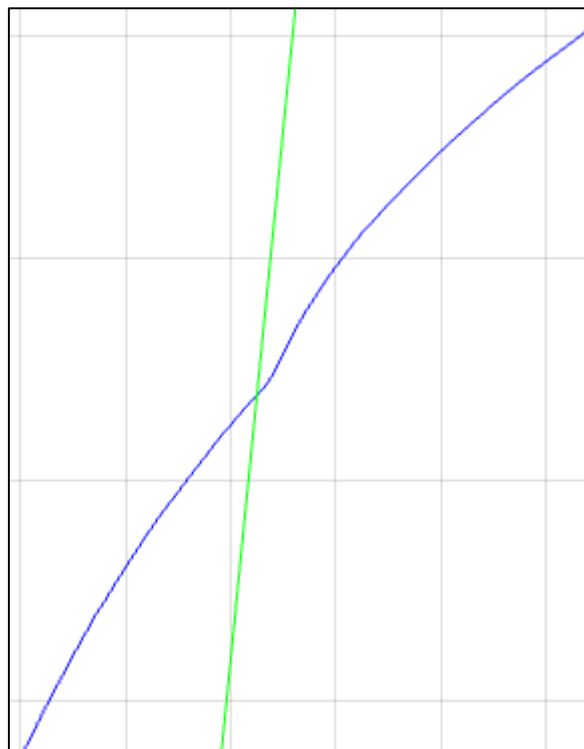


Figure 4.2.3-1 Yield point on stress-strain graph for specimen L1. Blue line is stress-strain graph and the green line is the E-modulus with 0.2% offset used to find $R_{p0.2}$. The intersection between the graph and the offset E-modulus line matches closely with the yield point on the graph.

4.2.4 E-modulus

Table 4.2-4 E-modulus of tensile tests, [GPa]

Specimen No.	Specimen type			
	U	T	Y	L
1	139	122	190	204
2	180	187	180	147
3	133	115	200	-
4	-	-	-	218
Mean	151	141	190	190
STD	25,6	39,7	10,0	37,6

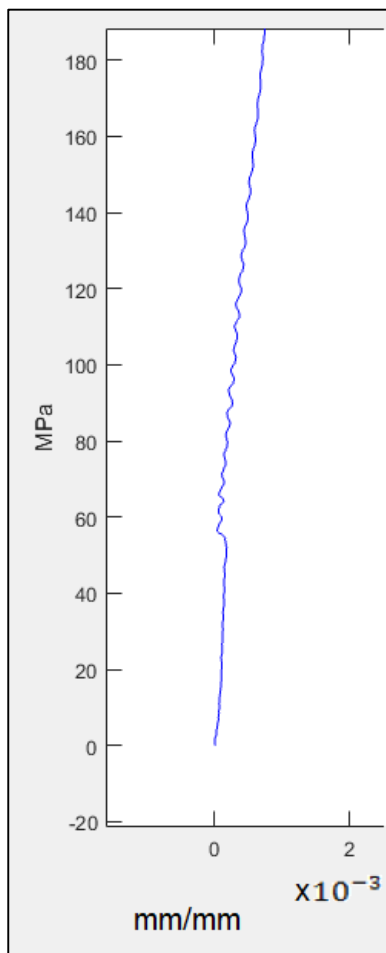


Figure 4.2.4-1 Uneven curve at start of tensile test, specimen U2.

The E-modulus varies quite much within the specimens, and the individual values are sometimes outside EOS specifications [6]. The mean values are just inside specifications, if the Y-specimens counts as a horizontal specimen, something that the other results from tensile testing suggests.

Specimen U2 has a significantly higher E-modulus than U1 and U3, as seen in Table 4.2-4. This might be caused of slipping of the extensometer as discussed in section 5.2.1. Figure 4.2.4-1 is the first part of the test and might show extensometer slipping in the start of the test. This was not found for specimen T2, L1, or L3, who also has much higher E-modulus.

Specimen T2 and T3 were compared in the SEM to look for differences, but no differences were found.

4.2.5 Elongation

Table 4.2-5 % elongation at UTS

Specimen No.	Specimen type			
	U	T	Y	L
1	30,5 %	31,4 %	26,4 %	25,4 %
2	29,3 %	28,9 %	25,9 %	24,3 %
3	29,2 %	31,4 %	24,8 %	-
4	-	-	-	25,0 %
Mean	29,7 %	30,6 %	25,7 %	24,9 %
STD	0,7 %	1,4 %	0,8 %	0,6 %

Table 4.2-5 and Table 4.2-6 show good elongation at tensile strength and fracture for all specimens. All results for elongation at fracture is within EOS [6] specification. Test results are consistent pairing U and T together as the vertically printed specimens, and Y and L as horizontally printed in their properties, compared to EOS specifications

Table 4.2-6 % elongation at fracture

Specimen No.	Specimen type			
	U	T	Y	L
1	41,1 %	40,3 %	33,4 %	32,4 %
2	40,2 %	38,2 %	30,2 %	32,2 %
3	38,4 %	41,3 %	32,6 %	-
4	-	-	-	31,9 %
Mean	39,9 %	39,9 %	32,1 %	32,2 %
STD	1,4 %	1,6 %	1,7 %	0,3 %

4.2.6 Fracture surface

The fracture surface was similar for all the specimens. It was characterised by a lot of topography with varying intensity within each specimen type as much as it did between the specimens. Around all the fracture surfaces the pores described in section 4.7.1 were present, as seen in Figure 4.2.6-1, and in more detail in Figure 4.2.6-2.

The fracture is of a ductile nature as would be expected with the long elongation. Cracks in the fracture surface can be seen in Figure 4.2.6-3. Figure 4.2.6-4 and Figure 4.2.6-5 supports this with the tearing of the microstructure evident at higher resolutions. These were present in all fracture surfaces.

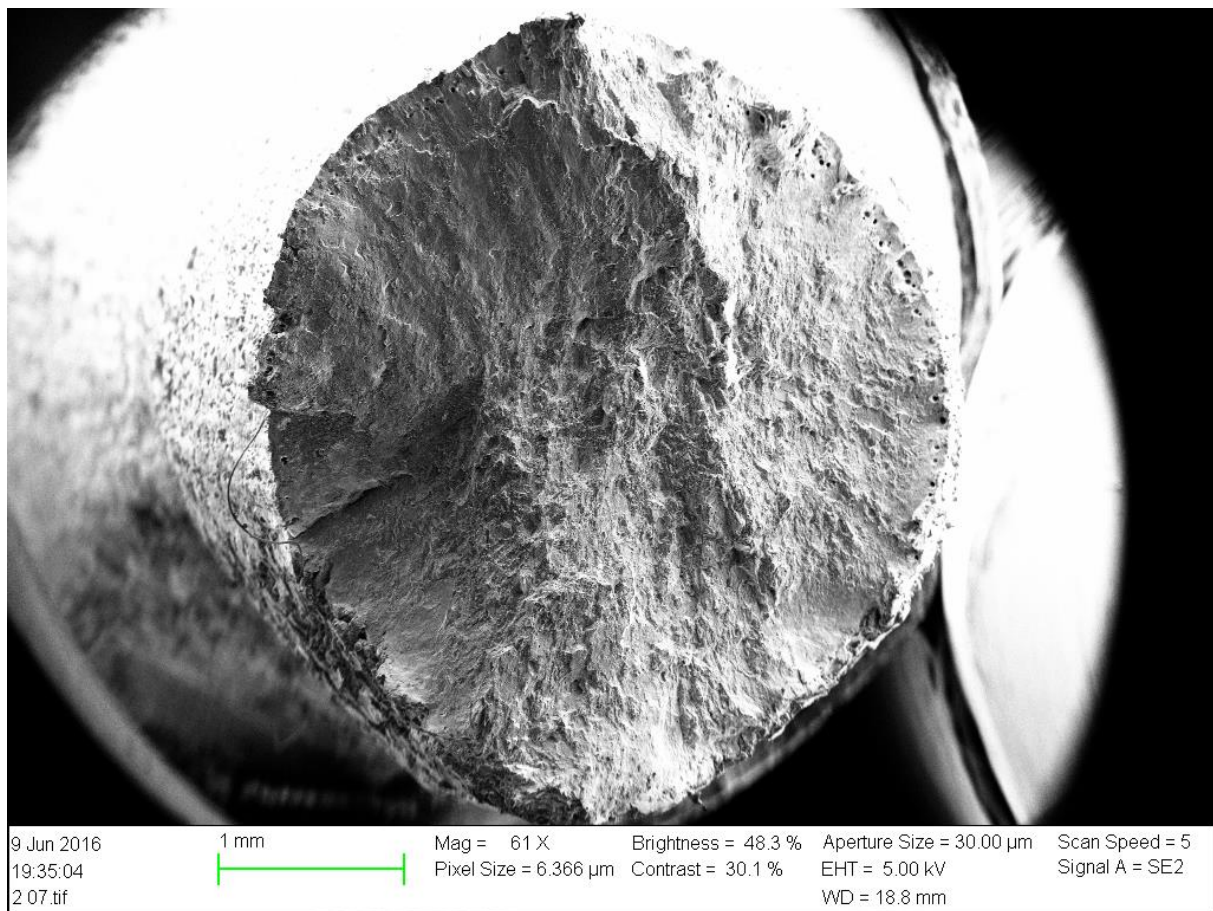


Figure 4.2.6-1 Fracture surface of specimen L2.

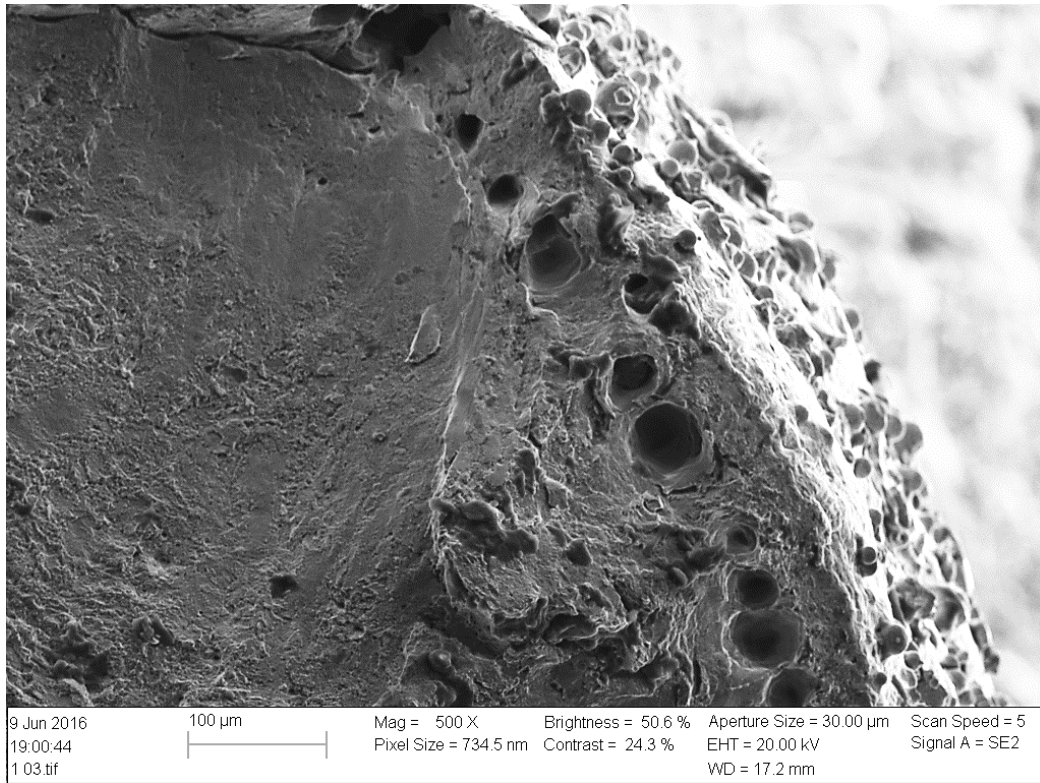


Figure 4.2.6-2 Pores on fracture surface of specimen T2

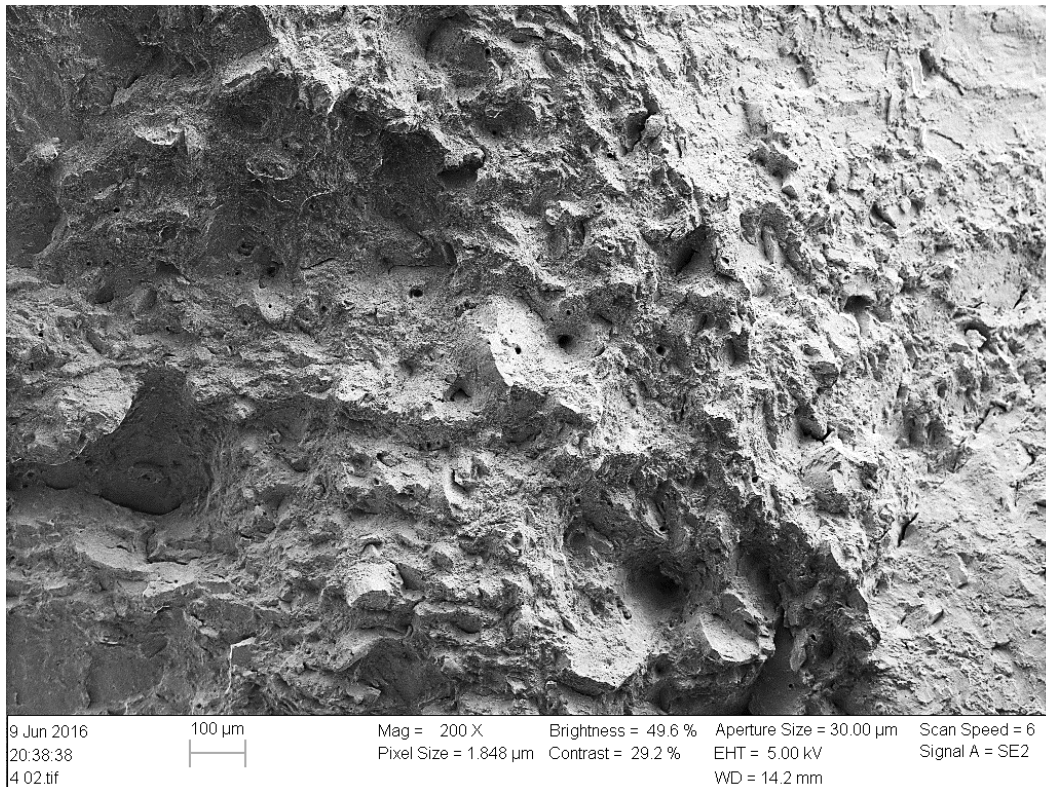


Figure 4.2.6-3 Specimen U2, cracks can be seen in the surface.

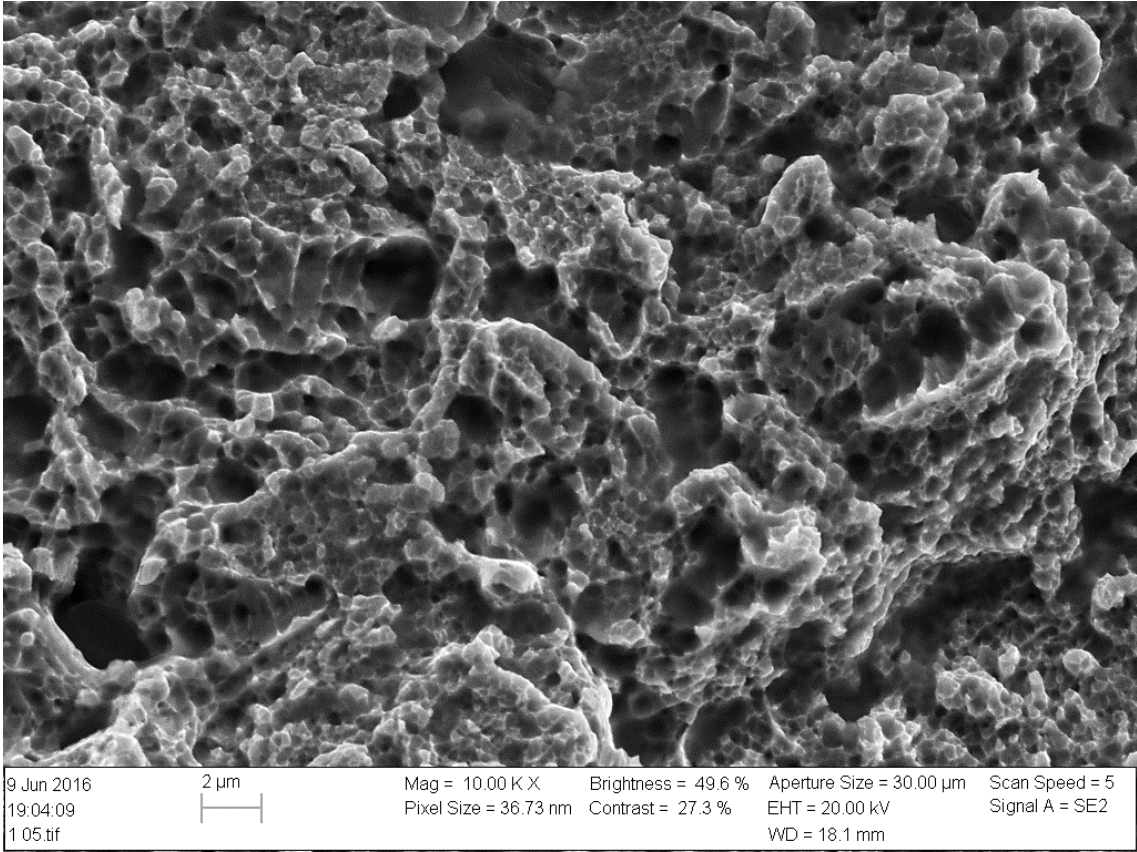


Figure 4.2.6-4 Specimen T2, showing tearing in the fracture surface.

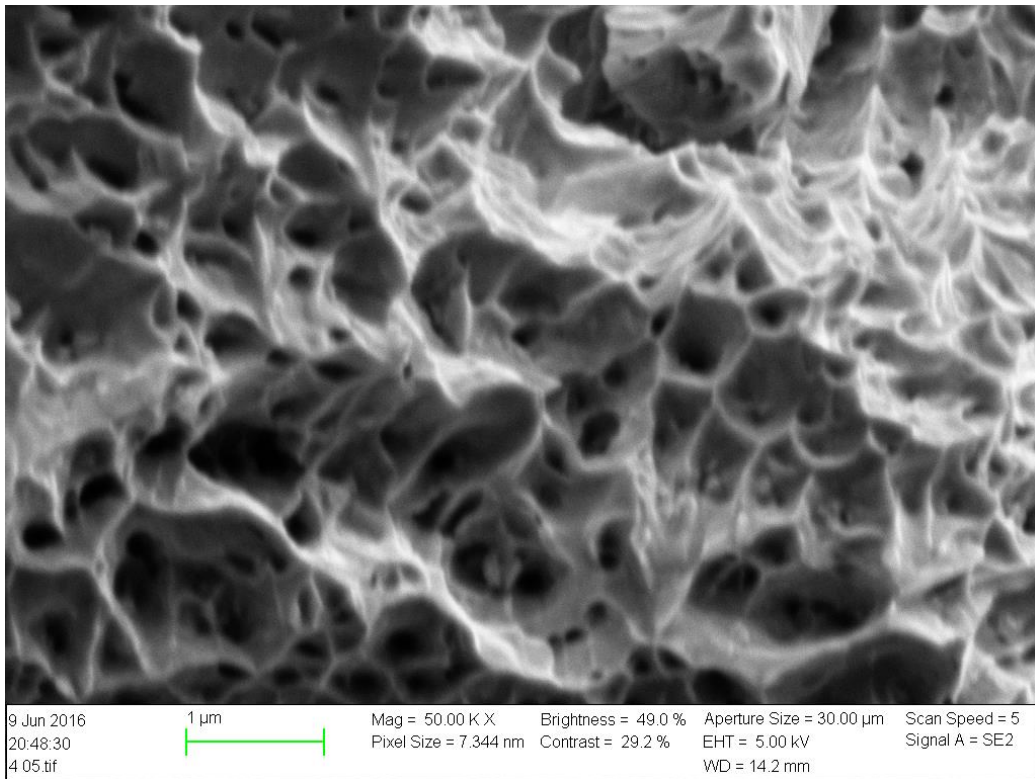


Figure 4.2.6-5 Specimen U2, showing tearing at higher resolution in fracture surface

4.3 CharpyV

4.3.1 Energy absorbed

Table 4.3-1 CharpyV test results, printed notch

	SI	AI	A_	LI
Mean	184	148	164	129
STD	7.69	1.0	3.4	3.3
DR mean	180	-	-	-
DR STD	1.41	-	-	-

Table 4.3-2 CharpyV test results, machined notch

	SII	AII	A=	LII	L=
Mean	194	174	189	153	155
STD	8.64	6.2	6.3	1.5	0.6
DR mean	189	-	186	-	-
DR STD	1.48	-	0.85	-	-

DR=Deviation Removed. If a test result was much higher than the other two results, it was deemed to be a result of not positioning the specimen correctly in the testing machine. To correct for this a new mean and STD was calculated without the deviating value. The new value was prefaced with DR as seen in both the tables above.

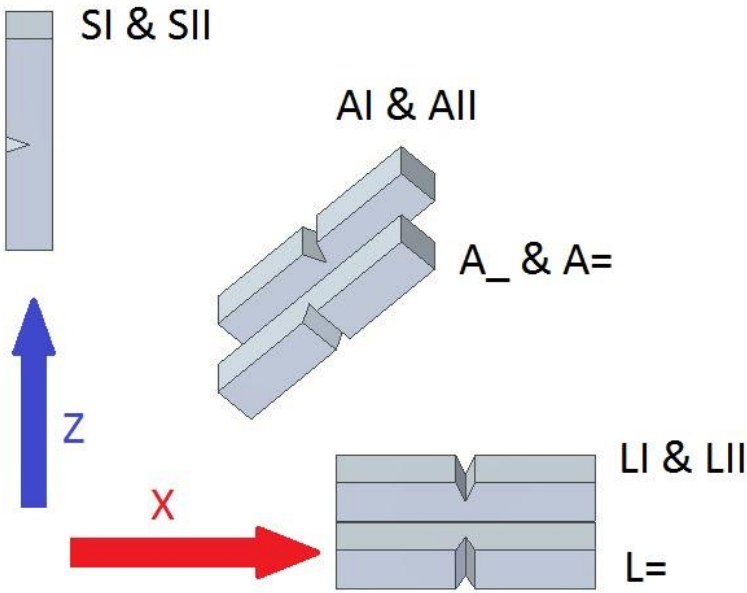


Figure 4.3.1-1 CharpyV specimen orientations in 3D-printer

The results from the digital and analogue readout corresponds to each other with the analogues readings being a little, 4-5 J, higher than the digital values. This confirms that the data is correctly noted. Since the digital readout had been calibrated, the digital readings are presented and used in the rest of the report.

Both the absorbed energy, and its standard deviation is varying for each specimen. The testing order was S, A, L; starting with the SI and ending with L= specimens. The standard deviation seems to get lower as more experience with testing was gained.

The printed notches in Table 4.3-1 shows lower absorbed impact energy than the machined notches in

Table 4.3-2. The difference is varying as seen in Table 4.3-3, and discussed in chapter 5.3.1.

Table 4.3-3 Comparison between printed and machined notch

	S I and II	A I and II	A _ and =	L I and II
Difference	9.1	26.0	21.9	23.9
% Difference ⁵	5.1	17.5	13.4	18.5

The absorbed energy varies with specimen orientation. The way the cleaving plane is cleaved also seems to have an impact for the A-specimens as seen in Table 4.3-1 and Table 4.3-1, while the L specimens did not seem to be affected.

4.3.2 Fracture surface

⁵ Calculated as: $\%Difference = \frac{Difference}{Printed\ notch} * 100$

4.4 Hardness Vickers

4.4.1 Resluts

Table 4.4-1 Vickers test results

Specimen	Test	No. of tests	Mean	STD	Note
L II 3 F	HV1	105	299	9.22	Polished
L II 3 S	HV1	38	286	7.41	Polished
S II 3 F	HV0.1	32	416	19.4	Grinded, 1200 grit
S II 3 F	HV0.1	15	311	13.2	Polished
S II 3 F	HV0.2	24	329	16.7	Polished
S II 3 F	HV 0.1	30	317	12.7	Polished
S II 3 S	HV5	6	278	5,53	Polished
S II 3 F	HV5	6	294	4,45	Polished
L II 3 S	HV5	6	301	9,40	Polished
L II 3 F	HV5	6	285	5,80	Polished

No indication of hardness changes near the top, side, of supported surface was found. Figure 4.4.1-1 shows a HV1 test varying as much along the edge as with the distance inwards. There was clear variation in hardness in of the material, but no clear connection with hitting the edge, or the middle of a grain, og at or near a melting zone line. HV5 test were done in the middle of the specimens and did not show any conclusive evidences since S II 3 S and F should be the same since they effectively have the same grain orientation. It is clear that surface preparation is important as the grinded surface in Table 4.4-1 has a significantly higher Vickers value than the test with a polished surface.

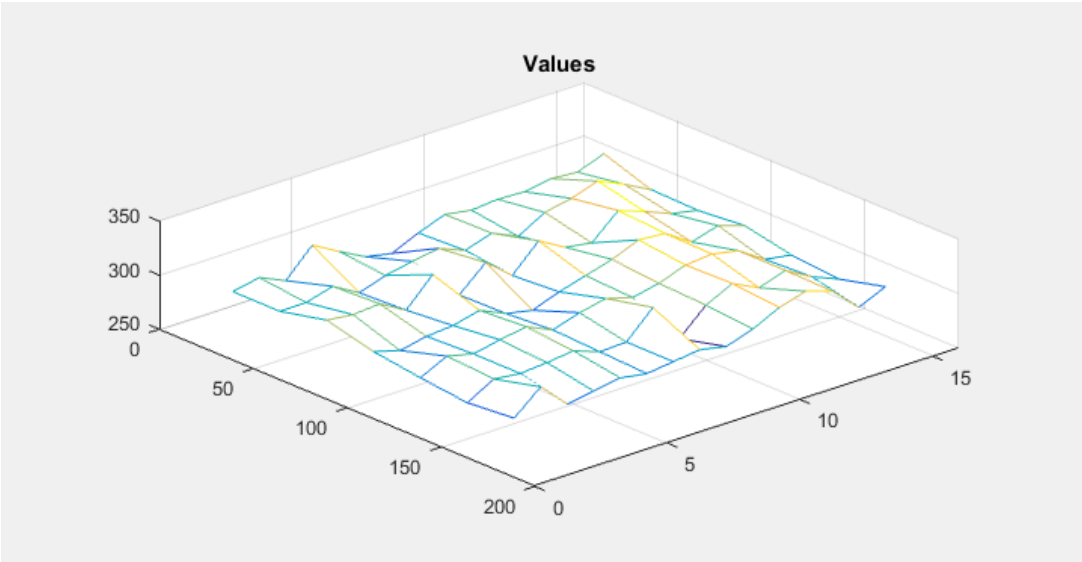


Figure 4.4.1-1 HV1 test on L II 3 F plotted in a 3D-plot. Left axis indicates distance from the edge of the specimen, right indicate test column No., vertical axis Vickers hardness

4.5 Corrosion

4.5.1 Introduction

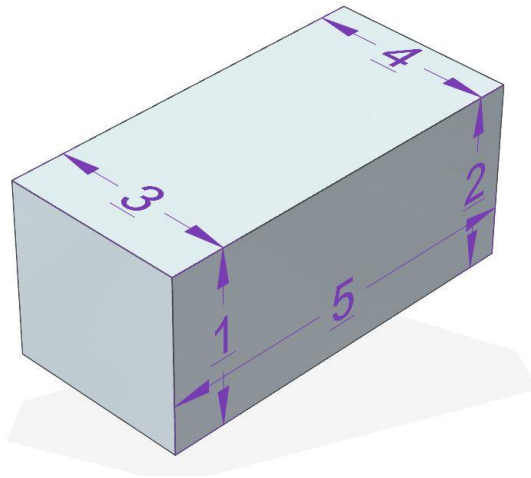


Figure 4.5.1-1 Illustration of corrosion specimen measurements

The physical measurements of the specimens are listed in Table 4.5-1 below, and an illustration in Figure 4.5.1-1 above to help explain the measurements. The deviation in mass measurements from before and after the test can be neglected as discussed in chapter 5.5.4.

4.5.2 Measurements

Table 4.5-1 Physical measurements and data of the corrosion specimens

Measurement/Data	Specimen		
	1	2	3
1	9.52 mm	9.52 mm	9.71 mm
2	9.55 mm	9.52 mm	9.49 mm
3	10.00 mm	10.02 mm	9.95 mm
4	9.99 mm	9.98 mm	9.93 mm
5	21.55 mm	20.37 mm	21.78 mm
Total Area	1032 mm ²	985.6 mm ²	1042 mm ²
mass pre-test	17.1260 g	16.1520 g	17.3223 g
mass post-test	17.1262 g	16.1519 g	17.3220 g
g/m ² difference	+ 0.1938	- 0.1015	- 0.2879

4.5.3 Microscopy

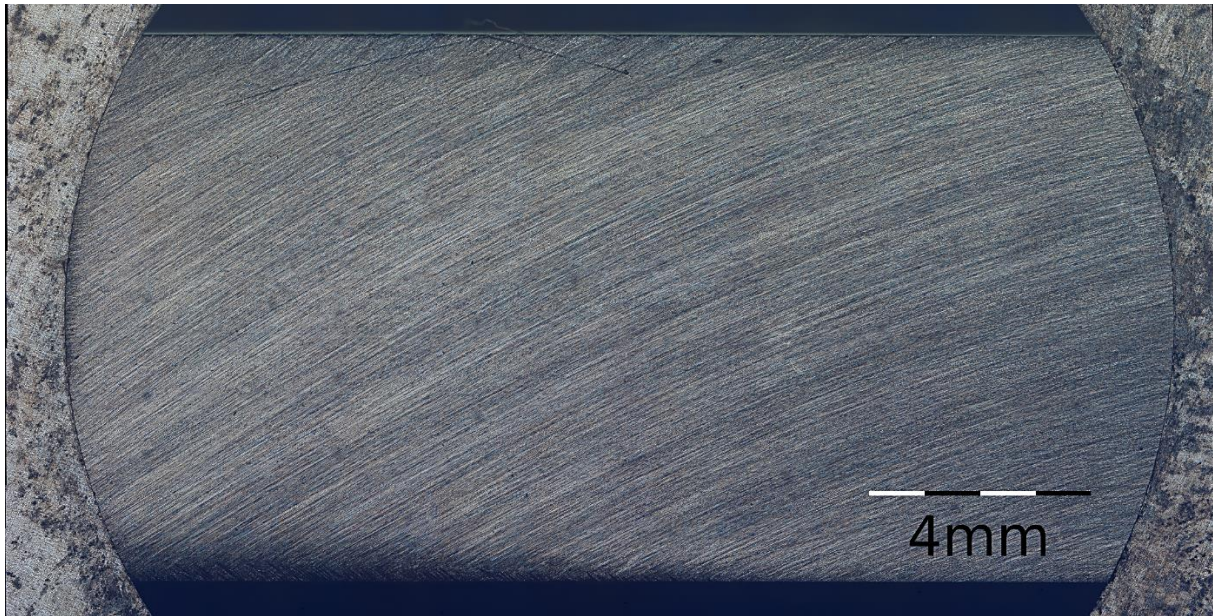


Figure 4.5.3-1 Part of one of the surfaces of corrosion specimen 3

The surfaces of the corrosion specimens were quite equal with some differences in grinding direction and other mechanical marks. Figure 4.5.3-1 is an example of the surface made of 100 pictures. The full image of 15925x8075px can be viewed in Attachment 4. There was no evidence of pitting found at 20x magnification, but some mechanical marks, oil from fingers, and dust were found as seen in Figure 4.5.3-2, Figure 4.5.3-3, and Figure 4.5.3-4

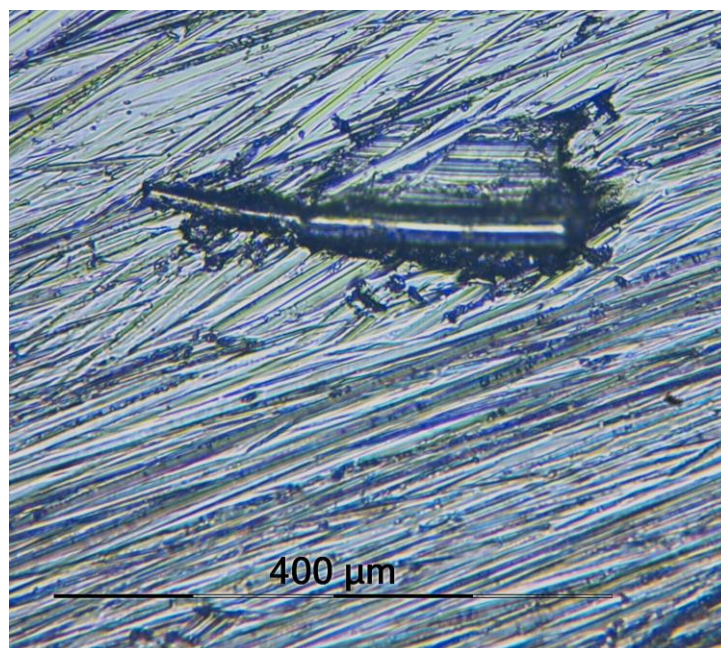


Figure 4.5.3-2 Mechanical mark on specimen 1

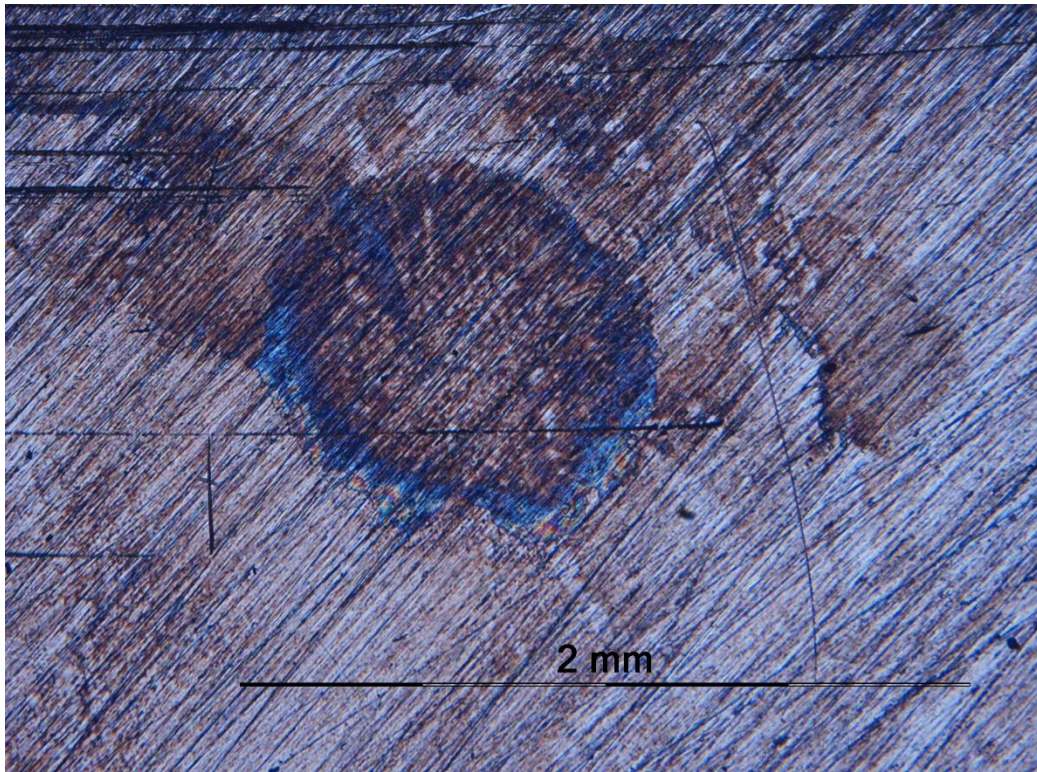


Figure 4.5.3-3 Oil from fingers on specimen 3

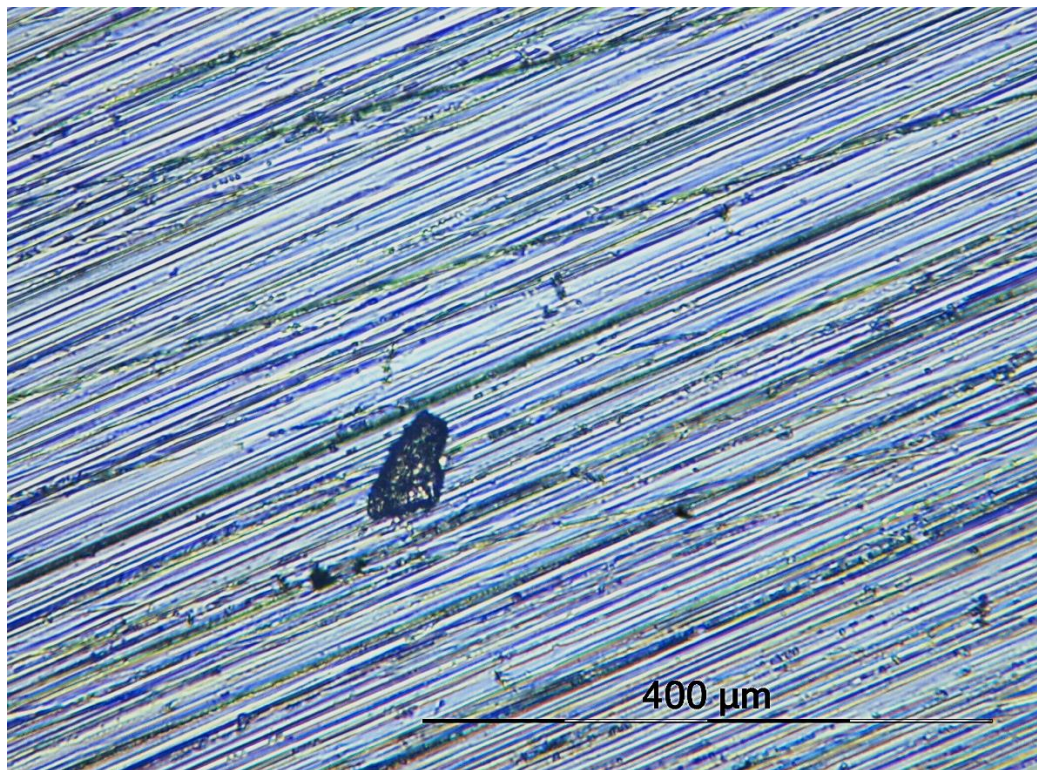


Figure 4.5.3-4 Dust on specimen 1

4.6 Light microscopy results

4.6.1 Layer angle

It was known that the laser changed direction from layer to layer, but not how much angular difference it was. Measurements done on the picture in Figure 4.6.1-1 shows an angular change of 67°

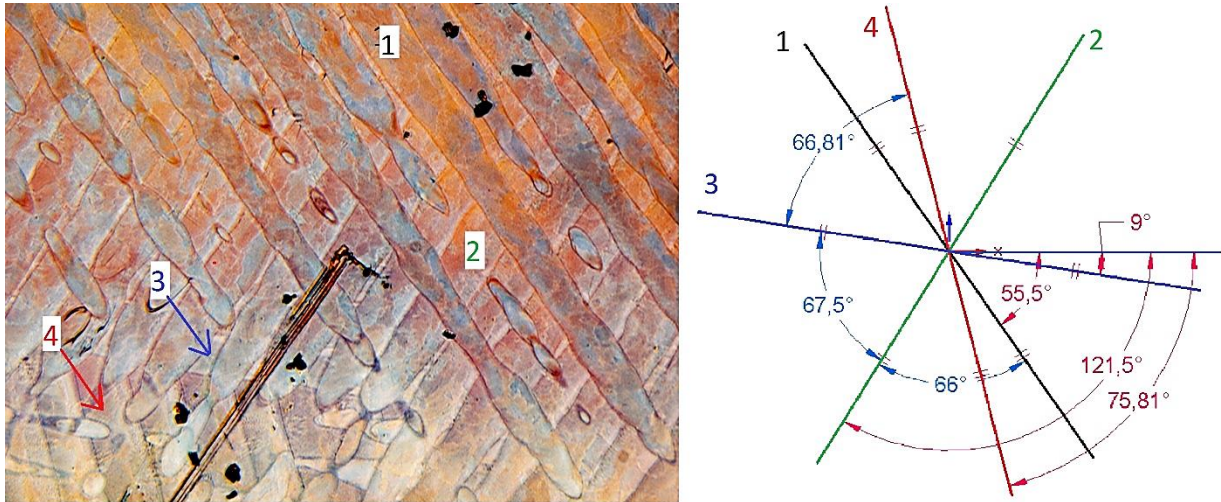


Figure 4.6.1-1 Multiple layers seen with laser angle difference in specimen L II 3 S.

4.6.2 Grain structure remaining over melting lines

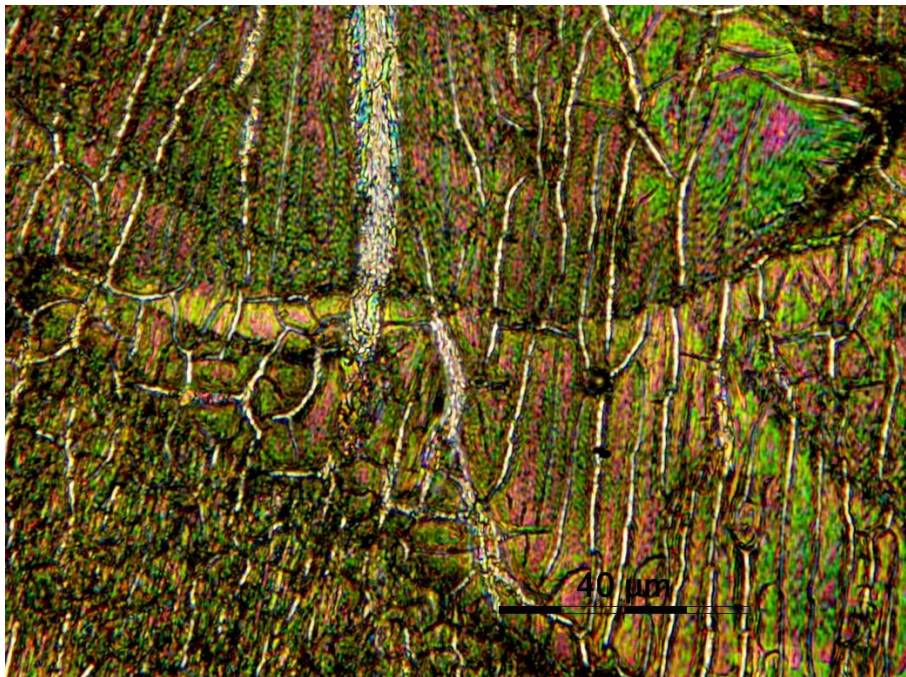


Figure 4.6.2-1 Grain growth across melting lines

Grains seem to continue to grow over a melting line (into a new melting pool or welding layer). This can be seen as grains grow across the melting lines, black curved lines, in Figure 4.6.2-1

4.7 SEM – microscopy

4.7.1 Pores

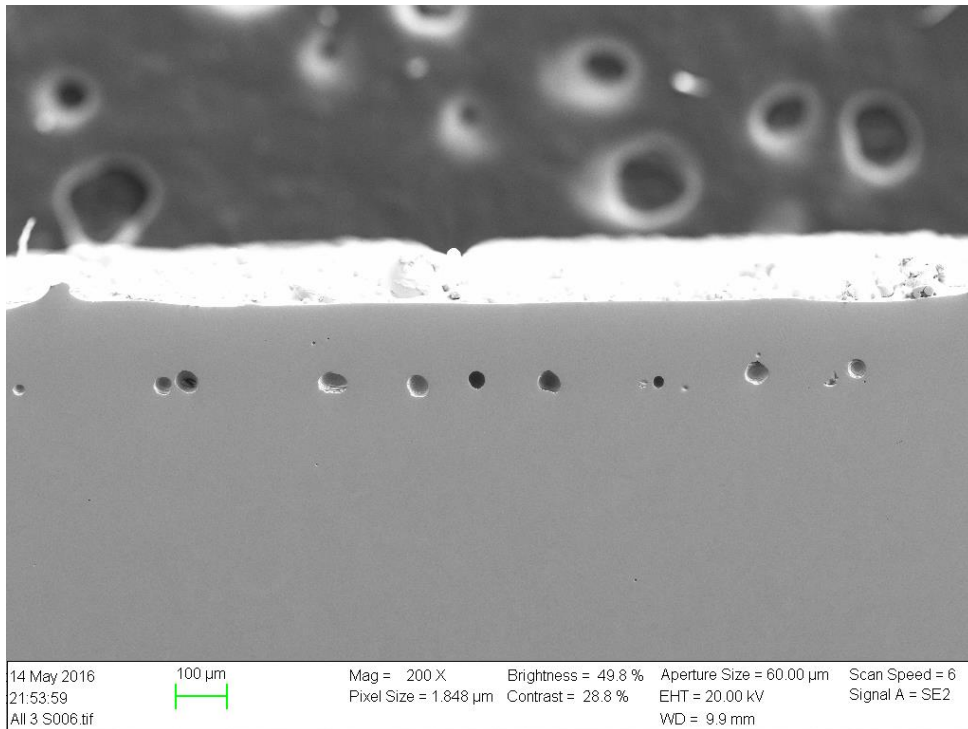


Figure 4.7.1-1 Pores near about 100 μ m from the edge of specimen A II 3 S

Pores were present along all the vertical surfaces, but not on the top surface. See Figure 4.7.1-1 above. When the DMLS machine melts the material, it first melts the outer contour, then du the infill. The pores were all located at the inner edge of this contour weld line. In the pores cracks were present as seen in Figure 4.7.1-2



Figure 4.7.1-2 Pore in surface of A II 3 S up close. Cracks visible at the bottom.

4.7.2 Dendritic structure

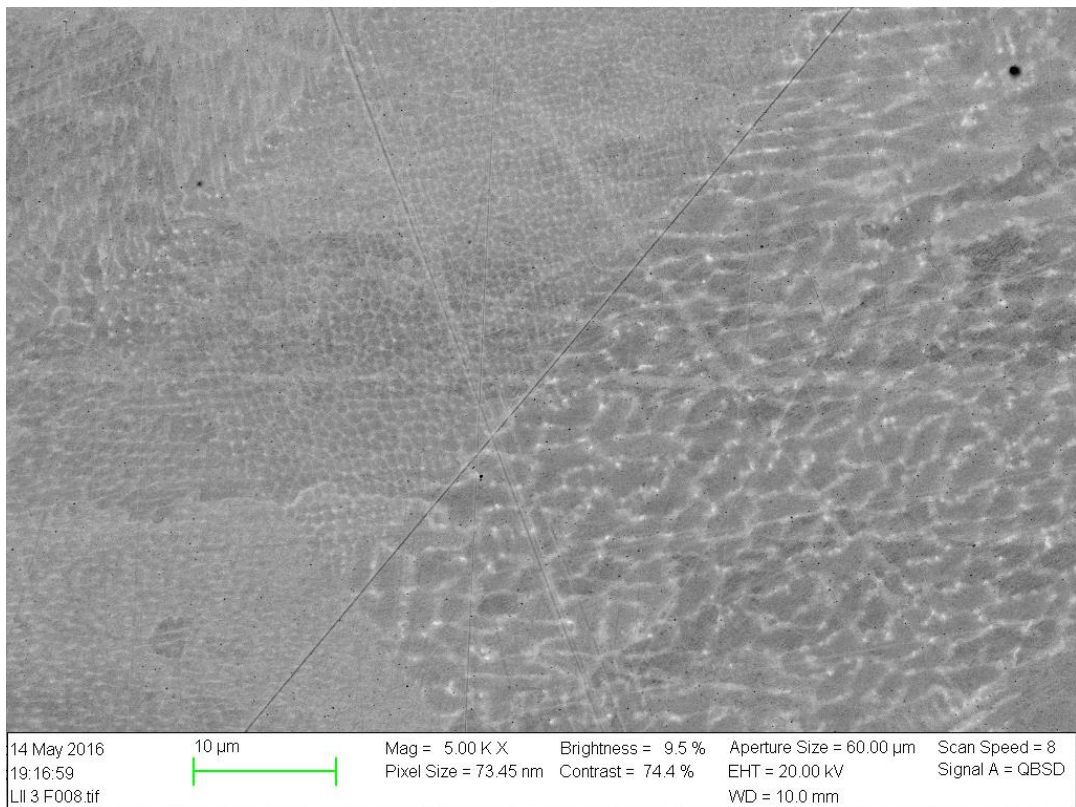


Figure 4.7.2-1 Backscatter image of dendritic structure of L II 3 F. Different grain orientations visible.

A dendritic structure similar to that found in welding was found using QBSD in the SEM, Figure 4.7.2-1. Elemental analysis was done with the EDS, and it was proven that the bright lines were rich in Molybdenum and Niobium as seen in Figure 4.7.2-2. Elevated levels of carbon were also found, Table 4.7-1. It was also richer in carbon than the matrix.

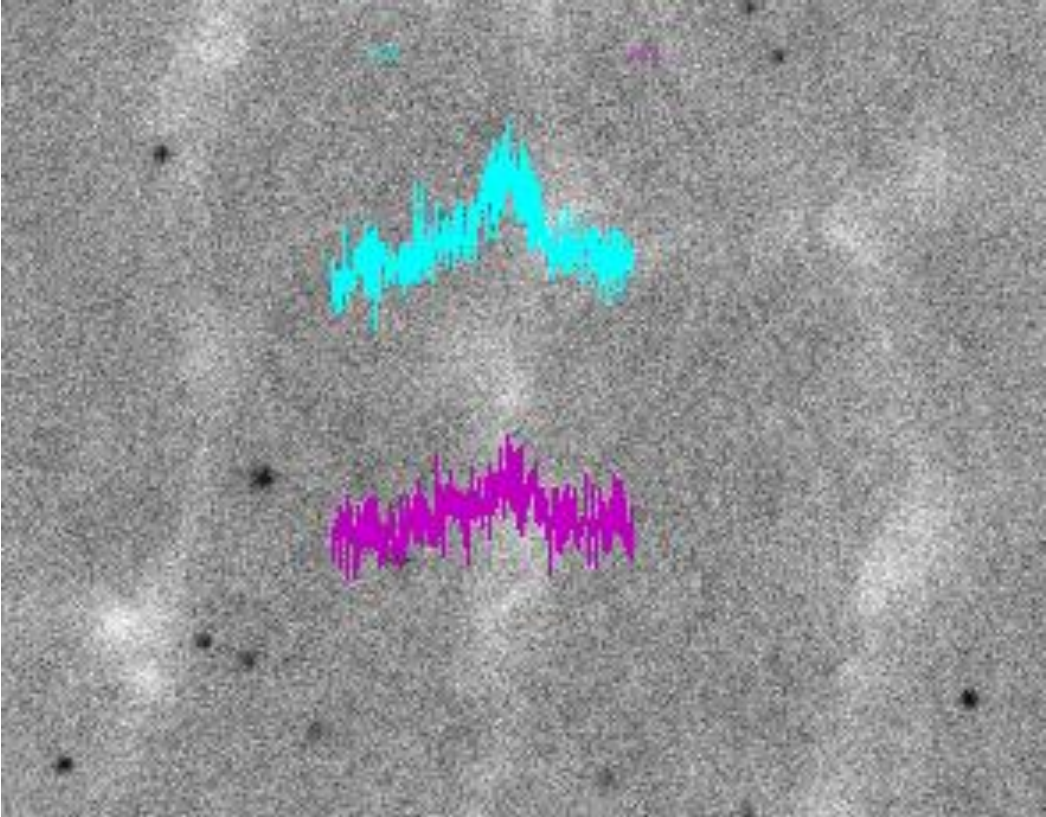


Figure 4.7.2-2 EDS line-mapping showing high amounts of Mo(magenta) and Nb(purple) at dendritic edges.

Table 4.7-1 EDS analysis of dendritic intersection, bright area, at 20kV

Elem	Wt %	At %	K-Ratio	Z	A	F
C K	17.81	49.52	0.0315	1.1397	0.1553	1.0002
O K	3.96	8.27	0.0084	1.1202	0.1890	1.0015
AlK	0.45	0.56	0.0015	1.0416	0.3118	1.0022
NbL	7.89	2.84	0.0539	0.8713	0.7832	1.0010
MoL	9.52	3.31	0.0684	0.8625	0.8321	1.0013
TiK	0.50	0.35	0.0045	0.9582	0.9145	1.0408
CrK	14.78	9.49	0.1420	0.9568	0.9584	1.0477
FeK	0.64	0.38	0.0063	0.9589	0.9511	1.0909
CoK	0.24	0.14	0.0022	0.9404	0.9646	1.0000
NiK	44.21	25.15	0.4200	0.9756	0.9738	1.0000
Total	100.00	100.00				

4.7.3 Aluminium particles

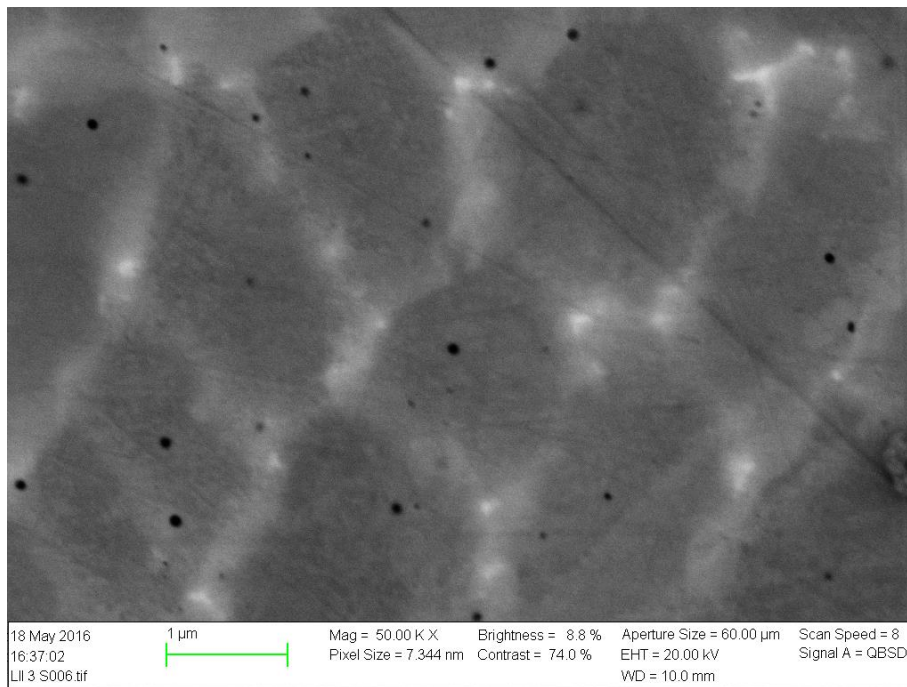


Figure 4.7.3-1 Black spots of around 67nm diameter, found in all specimens.

Black spots were found in all specimens. Their size is about 67nm in diameter, and they seem to be spread randomly around without any preferred location in regards to grain boundary or dendritic intersections. Figure 4.7.3-1 shows the distribution in specimen L II 3 S.

The particles were analysed by EDS and was found to be rich in aluminium, about 5 times richer than the matrix as seen in Table 4.7-2, and from the EDS line-map in Figure 4.7.3-2. No aluminium products have been used in the specimen preparation, with the exception of OP-A that was not used on specimens until EBSD was performed, that was the last SEM-work on polished surfaces.

Table 4.7-2 EDS analysis of black spot, at 20kV

Elem	Wt %	At %	K-Ratio	Z	A	F
C K	5.09	18.55	0.0084	1.1598	0.1430	1.0003
O K	5.12	14.03	0.0135	1.1398	0.2301	1.0019
AlK	2.64	4.28	0.0077	1.0594	0.2748	1.0016
NbL	4.00	1.88	0.0251	0.8887	0.7069	1.0011
MoL	9.13	4.17	0.0610	0.8797	0.7586	1.0015
TiK	0.44	0.40	0.0041	0.9758	0.9124	1.0491
CrK	18.18	15.32	0.1792	0.9747	0.9574	1.0561
FeK	0.80	0.63	0.0082	0.9771	0.9432	1.1040
CoK	0.28	0.21	0.0026	0.9585	0.9582	1.0000
NiK	54.32	40.53	0.5230	0.9944	0.9683	1.0000
Total	100.00	100.00				

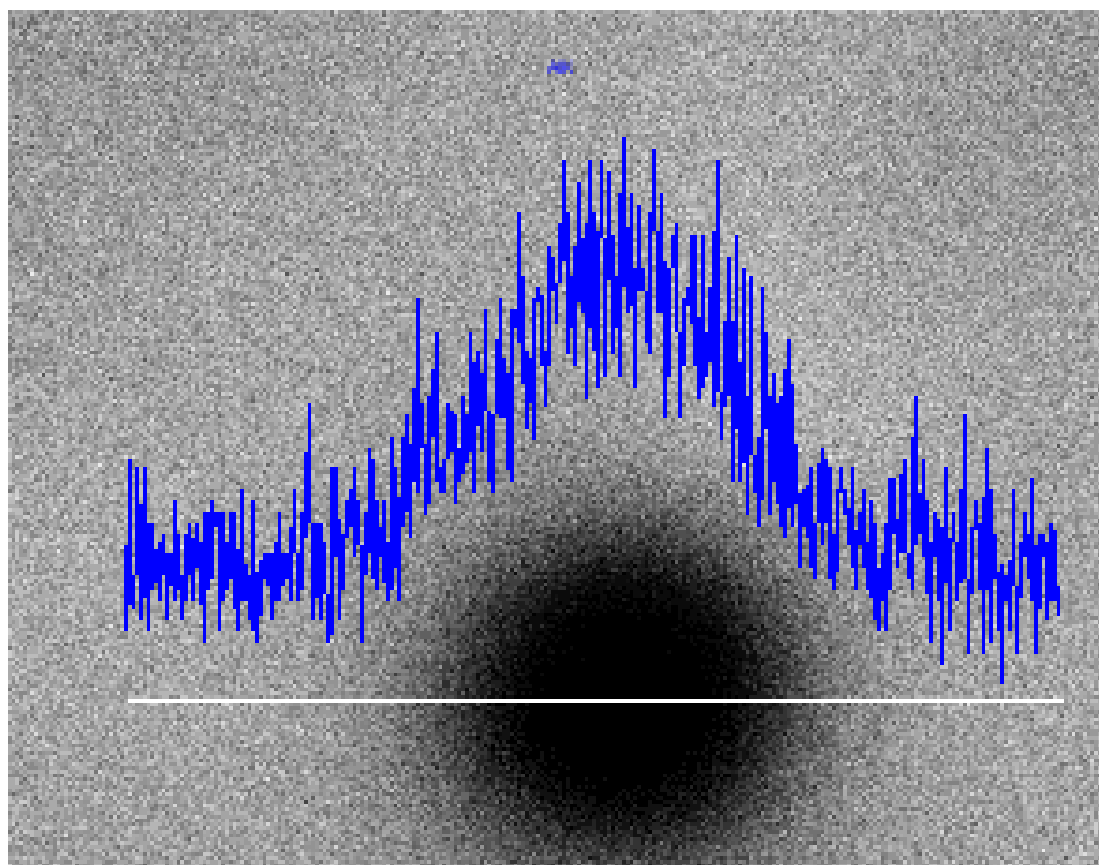


Figure 4.7.3-2 Increase in Al at dark spots

4.7.4 Crystal orientation, grain size. EBSD

Crystallographic orientation

Preferred crystallographic orientation was found by the use of EBSD. The colour key in Figure 4.7.4-1 can be used to evaluate Figure 4.7.4-2 and Figure 4.7.4-3 to see the preferred orientations. Figure 4.7.4-4 and Figure 4.7.4-5 shows the orientation density patterns.

Grain shape

It is clear from figure Figure 4.7.4-2 and Figure 4.7.4-3 that there is a significant difference in grain shape seen from the top (xy-plane), and from the side. The grains are stretched upwards in the build direction. The smaller grains in both figures is suspected to be remains of grains that have nearly been polished away.

Grain size

Grain size was calculated to be $8.17\mu\text{m}$, with a standard deviation of 9.5, in diameter seen from the top, and $9.07\mu\text{m}$, with a standard deviation of 12.6 seen from the side. Because of the remains of parts of grains as mentioned above the real grain diameter is probably larger, evident from the large standard deviations.

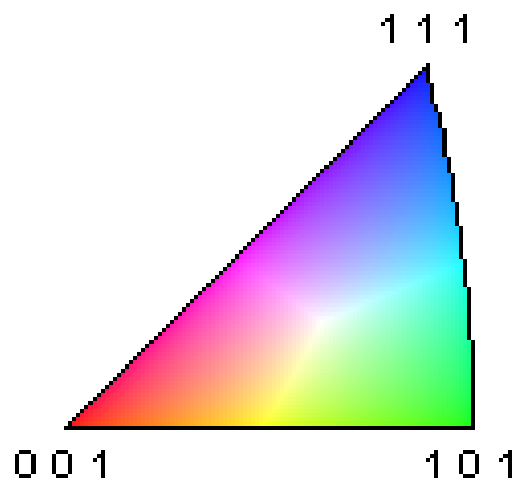


Figure 4.7.4-1 EBSD orientation colour key



Figure 4.7.4-2 Grain orientation, specimen seen from the top and down, xy-plane. 500x500 μm .

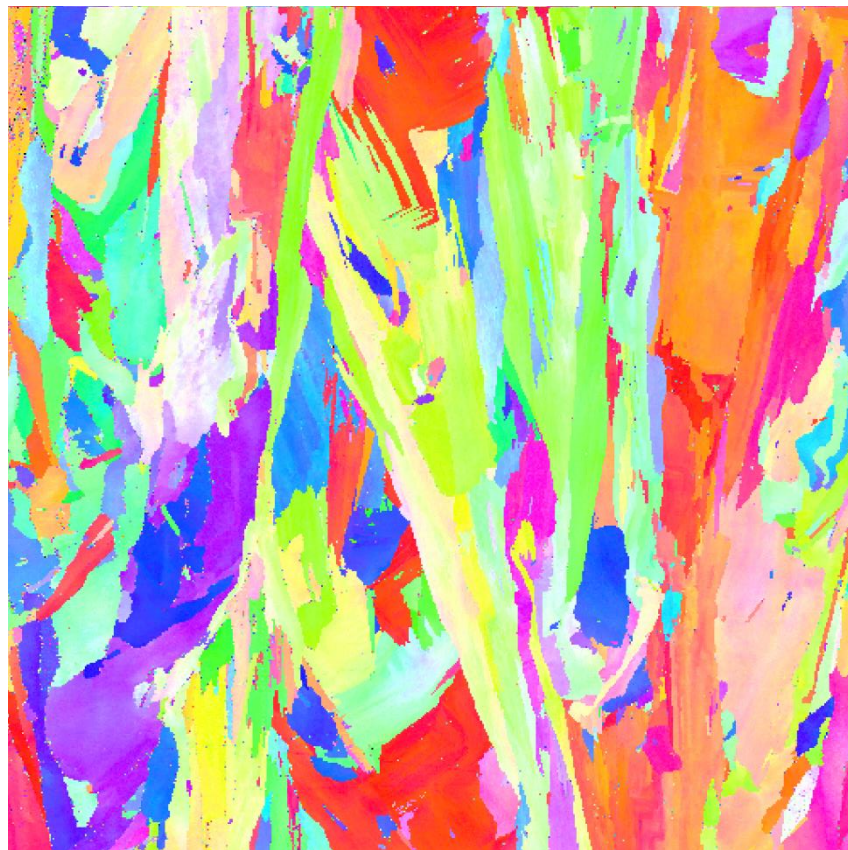


Figure 4.7.4-3 Grain orientation seen from the side, zx-plane. 500x500 μm resolution.

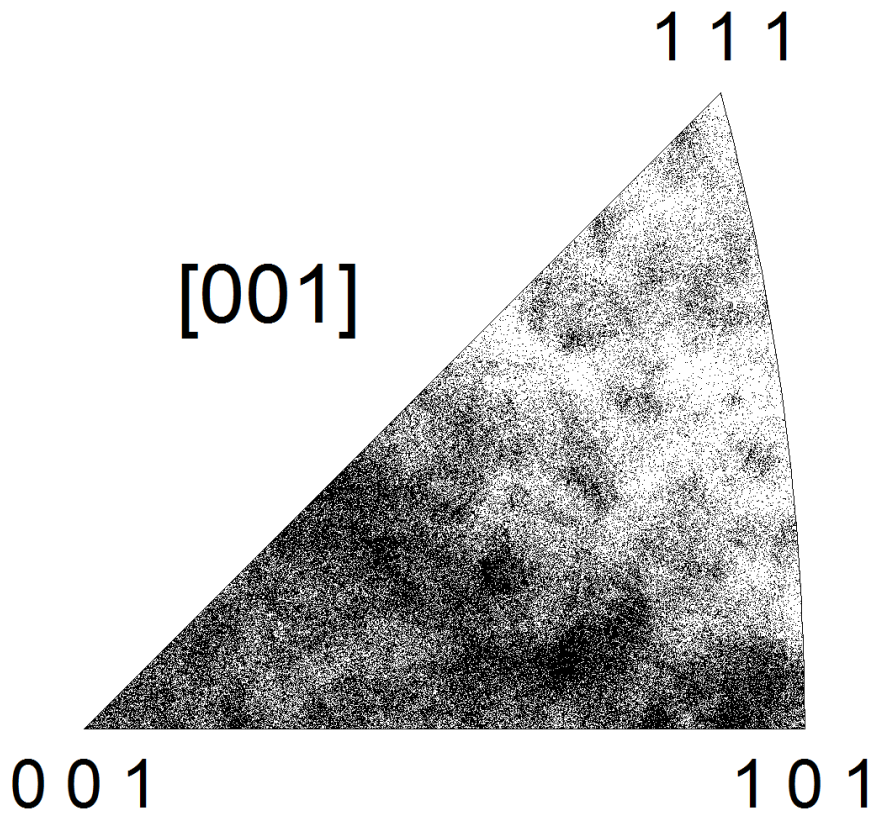


Figure 4.7.4-4 Grain orientation density seen from the top, xy -plane. Darker region is equal to higher presence.

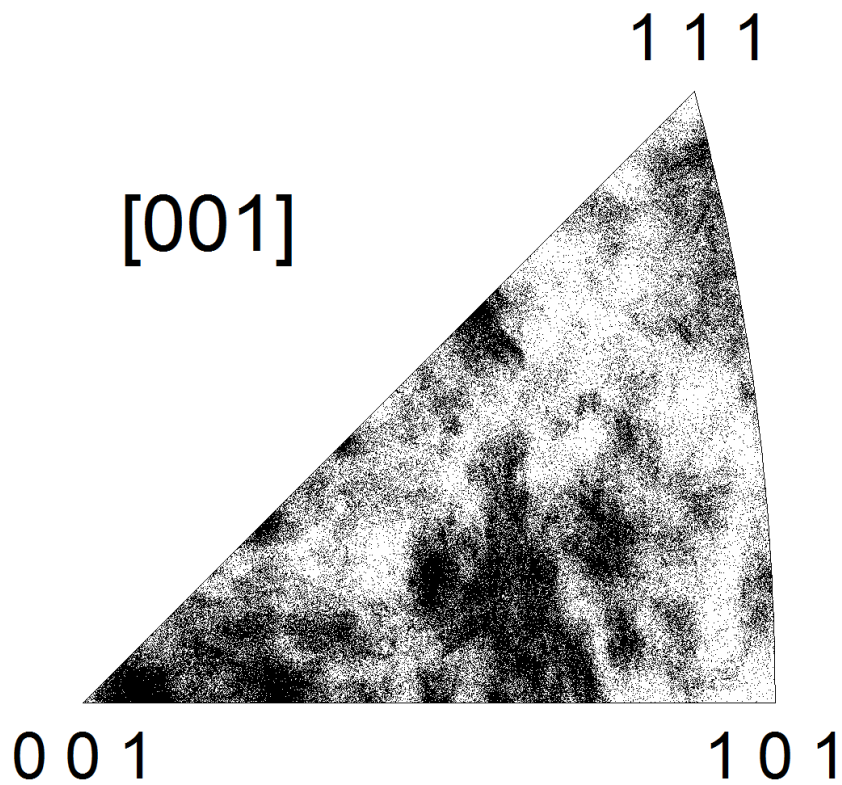


Figure 4.7.4-5 Grain orientation density seen from the side, zx -plane. Darker region is equal to higher presence.

Dendritic subgrain misorientation

There was suspected to be small, less than 1° , crystallographic misorientation between the dendrites. Images taken at higher magnification shows tint inside the grains, see Figure 4.7.4-6.

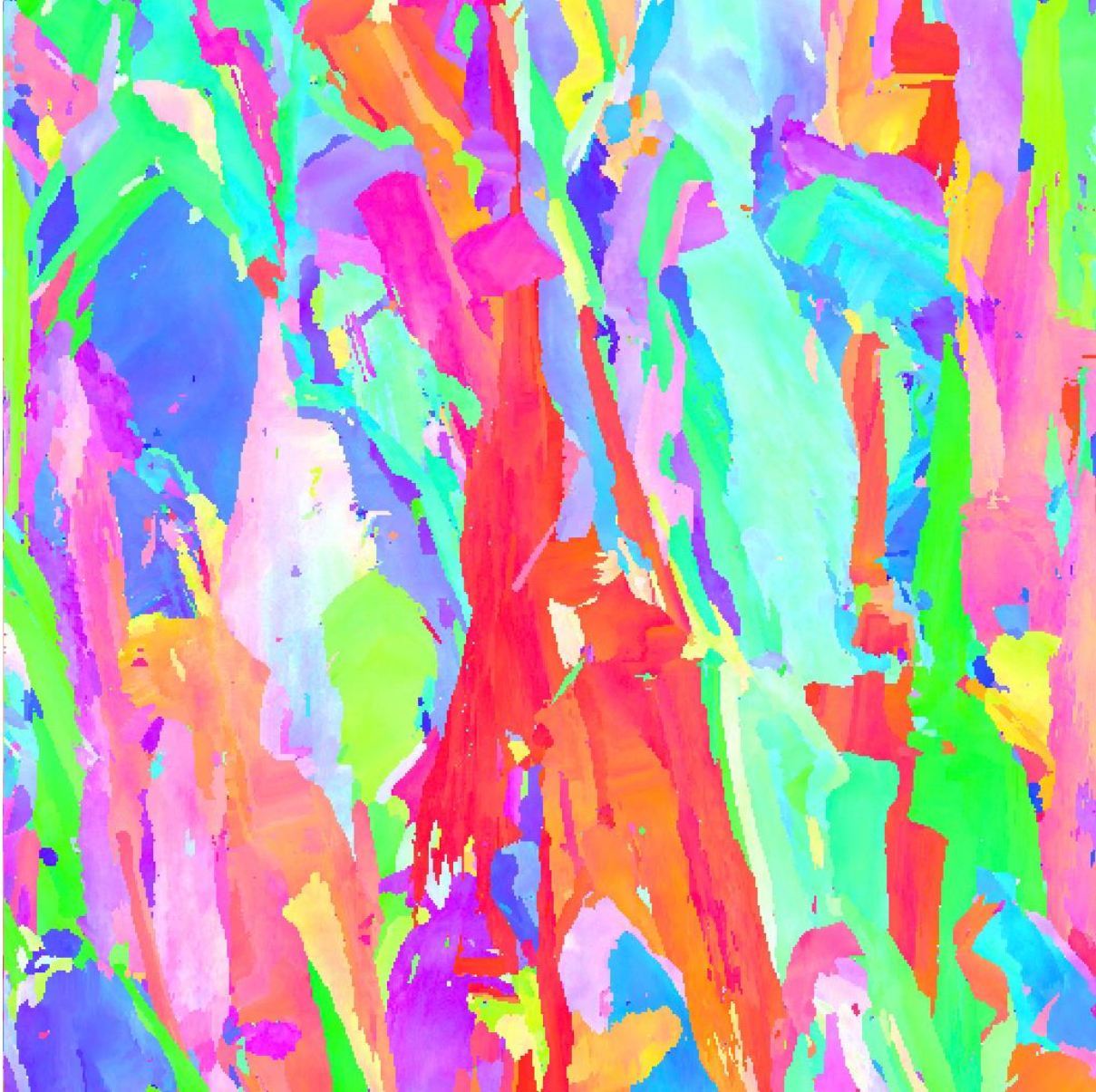


Figure 4.7.4-6 Grains showing tints indicating smaler changes in crystallographic orientation. Specimen seen from the side.

4.7.5 Elemental composition

With EDS the elemental composition of large areas of the specimen's surfaces was evaluated. Neglectable differences were found and below is the one of the analysis presented.

The results are near or within the range given in the EOS [6] specification.

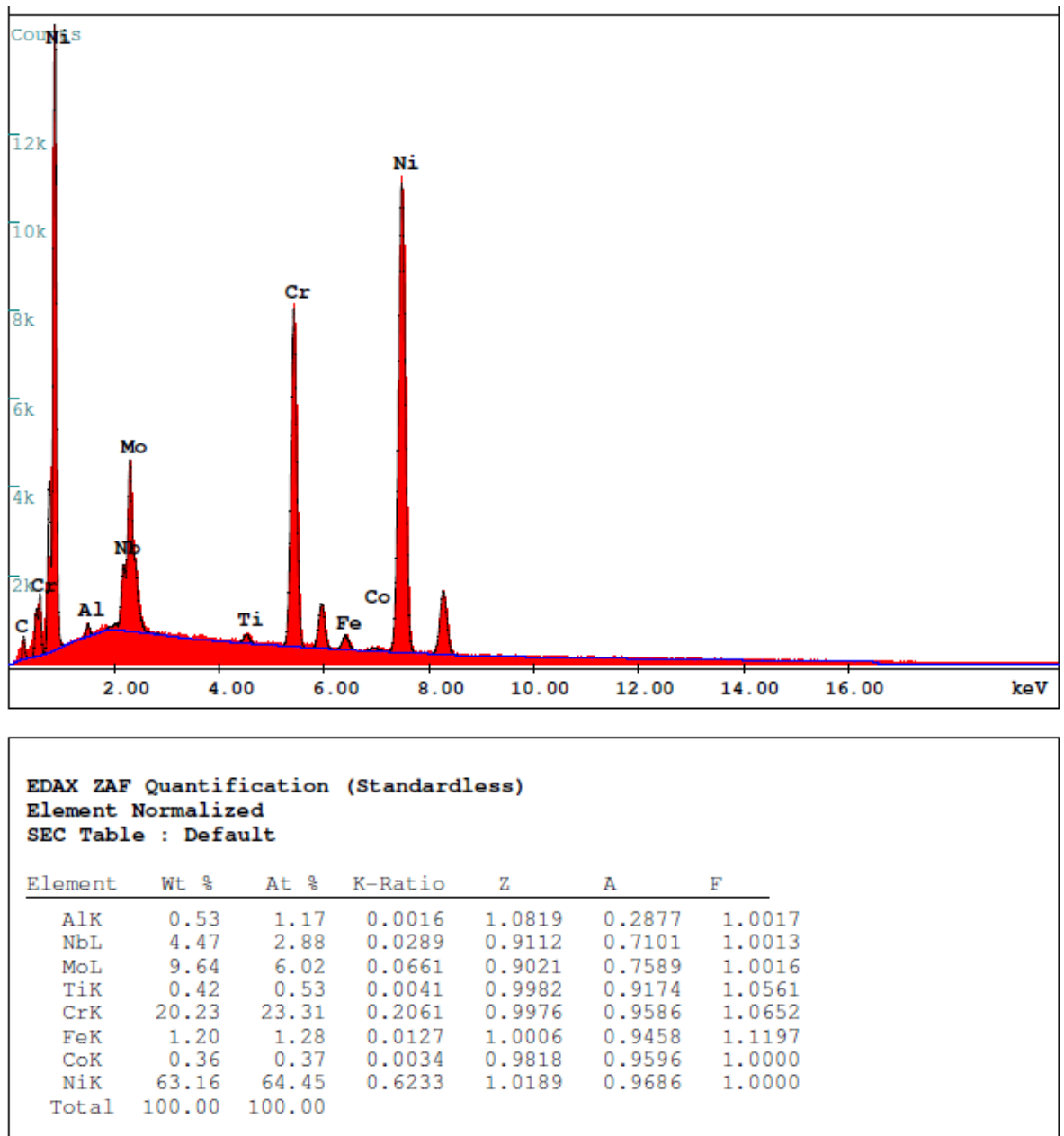


Figure 4.7.5-1 EDS analysis of the matrix, with plot and ZAF-table

5 Discussion

5.1 Initial measurements and inspection

5.1.1 Overhang and support surfaces

The specimens did show struggle with the overhang, creating a very rough surface. This creates both fracture initiation points, and makes it harder to measure the real cross section. These surfaces should probably be machined/polished, before use in any load bearing applications to avoid cracks.

5.1.2 Discoloration

All vertical specimens from print platter No.1, all specimens with a 1 in their name, showed a golden colour on the top of the part. Figure 3.2.2-1 shows an example of this. It is suspected that this was a result of oxidation. This might have happened if the specimens were brought out of the printer chamber when they were still hot, or if the argon atmosphere in the printer was contaminated at the end of the printing process.

5.1.3 Dimensional accuracy

The dimensional accuracy was over all good. The parts were generally a little bit large than they were supposed to, providing the possibility to remove material as opposed to them being to small which is harder to fix. The dimensional accuracy is considered impressive since this is a welding process.

5.1.4 Surface roughness

The surface roughness of the top and sides of the specimens were good. No measurement of the surface roughness has been done, but as seen in Figure 4.1.3-1 the surface is not generally rough, with the exception of overhand and support surfaces. In SEM particles were seen on the side surfaces that are believed to be metal powder from the printing proses that got stuck on the surface. These particles should be removed as they can be crack initialisation points, and they could get loose and contaminate the process that the part is installed in.

5.1.5 Thermal bending

There are clearly bending because og thermal shrinking as the welds solidifies and cools down. This is a known issue with the technology, and compensating measures are being developed to handle it.

5.2 Tensile

5.2.1 Modulus of elasticity (E-modulus)

The E-modulus varies quite much. This is expected to be a result of the extensometer slipping on the surface causing some specimens to get higher E-modulus than they should have. There was no definitive evidence of this behaviour in the test graphs, except for a few specimens. There is of course a possibility that the results are correct and that there are significant variations between specimens. The consistent elongation support this as there would be strange if the extensometer only would slip in the start. No evidences of differences were found when inspecting T2 and T3, that had a large difference in E-modulus, in the SEM. It is not certain if the stress strain graphs are curved enough to demand the alternative method for finding the E-modulus described in section 2.3.2. As mentioned in the results section the E-modulus found in this thesis should not counted upon, and only serves at information that could be beneficial for others to compare with, should they find similar characteristics.

Shouting down common suggestions

“This is a result from threads tightening” – suggested by nearly everyone.

The extensometer is measuring on the reduced cross section, and they record distance between them. This makes any elongation happening outside the extensometer irrelevant as it is not measured.

On the other hand, a sudden “jump” of the specimen because of thread tightening might cause the extensometer to slip on the surface.

“You should use the extension between the clamps in the machine to measure extension. They will be more precise” – suggested by surprisingly many engineering students

In short, read a standard, use common sense, make a drawing of it (it always helps)

With an even cross section, the spring constant, k , of a part can be calculated as:

$$k = \frac{A_{cross\ section} * E_modulus}{Lenght}$$

This is the reason why it is measured between the extensometers where the cross section is even. The whole specimen, including the mounts, has a much more complicated geometry. Compensating for that would probably induce even more errors than what might be present in the extensometer data.

5.2.2 % elongation

The elongation is as expected and within the range of EOS [6]. If the extensometer is slipping in the plastic region, it won't affect the end elongation as the plastic region ends at about 0.4% elongation, and the elongation at fracture is about a hundred times larger.

5.2.3 UTS and yield

UTS and yield strength was in the expected range.

The pores along the surface of specimen T did not seem to have a large impact of yield or UTS compared to the machined, and then pore free U specimen. 3 specimens with some variations in the results are not enough to properly conclude on this matter, but the difference seems to be nearly neglectable.

Some variation was present in specimen Y and L. This is probably because of the overhang and supported surface making the real cross section different from what was measured. To omit this, specimens with a larger cross sectional area should be used to investigate these orientations, since the surface would have a lower total effect on the area than for these small specimens.

5.2.4 Fracture surface

Evidence of cracks in Figure 4.2.6-5 and the images of the microstructure looking torn apart, together with the topology of the fracture surface and the large elongation at fracture, makes these fractures ductile. No clear fracture initiation point was found, and the sound of the fracture being really loud for such small specimens suggests that the fracture was nearly instant.

5.2.5 Y- specimen behaving like the L specimen

It is really interesting to see that the Y-specimens at 45° behave so similar to the L specimens in the tensile test. No clear suggestions to this behaviour has been found, but it no doubt has to do with the crystallographic orientation.

This might prove to be a really beneficial property of the material since it allows for the production of the material in its strongest form over a large angular range. This is important information when tailoring the orientation of a part in the build chamber to benefit from the anisotropic properties.

5.2.6 Anisotropic properties

The specimens showed clear anisotropic properties as expected- The main reason is expected to be because of the preferred crystallographic orientation

5.3 CharpyV

5.3.1 Difference between printed and machined notch

The specimens with the printed notch did show a lower Charpy value than the ones with the machined ones. Many factors can contribute to this and is discussed below

Machined vs printed notch radius

The difference in the notch radius between the printed and machined notch was larger, nearly on the opposite sides of the tolerance range. The printed notch had the largest radius, and the machined had the smallest. The radius was consistent in all printed and machined specimens. The difference can be seen in Figure 3.3.2-4 and Figure 3.3.2-6. Isolated this should make the machined specimens weaker since the stress concentration in a sharper notch is higher. This would suggest that with an identical notch radius, the difference would be even larger than it already is.

Dimension of the specimen's (machined vs printed)

The specimens with a printed notch had a cross section of 10.1x10.1 mm, giving little room for machining to final size. This was a problem as the supported and overhang surface was so rough as described in section 5.1.1. This causes the opposite side of the printed notch to still have some printed surface on it, making it possibly contributing with pores as discussed below, that lower the impact resistance.

Near side surface pores

The surface pores detected along the printed surface causes stress concentrations, that causes the impact resistance to lower. This is expected to be the main reason for the difference in CharpyV value between printed and machined notch specimens.

AI and AI vs A= and A_

Even though these specimens cleave the same plane, there was a clear difference in energy needed depending on the notch placement (cleaving from the top or from the side). This is an important when considering part orientation in the build chamber.

Orientation anisotropic properties

There are clear anisotropic properties in the material. The reason is thought to have most to do with grain shape and geometry. The elongated grains interlock in Z direction making them like roof tiles, but from the side, when the notch is vertical, the grains look more like a dense forest. It is easier to propagate a crack in between the trees than to find a way in-between the roof tiles. (to be certain of no misunderstanding our actual material is solid). This might be the

reason for the vertical specimens SI and SII having significantly larger impact resistance than the horizontal specimens Lxx.

5.4 Hardness Vickers

Results of the hardness test showed large variations within a test series. It is believed that these differences come from variations in the microstructure beneath the surface. It is clear that surface preparation can have a huge impact on the test values. The values are comparable to the ones provided by EOS [6] datasheet.

5.5 Corrosion

5.5.1 Presence of pitting

No pitting was found on the surface of the test specimens. Up to 1000x magnification was used on some parts and no clear signs of pitting was found. Some pitting might have taken place in the dents and pores that was already present on the surface. Thus it was not possible to totally exclude that there have been pitting.

5.5.2 Surface finishing impact on pitting

For stainless steel the pitting resistance of the surface increases as the roughness of the surface decreases [29]. In other words, the higher the grit of the finishing abrasive paper, the better pitting resistance is achieved. This was caused by a decrease in number of metastable pits on the surface that are prone to pitting, on the surface grinded with a higher number paper. Sources documenting this behaviour in Alloy 625 or other nickel based superalloys was not found, but a similar behaviour might be present. If it is then it would have two consequences.

The pitting test performed would not be valid as only a 120grit paper is suggested in the standard, and a finer paper, 500grit, was used. This could have caused the pitting resistance to increase and thus making the test incomparable with other test performed with the surface of 120grit paper. In the extreme case the test could be invalid.

Performing a new test with a finer surface finish, a higher grit paper, to be able to easier spot any pitting, even minor; would cause the pitting resistance to increase and thus invalidate the test.

Pickling was not performed since it was deemed unnecessary as the grinding, ultrasonic cleaning, and ethanol bath would clean the surfaces for oxides, oils, and other pollutants [30]. The effect of the etching, that a pickling process would perform, on the pitting resistance is unknown.

5.5.3 Measurement accuracy of the surface area

As the specimens didn't have completely parallel surfaces the calculated surface area does contain some uncertainties.

5.5.4 Mass deviation

The mass deviation seen in Table 4.5-1 is not large. Some of it is probably because of the inaccuracy of the scale, $\pm 0.0001\text{g}$. Another factor is that the scale is placed upon a proper surface, but only an old desk. This can cause some deviation according to the lab engineers at the university. The difference in the amount of dust, particles, and oils on the specimen should not be large enough to create this amount of deviation.

There were no signs of pitting at 20x magnification, but pitting might have started to occur in the mechanical marks and defects already present on the surface after the sanding.

5.6 Light microscopy

Clear indication of fusion lines was found in the Reichert-Joung microscope. Grain growth across these lines were also found.

5.7 SEM – microscopy

5.7.1 Pores

The pores found along the surface is probably a result of the printing process. To remove them and improve the process a re-melting of this zone could be done on the end of each layer to “melt them away”, or more precisely, melting them shut.

5.7.2 Dendrites

Dendrites was found like in welded material, and as seen by others analysing additive manufactured materials before. Proper analysis of them needs to be performed in the TEM, but there might be carbides in dendritic interfaces indicated by the higher Mo, Nb, and C content.

Further studies should be conducted.

5.7.3 Aluminium rich spots

The aluminium rich spots could be aluminium oxides, being part of the material, or contamination on the polishing discs. The acceleration voltage used to analyse tem, 20kV was too large to get accurate results, since the spot was about 67nm in diameter and the emission volume about 1000nm. More research should be done on them to identify if they are pollutants from polishing of part of the material

5.7.4 Crystallographic orientation

Results of the EBSD shows clear preferences in crystallographic orientation. There was also evidence of small tinting inside each grain that are thought to come from the dendrites having small crystallographic mismatches.

5.7.5 Material composition

The elemental composition was within the range of the specification from EOS, since the minor deviations probably comes from the use of general ZAF settings, and not a calibrated standard.

6 Conclusion

EOS alloy 625 is as specified in their documentation. No deviations were found with the exception of the E-modulus which varied a lot, but this was inconclusive. The material has clear anisotropic properties and preferred grain orientations.

Expanding on the information given in EOS documentation [6], there seems to be little difference between printing a specimen at 45° and horizontally, an interesting found that is valuable in a design perspective. The CharpyV test, that to the knowledge of the author no one has performed on this material before, showed clear anisotropic characteristics too. It was especially interesting to see that the difference in cleaving direction of the same plane was so significant at 45°

No cracks were found, and only a very few pores were found in the bulk material. Along the vertical or angled printed surface pores were regularly found about 100µm inside the material. Inside these pores there were found cracks, and they can themselves be stress concentrators that can cause crack initiation. This is believed to be the main reason for the differences in CharpyV values between printed and machined notch.

A dendritic structure with subgrains that showed small orientation mismatches were found, as previously found in welds. The dendrite boundaries had elevated levels of Molybdenum, Niobium, and Carbon. This could suggest that there is other phases and carbides present at these intersections. TEM-microscopy needs to be done to conclude on this subject. Aluminium rich spots of about 67nm in size were found in all specimens. Further research on them is needed.

The material was within specifications and holds little surprises. It shows great promise as a standard engineering material.

7 Further work

The E-modulus needs to be evaluated further to be able to conclude on the subject of its large variation.

Tensile test horizontally and at 45° needs to be done with a larger cross section to find more precise tensile and yield values.

TEM- microscopy should be done to investigate the dendritic phases and the aluminium rich spots.

8 References

- 1] The Smithsonian Institution, “Stone Tools | The Smithsonian Institution's Human Origins Program,” 24 May 2016. [Online]. Available: <http://humanorigins.si.edu/evidence/behavior/stone-tools>. [Accessed 25 May 2016].
- 2] Wikipedia contributors, “3D printing,” Wikipedia, The Free Encyclopedia, 23 May 2016. [Online]. Available: https://en.wikipedia.org/w/index.php?title=3D_printing&oldid=721641345. [Accessed 25 May 2016].
- 3] Oxford Dictionaries, “Superalloy,” Oxford University Press, [Online]. Available: <http://www.oxforddictionaries.com/definition/english/superalloy>. [Accessed 25 May 2016].
- 4] Wikipedia contributors, “Superalloy,” Wikipedia, The Free Encyclopedia., 14 May 2016. [Online]. Available: <https://en.wikipedia.org/w/index.php?title=Superalloy&oldid=720183579>. [Accessed 25 May 2016].
- 5] R. Bowman, “Superalloys: A Primer and History,” The Minerals, Metals & Materials Society, 2000. [Online]. Available: <http://www.tms.org/meetings/specialty/superalloys2000/superalloyshistory.html>. [Accessed 25 May 2016].
- 6] EOS GmbH - Electro Optical Systems, “EOS NickelAlloy IN625,” 2011. [Online]. Available: http://ip-saas-eos-cms.s3.amazonaws.com/public/d1327facdca0e32a/373a60ec4f5c891b7dbcdf572e37d3b0/EOS_NickelAlloy_IN625_en.pdf. [Accessed 18 February 2016].
- 7] Special Metals Corporation, “Inconel alloy 625,” [Online]. Available: <https://www.google.no/url?sa=t&rct=j&q=&esrc=s&source=web&cd=1&cad=rja&uact=8&ved=0ahUKEwj6zYX3r6XNAhVLApoKHXIDAA4QFggeMAA&url=http%3A%2F%2Fwww.specialmetals.com%2Fassets%2Fdocuments%2Falloys%2Finconel%2Finconel-alloy-625.pdf&usq=AFQjCNHTzkhLSCGiLEmW1aI-V>. [Accessed 25 April 2016].

8] M. ROZMUS-GÓRNIKOWSKA, Ł. CIENIEK, M. Blicharski and J. KUSINSKI, "MICROSTRUCTURE AND MICROSEGREGATION OF AN INCONEL 625 WELD OVERLAY PRODUCED ON STEEL PIPES BY," *Archives of Metallurgy and Materials* , vol. 59, no. 3, p. 1081–1084, 2014.

9] Proto Labs, Inc, "Why DMLS is a Reliable Additive Alternative for Complex Metal Parts," Proto Labs, Inc, [Online]. Available: <https://www.protolabs.com/resources/design-tips/united-states/2015-05/>. [Accessed 4 June 2016].

10] Materialgeeza, "SLS system schematic," Wikimedia Commons, 2008.

11] R. Brooke, "Airbus A320 nacelle hinge bracket," Rapid News Publications Ltd, 2013.

12] P. Zelinski, "How Do You Make a Howitzer Less Heavy?," Modern Machine Shop, 2 June 2014. [Online]. Available: <http://www.mmsonline.com/blog/post/how-do-you-make-a-howitzer-less-heavy>. [Accessed 4 June 2016].

13] International Organization for Standardization, NS-EN ISO 6892-1:2009; Metallic materials - Tensile testing - Part 1: Method of test at room temperature (ISO 6892-1:2009), Standards Norway, 2009.

14] Heavy Engineering Research Association, "Mechanical Testing of Welds - Part 3," [Online]. Available: https://www.hera.org.nz/Category?Action=View&Category_id=518. [Accessed 10 June 2016].

15] International Organization for Standardization, NS-EN ISO 148-1:2009; Metallic materials - Charpy pendulum impact test - Part 1: Test method (ISO 148-1:2009), Standards Norway, 2009.

16] International Organization for Standardization, NS-EN ISO 6507-1:2005 Metallic materials -- Vickers hardness test -- Part 1: Test method, Standards Norway, 2005.

17] Wikipedia contributors, "Visible spectrum," Wikipedia, The Free Encyclopedia. , May 2016. [Online]. Available:

https://en.wikipedia.org/w/index.php?title=Visible_spectrum&oldid=720526851.

[Accessed 10 June 2016].

- 18] Wikipedia contributors, "Optical microscope," Wikipedia, The Free Encyclopedia, 22 May 2016. [Online]. Available: https://en.wikipedia.org/w/index.php?title=Optical_microscope&oldid=721491965. [Accessed 12 June 2016].

- 19] Nothing Nerdy contributors, "Thin-film interference," Nothing Nerdy, [Online]. Available: <http://nothingnerdy.wikispaces.com/THIN-FILM+INTERFERENCE>. [Accessed 12 June 2016].

- 20] The University of Utah, "Introduction to Electron Microscopy - Advanced Microscopy - Imaging Facilities - The University of Utah.," The University of Utah, [Online]. Available: <http://advanced-microscopy.utah.edu/education/electron-micro/>. [Accessed 12 June 2016].

- 21] P. Potts, A Handbook of Silicate Rock Analysis, Springer, 1987.

- 22] K. RAJAGOPAL, Textbook Of Engineering Physics, Part 1, New Delhi: PHI Learning Private Limited, 2008.

- 23] J. H. Wittke, "Detection of Signals - Electron Microprobe Laboratory - Northern Arizona University," Northern Arizona University, 2015. [Online]. Available: <http://nau.edu/cefns/labs/electron-microprobe/glg-510-class-notes/detection-of-signals/>. [Accessed 12 June 2016].

- 24] BenBritton, "Electron Backscatter Diffraction Pattern from a Single Crystal of Silicon," Wikimedia Commons.

- 25] NORSOK committee SN/K 114/EG M, NORSOK MDS-630 6:2013, Standard Norge, 2003.

- 26] ASTM International, Subcommittee: G01.05, ASTM G48-11(2015), Standard Test Methods for Pitting and Crevice Corrosion Resistance of Stainless Steels and Related Alloys by Use of Ferric Chloride Solution, West Conshohocken, PA: ASTM International, 2015.

27] E. H. Kvåle and S. Randeberg, “Deformasjonsmekanismer og mikrostruktur i kaldvalset og rekrystallisert Inconel 625 UNS00625,” University of Stavanger, Stavanger, 2016.

28] G. V. Voort, “Metallographic Specimen Preparation for Electron Backscattered Diffraction,” VACAERO International Inc, [Online]. Available: <http://vacaero.com/information-resources/metallography-with-george-vander-voort/1131-metallographic-specimen-preparation-for-electron-backscattered-diffraction.html>. [Accessed 28 May 2016].

29] T. Hong and M. Nagumo, “Effect of surface roughness on early stages of pitting corrosion of Type 301 stainless steel,” *Corrosion Science*, vol. 39, no. 9, p. 1665–1672, 1997.

30] Wikipedia contributors, “Pickling (metal),” Wikipedia, The Free Encyclopedia, 17 April 2016. [Online]. Available: [https://en.wikipedia.org/w/index.php?title=Pickling_\(metal\)&oldid=715700428](https://en.wikipedia.org/w/index.php?title=Pickling_(metal)&oldid=715700428). [Accessed 6 May 2016].

31] High Temp Metals, “Inconel 625 Technical Data,” High Temp Metals , 2015. [Online]. Available: <http://www.hightempmetals.com/techdata/hitempInconel625data.php>. [Accessed 11 May 2016].

32] Struers A/S, “OP-S, 0.04 µm. 1 l (40700000),” Struers A/S, [Online]. Available: https://e-shop.struers.com/NO/EN/products/Polishing/Silica_Oxide/OP-S_004_m_1_l%2840700000%29.aspx. [Accessed 29 May 2016].

33] Struers A/S, “OP-A, 0.02 µm. 500 ml (40700021),” Struers A/S, [Online]. Available: https://e-shop.struers.com/IE/EN/products/Polishing/Aluminium_Oxide/OP-A_500_ml%2840700021%29.aspx. [Accessed 29 May 2016].

34] Learn EASY, “Finding YS, UTS, E and Toughness,” [Online]. Available: <http://www.learneasy.info/MDME/MEMmods/MEM23061A/Shenck/Schenck.html>. [Accessed 20 May 2016].

35] Cause of Colour, “Iridescence | Causes of Color:,” webexhibits.org, [Online]. Available: <http://www.webexhibits.org/causesofcolor/15.html>. [Accessed 12 June 2016].

J. H. Wittke, "Signals - Electron Microprobe Laboratory - Northern Arizona University," Northern Arizona University, 2015. [Online]. Available: <http://nau.edu/CEFNS/Labs/Electron-Microprobe/GLG-510-Class-Notes/Signals/>. [Accessed 12 June 2016].

Phenom-World BV, "Topographic and Compositional Analysis in SEM with Backscattered Electron Imaging," AZoNetwork, 7 March 2014. [Online]. Available: <http://www.azom.com/article.aspx?ArticleID=10707>. [Accessed 13 June 2016].

Attachments

7 Raw tensile test data

8 Raw CharpyV data